UNIVERSITY OF OKLAHOMA

GRADUATE COLLEGE

GAIT PERFORMANCE AND CONTROL OF A PROSTHETIC ANKLE JOINT FOR BELOW-KNEE AMPUTEES

A DISSERTATION

SUBMITTED TO THE GRADUATE FACULTY

in partial fulfillment of the requirements for the

Degree of

DOCTOR OF PHILOSOPHY

By

ANH THE MAI
Norman, Oklahoma
2015

GAIT PERFORMANCE AND CONTROL OF A PROSTHETIC ANKLE JOINT FOR BELOW-KNEE AMPUTEES

A DISSERTATION APPROVED FOR THE
SCHOOL OF ELECTRICAL AND COMPUTER ENGINEERING

BY

_____
Dr. Sesh Commuri, Chair

_____
Dr. Musharraf Zaman

_____
Dr. Thordur Runolfsson

_____
Dr. Choon Yik Tang

_____
Dr. Tian-You Yu

To my parents.

Acknowledgements

First and foremost, I would like to express my special appreciation to my advisor Dr. Sesh Commuri. He has always motivated, supported, and guided me during my graduate study. I specially thank him for not only being my supervisor, but also for being my mentor and for giving me various opportunities to learn from him. This dissertation would not be possible without all his help.

My gratitude goes to Dr. Musharraf Zaman, Dr. Thordur Runolfsson, Dr. Choon Yik Tang, and Dr. Tian-You Yu for serving on my doctoral committee and advising me at all stages of my doctoral study. I thank Dr. Zaman for sharing his knowledge and experience in multidisciplinary research areas. My appreciation also goes to Dr. Runolfsson, Dr. Tang, and Dr. Yu not only for the knowledge I gained in their classes and as their teaching assistant, but also for their enthusiasm in guiding and mentoring me.

The doctors, physicians, and graduate students from the University of Oklahoma Health Sciences Center deserve acknowledgement for their assistance and guidance in carrying out the clinical work reported in this dissertation. I would especially like to mention the help and support from Dr. Carol Dionne, Dr. William Ertl, Mr. Jonathan Day, Dr. James Regens, Dr. Derek Crawford, Mrs. Jaret Mary Quitoriano, and Ms. Aimee Giuliano. My special appreciation extends to the subjects who participated in the gait studies.

I would like to thank my friends and lab mates in the School of Electrical and Computer Engineering for all their help. I want to single out Dr. Phuong Pham, Dr. Chuong Nguyen, Mr. Harish Gadigota, Mr. Damian Vigouroux, Dr. Fares Beainy, Mr. Syed

Imran and Mrs. Fauzia Ahmed for all the invaluable time spent discussing research and graduate life.

My heartfelt gratitude goes to my host family – aunt Ha Flanagan and late uncle Larry Flanagan, and my Vietnamese friends in Norman, Oklahoma, a place I have considered my second home during the last 9 years. I would like to thank Mr. Hien Hoang, Mrs. Hoat Tran, Dr. Trung Tran, Mrs. Tram Truong, Dr. Dzung Tran, Dr. Thu Nguyen, Drs. Son Hoang and Huong Pham, Dr. Phuong Do, and Mrs. Anh Nguyen for making my time at the University of Oklahoma full of unforgettable memories.

I would like to thank my overseas family members, my dad Mr. Chinh Mai, my mom Mrs. Thao Nguyen, my bother Mr. Anh Mai and his family, and my mother-in-law Dr. Minh Phan. Their unconditional love and confidence in me helped me stay focused and motivated during my doctoral study.

Last but not least, my deepest appreciation goes to my wife, Dr. Linh Do, and my daughter, Han Mai, for loving me, supporting me, and always being by my side through the challenging moments. Their love, patience, and sacrifices are my greatest motivation in completing this dissertation.

Table of Contents

List of Tables

List of Figures

Abstract

Traumatic events such as accidents or vascular and circulatory disorders often lead to amputation of the lower limb below the knee joint. The surgery is followed by fitting of a prosthetic device and rehabilitation process to help the individual recover mobility. The recovered gait of the individual depends to a large extent on his/her health, the amputation technique, and the functional level of the prosthesis. Prior research in amputee gait has focused mostly on assessing gait symmetry, movement of the healthy joints, activities of the unaffected muscles, and the metabolic energy consumption in individuals who had undergone traditional amputation. Very little research has been carried out on the performance of individuals with non-traditional amputation procedures designed to maximize the ability of the residual limb to support body weight at the extremity and to maintain the ability of the affected muscles. Moreover, majority of the studies were limited to gait tests in laboratory environments which restricted the mobility of the individuals.

Current ankle/foot prostheses for people with below-knee amputation are primarily passive devices whose performance cannot be adapted or optimized to meet the requirements of different users. The adverse consequences of wearing poorly functioning prosthetic feet include asymmetric gait, increased metabolic consumption, limited blood flow, instability, and pain. Over the long term, the amputees, especially ones with diabetes, might have to undergo hip replacement procedure and use wheel-chair on a daily basis.

There exists a high and increasing demand for an advanced prosthetic foot that is comfortable and able to replicate the function of the biological foot. Some of the factors

hindering the development and performance validation of such an actively controlled foot are the lack of complete understanding of the gait, the interaction between the residual limb and the controller, presence of human in the control loop, unknown interaction between the terrain and the foot, and stringent requirements on the mechanical power and rigidity of the foot.

This dissertation aims to address these shortcomings in a systematic fashion in order to develop an intelligent ankle/foot prosthesis system. The following are the key steps in the process adopted in this dissertation.

- First, a gait monitoring device and algorithms for gait analysis will be developed to study the gait of people with below-knee amputation in real time during work-related activities. Experimental protocols are then designed to collect gait data from individuals with below-knee amputation in order to understand the activity of the residual muscles and the ability of the prosthetic device to support body weight during gait.
- The dependence of the interfacial socket forces and electromyography signals from the muscles in the residual limb on the type of the gait and gait-related events will then be studied. The use of this dependence to recognize user gait and the corresponding ankle displacement pattern for the controlled prosthetic foot will be investigated.
- Finally, hierarchical learning-based control strategies will be developed to adaptively compensate for the unknown, changing ankle dynamics and drive the prosthetic ankle joint along the desired trajectories. It is anticipated that the learning capabilities of these control strategies will enable the prosthetic ankle

joint to not only replicate the movement of the healthy ankle, but also improve the stability of the gait and optimize the performance.

The above approaches are demonstrated in this dissertation in two parts. The analysis of the gait of a group of otherwise healthy men with non-traditional amputation technique called transtibial osteomyoplastic amputation (TOA) is considered in the first part of the dissertation. The TOA procedure is prescribed for healthy, young individuals who desire a very active lifestyle. TOA offers stable bony residuum capable of bearing the weight of the individual and residual muscles that are active throughout the gait cycle. The gait study carried out in this dissertation is shown to confirm loading at the distal end-bearing area of the residual limb and active contraction of the residual muscles below the knee during gait of all participants. The interfacial forces in the socket and the activity of the residual muscles in subjects with TOA are shown to be related to and dependent on the type of gait, as well as the type of prosthetic feet used. In addition, the potential of residuum socket interface forces in recognition of the gait is also demonstrated.

Learning-based control of the prosthetic ankle joint is addressed in the second part of the dissertation. Two hierarchical learning-based control algorithms that take into account the ankle dynamics, foot-ground interaction, and the movement of upper body are considered. The first strategy uses an artificial neural network-based feedback linearization controller to learn the unknown and changing dynamics of the ankle joint and to track a desired ankle displacement profile. In the second strategy, a neural dynamic programming-based controller that can track an ankle displacement profile while optimizing a cost function based on the tracking error is considered. Actual gait

data obtained from the subjects in the first part of this dissertation is used to study the effectiveness of the control strategy. For the first time, an adaptive controller has been demonstrated that can address changes in terrain and in user requirements to provide consistent and stable functioning of the prosthetic ankle. It is anticipated that the strategy developed in this dissertation will help build an intelligent prosthetic foot that can significantly improve the mobility and long-term health of people with amputation of the lower limb.

Chapter 1: Introduction

1.1 Motivation

Impaired mobility has far-reaching consequences on the health and economic well-being of an individual and the society. In 2008, 1.6 million Americans, or roughly 1 in 190 persons, were living with a loss of a limb [1]. Amongst them, 62% had undergone an amputation of the lower extremity. It is anticipated that the number of people living with limb loss would increase to 3.6 million by the year 2050, with over 1.4 million of them being under 65 years of age.

Amputation of a limb below the knee is prescribed for people who have undergone extreme trauma or those suffering from vascular or circulatory disorders. These individuals are then fitted with a prosthetic device designed to comfortably fit their residual limb and restore a minimum level of comfort and mobility. It comprised of a socket that is designed to fit the residual limb, a shank that connects the socket to the foot, and a flat foot typically with fixed ankle capable of flexing and supporting body weight during gait. Below-knee prosthetic feet are divided into three categories: conventional feet that merely support body weight and basic walking tasks; energy storage and return feet that release stored energy to facilitate forward motion during walking; and powered, controlled prosthetic feet (bionic feet) whose primary goal is to replicate the biomechanics of the healthy limb.

Gait of below knee amputees has been studied in the literature primarily with a goal of understanding the effect of amputation on the mobility of the individual. Temporal-spatial gait parameters (e.g., stance time, gait time, step length, stride length), kinematic measurements (e.g., angular joint trajectories, angular joint velocities) kinetic

measurements (e.g., joint forces, reaction forces), muscular measurements (e.g., muscle contraction, muscle force) and energy expenditure (e.g., oxygen consumption, heart rate) were usually recorded in a laboratory setting from subjects during gait. These methods mainly focused on assessing the asymmetry between the intact side and the amputated side, movement of the residual limb and muscle activity during gait. Some researchers also investigated the ability of amputees to adapt to varying terrain and gait, and effect of prosthetic components on the gait of the individual [2-7]. However, very limited research has been conducted to study the ability of the residual limb to support the body weight at the distal areas and the contraction of the residual muscles or the effect of end-bearing and muscle contractions on the stability of the gait.

Clinical studies indicate that between 68 to 88% of amputees wear prostheses at least 7 hours a day [8, 9] and desire an active lifestyle [10]. These people need highly functional prostheses in order to maintain healthy and high quality of life [1]. However, the prostheses that are currently available for people with below-knee (transtibial) amputation are passive devices that focus primarily on the ability of the individual to bear his/her body weight on the affected limb, have adequate balance, and retain a minimal degree of mobility. The studies also indicate that a high percentage of below-knee prosthesis users suffer on a daily basis from discomfort arising from inadequate prostheses [11, 12]. Further, individuals with unilateral below-knee amputation have asymmetric gait and tend to favor the intact side while walking [13, 14]. In the short term, the use of passive prosthetic foot with fixed ankle can lead to asymmetric gait [13, 14], increased muscle contraction on the intact side [15], and higher metabolic energy expenditure in an individual [16]. Long-term health complications such as osteoarthritis,

osteoporosis, back pain, and other musculoskeletal problems can also be linked to the poor fit and improper alignment of the prosthesis and can lead to poor overall quality of life of the individuals [17].

Development and performance verification of the bionic feet have drawn much attention recently due to the advances in computational and control technology. Several bionic feet including Proprio Foot [18] and BIOM [19] have been commercialized. These feet are typically equipped with active components to modify the dynamic characteristics of the prosthetic ankle joint during gait. However, these prosthetic devices utilize a classical control technique, e.g., PD control, with fixed control parameters. Therefore, although amputee gait improvement have been observed in several case studies [20-22], the performance of these prosthetic feet might be degraded in the presence of disturbances created by the walking terrain, human body movement, and unknown intent of the users.

The development of an intelligent prosthetic ankle that can replicate the functioning of the biological ankle can have far-reaching impact on the quality of life of people with below-knee amputation and is the motivation for the research presented in this dissertation.

1.2 Scope of the dissertation

This dissertation aims to address the shortcomings of existing prosthetic feet in a systematic fashion in order to develop an intelligent ankle/foot prosthesis system. The following are the key steps in the process adopted in this dissertation.

- First, a gait monitoring device and algorithms for gait analysis will be developed to study the gait of people with below-knee amputation in real time during

work-related activities. Experimental protocols are then designed to collect gait data from individuals with below-knee amputation in order to understand the activity of the residual muscles and the ability of the prosthetic device to support body weight during gait.

- The dependence of the interfacial socket forces and electromyography signals from the muscles in the residual limb on the type of the gait and gait-related events will then be studied. The use of this dependence to recognize user gait and the corresponding ankle displacement pattern for the controlled prosthetic foot will be investigated.
- Finally, hierarchical learning-based control strategies will be developed to adaptively compensate for the unknown, changing ankle dynamics and drive the prosthetic ankle joint along the desired trajectories. It is anticipated that the learning capabilities of these control strategies will enable the prosthetic ankle joint to not only replicate the movement of the healthy ankle, but also improve the stability of the gait and optimize the performance.

The above approaches are demonstrated in this dissertation in two parts. The first part presents the analysis of the gait of a group of otherwise healthy men with non-traditional below-knee amputation called transtibial osteomyoplastic amputation, or TOA. The TOA procedure is prescribed for healthy, young individuals who desire a very active lifestyle. TOA offers stable bony residuum capable of bearing the weight of the individual and residual muscles that are active throughout the gait cycle. Expected outcomes of the TOA procedure are confirmed through the presence of loading at the distal end-bearing area of the residual limb and active contraction of the residual

muscles below the knee. The interfacial forces in the socket and the activity of the residual muscles in individuals with TOA are found to be related to and dependent on the type of gait, as well as the type of prosthetic feet used. In addition, the potential of residuum socket interface forces in recognition of the gait is also demonstrated.

In the second part of the dissertation, learning-based control of the prosthetic ankle joint is addressed. Two hierarchical learning-based control algorithms that take into account the ankle dynamics, foot-ground interaction, and the movement of upper body are considered. The first strategy uses an artificial neural network-based feedback linearization controller to learn the unknown and changing dynamics of the ankle joint and to track a desired ankle displacement profile. In the second strategy, a neural dynamic programming-based controller that can track an ankle displacement profile while optimizing a cost function based on the tracking error is considered. Actual gait data obtained from the subjects in the first part of this dissertation is used to study the effectiveness of the control strategy. For the first time, an adaptive controller has been demonstrated that can address changes in terrain and in user requirements to provide consistent and stable functioning of the prosthetic ankle. It is anticipated that the strategy developed in this dissertation will help build an intelligent prosthetic foot that can significantly improve the mobility and long-term health of people with amputation of the lower limb.

1.3 Contributions of the dissertation

This dissertation addressed the development of an intelligent ankle prosthesis. For the first time, a systematic procedure was presented that was mathematically rigorous and guaranteed the stability of the prosthetic limb which could adapt to changing gait and

terrain conditions and optimized the performance over time. The dissertation also added key knowledge to our understanding of amputee gait and the effects of different prosthetic components on the gait. Key contributions of this dissertation are listed below.

a) *Develop a procedure to detect abnormality in amputee gait.*

   In this dissertation, the mobile gait monitoring device named OUPAM (OU Prosthetic Activity Monitor [23]) was used to capture the gait data and Matlab-based analysis utilities were developed to segment the data and extract critical gait parameters such as stance time and swing time. These parameters were shown to be crucial in detecting asymmetry in gait and also in capturing the effect of prosthetic components in gait.

b) *Confirm the expected outcomes of the TOA procedure.*

   In this dissertation, the expected outcomes of the TOA procedure in retrieval of the residual limb function through the presence of loading at the distal end-bearing area of the residual limb and active contraction of the residual muscles under the knee were successfully confirmed by quantitative measurements for the first time. The dependence of the interfacial force and residual muscle activities on the type of prosthetic feet and type of gait was clearly demonstrated and filled an important gap in the literature.

c) *Provide a method for recognizing the gait in real time and planning a desired ankle displacement profile for the recognized gait.*

   A new method for recognizing the type of gait in real time using residuum socket interface force and residual muscle activities was introduced in this

dissertation. Such method could be adopted for the synthesis of the desired ankle displacement profile which was appropriate for the recognized gait and could be used for control of a prosthetic foot.

d) *Develop intelligent control strategies that adapt to the changes in gait and terrain and improve the gait performance over time.*

   Finally, learning-based control strategies with hierarchical structures were implemented to adaptively compensate for the unknown, changing ankle dynamics and drive the prosthetic ankle joint along the desired trajectories. With the learning capabilities of these control strategies and the incorporation of the actual gait data, the prosthetic ankle joint could not only replicate the healthy ankle movement, but also improve the gait stability and optimize the gait performance

1.4 Organization of the dissertation

The rest of this dissertation is organized as follows.

- Necessary backgrounds for the research carried out in this dissertation are provided in Chapter 2. These include the human gait cycle and the ankle joint characteristics during gait, below-knee amputation and outcomes, prosthetic sockets, residuum socket interface force, and residual muscles contractions. An overview of gait analysis and the development of prosthetic feet for below-knee amputees are also presented in this chapter.

The first part of this dissertation, which includes Chapter 3 to Chapter 6, focuses on the gait analysis for participants with unilateral transtibial osteomyoplastic amputation.

- In Chapter 3, temporal-spatial gait parameters and muscle activities in subjects with unilateral TOA are investigated in order to highlight the consequences of undergoing a below-knee amputation on these factors.
- The effect of three prosthetic feet including Renegade Foot® (Freedom Innovations©), Venture Foot™ (College Park©), and Proprio Foot® (Össur) on the residuum socket interface force of an individual with unilateral TOA is elucidated in Chapter 4.
- In Chapter 5, the restoration of the residual tibialis anterior and gastrocnemius muscles and their relationship with the socket contact force under the residual limb are investigated.
- Dependence of the residuum socket interface force and residual muscle activities on the changing walking speeds is assessed in Chapter 6. Potential of these measurements in recognition of the gait types is also evaluated in this chapter.

In the second part of this dissertation, Chapter 7 to Chapter 9 concentrate on modeling and control of the prosthetic ankle joint in the framework which incorporates the ankle dynamics as well as its interaction with the unaffected joints and walking terrain.

- In Chapter 7, the framework in which the dynamics of the prosthetic ankle joint during gait are described and the goal for control of the prosthetic ankle joint in that framework are discussed.
- The implementation of an artificial neural network for control of the prosthetic ankle joint is described in Chapter 8. The resulted hierarchical controller is shown to adaptively compensate for the unmodeled dynamics and disturbances

during changing gait conditions and provide closed loop stability with guaranteed tracking performance.

- In Chapter 9, the implementation and performance of an adaptive dynamic programming-based structure, named direct neural dynamic programming, for control of an active prosthetic ankle joint are presented.

Finally, conclusions of the dissertation and outlines for the future research are discussed in Chapter 10.

Chapter 2: Background of Gait Analysis and Prostheses for People with Below-knee Amputation

This chapter covers the backgrounds on the human gait analysis and summarizes recent results and trends in improving the mobility of people with below-knee amputation. Definition of the human gait cycle, description of each gait phase and the biomechanical characteristics of the human ankle joint during gait are first discussed. Below-knee amputation procedures and the need for studying the residuum socket interface (RSI) force and residual muscle activities are then presented. Common approaches in gait analysis for people with below-knee amputation are discussed with a focus on understanding the goals required for such studies. The chapter concludes with an overview of the current status of below-knee prosthetic feet, the desired performance and challenges in development of advance prostheses.

2.1 Human gait cycle and the ankle joint during gait

Walking constitutes a very important aspect of human locomotion. The sequence of foot movements by which a person moves forward is called 'gait'. A typical human gait cycle is shown in Figure 2.1 [24] and can be divided into two phases: the stance phase when a foot contacts with the ground and the swing phase when a foot is swinging in the air [25]. According to [26], the stance phase constitutes approximately 62% of the gait cycle and includes five sub-phases: *Initial Contact*, *Loading Response*, *Mid-stance*, *Terminal Stance*, and *Pre-swing* . The swing phase constitutes the remaining 38% of the gait cycle and comprises of three sub-phases*: Initial Swing*, *Mid-swing*, and *Terminal Swing*.

Initial Contact of the stance phase is a time instance at which the leading foot hits the ground while the opposite foot is still in contact with the ground. At this point, the body weight starts shifting to the leading foot. The *Loading Response* phase starts after the *Initial Contact*, and comprises 10% of the gait cycle. During this phase, the foot gradually comes into full contact with the ground and entire body weight is transferred from the trailing foot to the leading foot. This phase terminates when the leading foot supports the entire body weight and the trailing foot starts *Initial Swing* by lifting off the ground. The *Mid-stance* phase starts at the end of the *Loading Response* phase and terminates when the opposite foot aligns with the stance foot. This phase constitutes 10 to 30% of the gait cycle. The *Terminal Stance* phase which constitutes 30 to 50% of the gait cycle, starts at the end of *Mid-stance* and terminates after the opposite foot finishes *Mid-swing*, *Terminal Swing* and contacts the ground. This marks the occurrence of *Initial Contact* and starts a new gait sequence on the opposite foot.

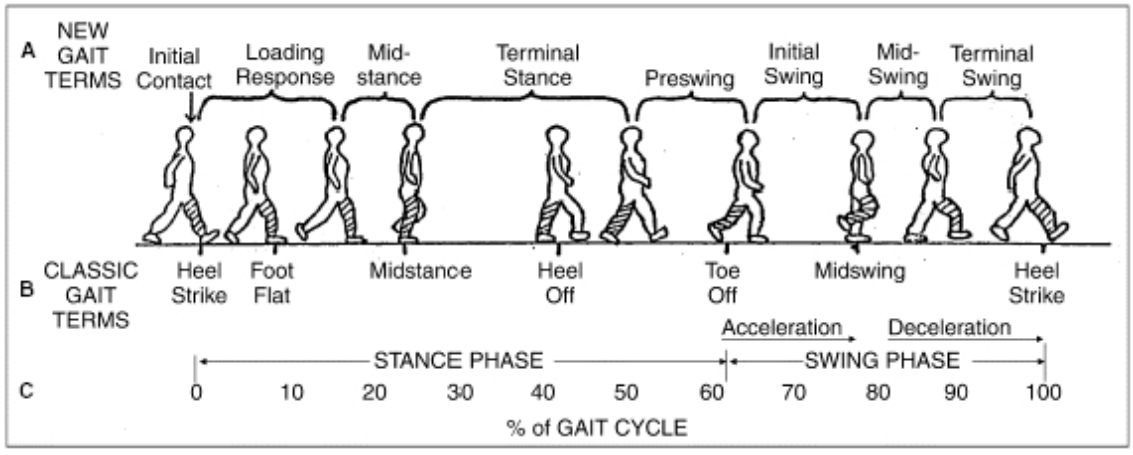

Figure 2.1. Human gait cycle [24].

As can be seen in Figure 2.1, the human foot is subjected to varying loads and torques as it transitions through the gait cycle. The unique design of the human ankle and foot

enables them to absorb shock and generate energy for propulsion. Further, the ankle can guarantee stability, mobility, and withstand 1.5 times the body weight during normal ambulation and 8 times the body weight during running [27]. During gait, the ankle can adjust the stiffness of the ankle joint, perform dorsiflexion and plantarflexion of the foot, and provide propulsion power to aid the human body as it moves forward. These capabilities help humans walk effortlessly in different walking conditions (changing walking speed, varying step length, etc.) on different terrains (level ground, ramps, staircases, etc.) and with individual preferences such as type of shoes, height of a heel, carrying heavy objects, etc.

During gait on level ground, the human ankle joint follows a typical trajectory as shown in Figure 2.2. The displacement profile in Figure 2.2 [28] is shown normalized with respect to the gait cycle and is related to the phases and events of the gait [24, 25, 28]. This joint displacement profile is typical for all humans and is presumed to minimize the energy consumption during gait [29, 30].

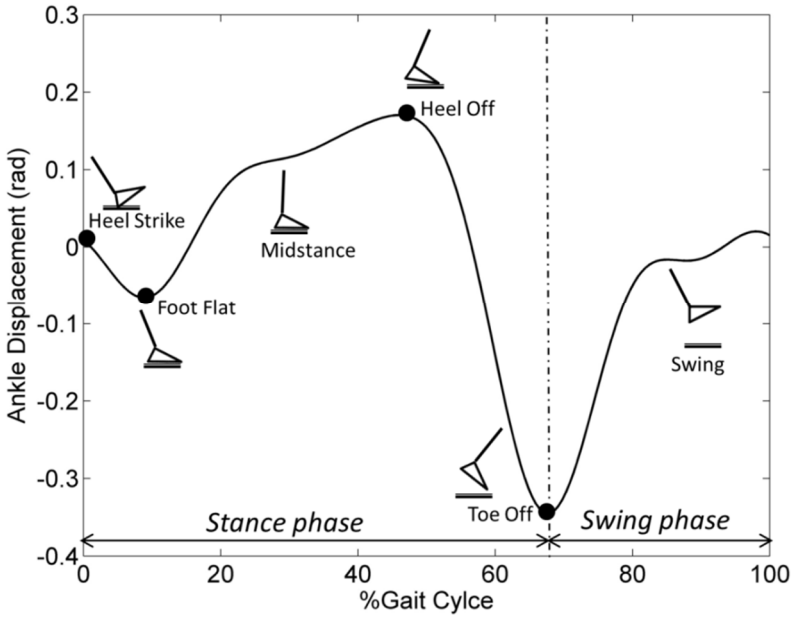

Figure 2.2. Typical human ankle displacement profile.

It is also known that during the gait of non-amputee subjects, dorsiflexion and plantarflexion of the foot are achieved by the contraction of the tibialis anterior (TA) and gastrocnemius (GAS) muscles. Contractions of those muscles have been studied by analyzing electromyography (EMG) signals obtained using either surface electrodes or needle electrodes [31, 32]. In principle, large muscle contractions are indicated by EMG signals with higher magnitudes. Normalized EMG signals over one gait cycle of tibialis anterior and gastrocnemius muscles [31] (Appendix Table 5.22 and Table 5.24) are shown in Figure 2.3.

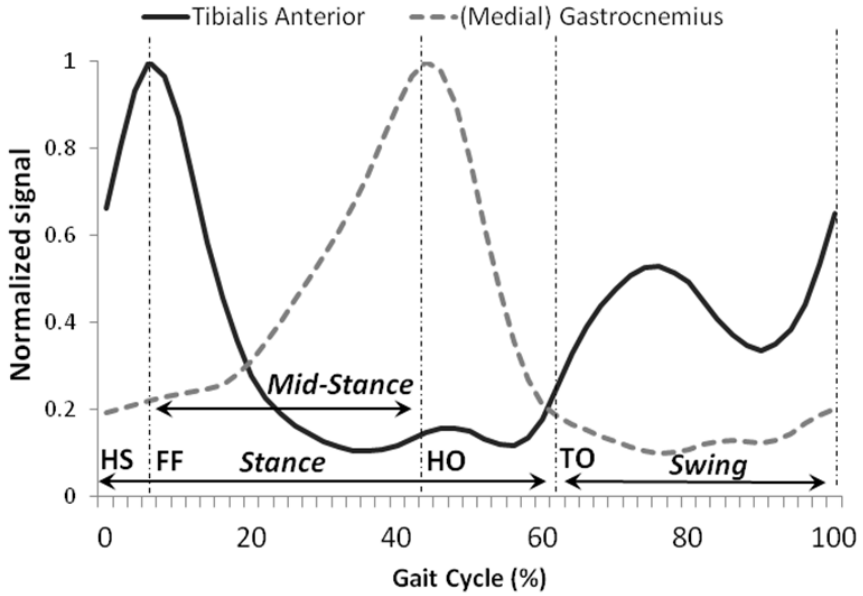

Figure 2.3. Normalized tibialis anterior and gastrocnemius muscle activities. This figure is reproduced using data from [31] (HS – *Heel Strike*; FF – *Foot Flat*; HO – *Heel Off*; TO – *Toe Off*).

The mechanisms of the tibialis anterior and gastrocnemius muscles in Figure 2.3 and their relationships to gait phases and ankle movement in Figure 2.2 are explained as follows [31, 33]. At the *Initial Contact* (or *Heel Strike*), the tibialis anterior contracts at its highest level (EMG signal reaches the highest magnitude) controlling plantarflexion

through eccentric contraction. After the foot is completely flat on the ground (*Foot Flat*) and during *Mid-stance*, this muscle contributes very little to the movement of the foot relative to the leg. As the body weight is shifted toward the opposite limb, the weight bearing heel starts to lift off from the ground (*Heel Off*), and EMG activity of the TA is increased until *Toe Off*. The TA muscle is also active during the swing phase while dorsiflexing the foot and providing toe clearance. In contrast, the gastrocnemius is more active during *Foot Flat* and *Mid-stance* to control tibial progression and generate propulsion power. Gastrocnemius plays little role during the swing phase as well as between the *Heel Strike* and *Foot Flat* phases of the gait [25, 31].

It can be seen that during the gait cycle, the human ankle joint adjusts its characteristics to accommodate movements of the human body. The ankle has low stiffness at *Heel Strike* to allow for controlled plantarflexion of the foot during the initial *Loading Response* phase. On the other hand, the ankle demonstrates high stiffness between *Mid-stance* and *Heel Off*. The quasi-stiffness of the ankle joint, denoted by the slope of the ankle moment versus the ankle angle curve during the stance phase, appears to change during gait and the relationship between the moment and angle during loading becomes more nonlinear as the walking speed increases [34]. These characteristics imply that the human ankle joint can be represented by a rotational spring and a damper for slow to normal walking speeds. However, to replicate the characteristics of the human ankle during walking at fast speeds, an augmented system would be necessary [34, 35].

2.2 Below-knee amputation

Below-knee or transtibial amputations (TTA) are typically performed on people who suffer from vascular or circulatory disorders or who experience traumatic events such as

combat wounds or traffic accidents. The ideal amputated length is from the proximal one third to the middle of the limb [36]. One way to classify below-knee amputation is based on whether the procedure aims to provide end-bearing for the residual limb and/or retain the contraction/elongation of the residual muscles. In traditional lower limb amputation, the distal end of the residual limb is not allowed to bear weight and the residual muscles (tibialis anterior, gastrocnemius) are left disconnected at the distal end of the limb. As a result, people with traditional amputation are typically fitted with a patellar tendon bearing (PTB) socket, wherein the loading is mainly distributed around the anterior area under the knee cap (patellar). Such concentrated loading of the body weight can lead to sores and frequent joint pains. A loss of the length-tension relationship in these unsecured muscles can also lead to a decrease in muscle contraction, blood circulation, and gait performance [37]. On the other hand, there are techniques that allow the amputated limb to bear weight at the extremity (e.g., Lisfranc amputation, Syme amputation, Ertl transtibial osteomyoplastic amputation) or enable the residual muscles to contract during gait (e.g., myoplasty, myodesis) [36].

In the transtibial osteomyoplastic amputation (TOA) procedure, the fibular and the tibial ends are connected to each other by a “bony bridge” (Figure 2.4) which helps stabilize the anatomy of the residual limb and allows weight bearing at the distal end [38]. This procedure aims to add rigidity to the lower limb extremity, aid load transfer between the residual limb and the prosthetic socket, provide more uniform load distribution on the residual limb by enabling amputees to wear total surface bearing (TSB) sockets, and provide stability during the gait. This procedure reduces the incidence of sores seen with PTB sockets and allows for increased weight to be supported by the amputated

limb [39]. In addition, TOA procedure also secures the distal ends of the residual tibialis anterior and residual gastrocnemius to the bony foundation to re-establish the length-tension relationships of these muscles. It is anticipated that each of these residual muscles has a contraction profile similar to that of the corresponding muscle of non-amputee subjects. Some researchers have studied the gait characteristics of people with TOA in order to understand the outcomes and maximize the potential advantages of the procedure [40, 41]. **While personal anecdotes validate the clinical outcomes of the TOA procedure, there has been no clinical evaluation or quantitative data in the literature on the success of this procedure.**

Figure 2.4. Radiograph of the bony bridge in transtibial osteomyoplastic amputation procedure [42].

2.3 Prosthetic sockets and residuum socket interface force

The prosthetic socket plays a critical role in providing comfort, appropriate load transmission, and efficient movement control in people with below-knee amputation [43]. Adverse consequences of ill-fitting socket or improper loading include soft tissue injury, bleeding, bruising, pressure sores, and pain, which in the short term reduce the functional ability of people with amputation. If left unaddressed, these can diminish their health and quality of life [44, 45].

The force distribution at the interface between the prosthetic socket and the residual limb is a critical consideration in the design and fit of a socket to a patient [46-48]. Proper distribution of an individual's weight across the surface of the residuum plays a critical role in the comfort and function in people with TTA [49, 50]. Further, the design of the socket is dictated by the type of amputation that was performed on the subject.

The load distribution inside the socket depends on a combination of factors, including the method of construction of the socket (pressure casting, hand casting, etc.) [45, 51-53], socket and prosthetic alignment [46, 54], suspension system of the prosthesis [55], and the type of gait [20, 56]. Computational methods such as finite element analysis [57], artificial neural network, and magnetic resonance image scan can be used to measure the residuum socket interface pressure/force and understand the load distribution and its characteristics during gait [48, 58]. These advanced tools have potential in predicting the RSI force distribution and in aiding the design and fabrication of the prosthetic sockets [47, 59, 60]. **However, there is no device that is currently available in the market that can simultaneously measure and analyze the interfacial forces and EMG signals during actual gait.** There exists a high demand

for subject-specific wearable measurement systems which are capable of real-time monitoring of the socket force and real-time evaluation of prosthetic fit and gait performance [61, 62].

2.4 Residual muscles

Electromyography signals which are captured by placing electrodes on the muscle bellies from the lower limbs can provide insight into how the muscular systems generate joint movements and stabilize limbs for both normal and pathological gait analysis [25, 28]. Since the magnitude of the electrical signals generated by muscles during gait is very small, measurement and analysis of EMG signals from muscles require specialized hardware and procedures [32, 63]. Muscle contraction profiles from the lower limbs and their dependence on the walking speed and walking terrain can also be used to explain the variations in ambulatory energy consumption [64].

For individuals with below-knee amputation, alterations in lower limb muscles compared to those of able bodied also indicate the compensation strategies for the missing limb [65, 66]. However, most of the studies on muscle contraction focus on the muscles which are outside the prosthetic socket or in other words, above the knee. Measurement of the activity of the residual muscles below the knee of the residual limb requires the surface electrodes to have high sensitivity and be thin enough for placement inside the prosthetic socket. Recently, there has been increasing interest in characterizing the contractions of the below-knee residual muscles in order to observe the recovery of those muscles after amputation [67], explain their activities during gait [68, 69], and evaluate the potential of those muscles in gait recognition and prosthetic development [70]. **However, activities of the residual muscles inside the socket and**

their relationships to the variations of the RSI forces in individuals with TOA during actual gait have not been adequately addressed.

2.5 Overview of gait analysis for individuals with below-knee amputation

Gait analysis has been extensively performed in the last few decades to characterize the human gait, study the performance of the human joints and muscles during gait, and understand the reasons for pathological gait [25, 31]. Different gait analysis systems have been developed to capture the temporal-spatial gait parameters, joint movements, ground reaction forces, muscle contractions, and metabolic energy consumption in order to obtain a complete picture of the gait mechanism [26, 71, 72]. In recent years, there has been an increasing number of applications of computational tools such as artificial intelligence, digital signal modeling and processing in gait analysis, especially in recognition of abnormal gait phenomena and classification of gait pathologies [73-76]. Results from gait analysis of abled bodied individuals provide insight into the development of prosthetic feet [34, 77, 78]. Gait analysis using wearable sensors [79] or mobile gait labs has also drawn much attention. VICON [80], Organic Motion [81], and IDEEA [82] are examples of some of such systems.

Gait analyses for below-knee amputees have also been carried out to study the effect of amputation on standard gait measurements such as gait asymmetry, joint movements, and muscle activities that contribute to higher energy consumption [3, 83]. Gait analysis also considers the interfacial contact force between the prosthetic socket and the residual limb as well as the contraction of the residual muscles. Standard gait measurements from the amputees are usually compared to that of able bodied subjects to understand the consequence of amputation procedure as well as the individual's

strategy to adapt to the changes in gait and mobility [14, 84]. Gait measurements are also compared among subjects wearing different prosthetic systems to evaluate the effectiveness of the prosthetic feet and socket design [3-5]. Outcomes of rehabilitation process can also be beneficial from the gait analysis results [85]. While gait analysis can provide insight into the gait performance and effect of prosthetic components, one has to take into account the discrepancies in amputation techniques, socket concepts, prosthetic foot models, and activity levels of the amputees before any conclusions can be drawn [86].

2.6 Development of prosthetic feet for people with below-knee amputation

Recovery of full locomotion capability in TTA's requires the development of highly functional prosthetic foot that can replicate the biomechanics of a healthy ankle joint and adapt to amputees' gait. However, existing prosthetic devices are designed primarily to support body weight and provide stability during stance and gait. The state of the art in prosthetic feet and the requirements for the next generation intelligent feet are discussed in this section.

2.6.1 Current status of prosthetic feet

Below-knee prosthetic feet can be divided into three categories: conventional feet, energy storage and return feet (ESR), and controlled prosthetic feet [77]. Conventional foot, such as solid ankle cushion heel (SACH) foot or Single Axis Foot mainly helps support the body weight and aid in basic walking. Although these feet have limited functionality, they are still very popular, especially in rural areas and in developing countries due to their low cost, simple design, and easy maintenance.

Energy storage and return feet (e.g., Flex Foot, Venture Foot) have spring-like components to store the energy that the human body asserts during the *Loading Response* phase and then release that stored energy during the end of *Terminal Stance* and *Pre-swing* to help propel the body forward. It has been shown in some studies that the energy storage and return prosthetic feet help improve the gait and energy expenditure [5, 87, 88]. However, other studies did not find evidence of significant improvement of ESR prostheses over the SACH foot [89, 90] and benefit of such designs on knee and hip output powers are still unclear [91]. Moreover, none of the current ESR prosthetic feet can return the required energy (1.7 times the body weight) during push off (*Terminal Stance*) phase [77, 92] or dorsiflex the ankle joint to reduce the incidence of tripping during the swing phase of the gait.

Some advanced prosthetic feet are equipped with active components that can modify the characteristics (ankle joint stiffness and joint movements) of the prosthetic ankle joint in order to adapt to changing terrain and gait needs. These prosthetic feet have either pneumatically driven or electrically driven actuators which generate enough torque to modify ankle movement and provide propulsion energy during gait. Commercially available below-knee controlled prostheses such as Proprio Foot [18] and BIOM Ankle system [19, 93] are capable of manipulating the movement of the ankle joint [77, 94]. Improved gait performance obtained using these controlled prostheses has been reported in several case studies [20-22]. Performance of other active foot prototypes such as SPARKy [95] and PPAMs [96] in generating ankle movement and push-off power during late stance phase is also promising. However, both systematic and subject-

specific tests are necessary in order to fully evaluate the benefits of these bionic feet [21, 92, 97].

2.6.2 Desired performance of the controlled prosthetic feet

The lack of an active prosthetic joint that can dynamically adapt to changing terrain and gait needs is a limiting factor in attaining adequate comfort and mobility in below-knee amputees. **Thus, it is necessary to design a prosthetic device and an associated control mechanism that can replicate the biological ankle joint in altering its stiffness and movement during gait [34], providing enough propulsion power, adapting to walking environment in real time, while being robust to dynamic uncertainties of the prosthetic ankle, measurement noises, and actuator noises.** The outcomes of these advanced prosthetic feet would be evaluated by accessing the improvement in the gait symmetry, reduction in the unnecessary kinematics and muscle compensation, and decrease in the metabolic energy consumption.

However, developing a prosthetic foot that meets the desired performance described above is not easy and has to overcome several challenges. Important among these challenges are the following.

- Mechanical design of the prosthetic foot has to be rigid, able to support the body weight, and provide shock absorption during gait activities. Power requirement (i.e., batteries) and joint actuators also create challenges for a proper implementation of the prosthetic feet. In addition, the rigidity and power required during the gait are usually varying depending on the activity pursued by the individual.

- The lack of an accurate dynamic model describing the characteristics of the prosthetic ankle and the variations of the biomechanics of a human ankle during different walking conditions make it difficult to apply the traditional control approaches to this problem. The addition of human-in-the-loop further makes the system much more complicated and highly nonlinear.
- Wearable sensors can be attached to the prosthetic foot or the human body in order to capture the user intent or gait variations. However, accessibility to the measured signals, reliability of the captured data, portability of the measurement systems, and data processing and interpretation are not trivial tasks.
- Changing gait types and walking terrains create another obstacle for the traditional control approaches which have fixed control structure and parameters. It is noted that the currently available powered prosthetic feet are typically controlled using classical techniques, e.g., PD control. Once the controller is tuned, its parameters are usually fixed irrespectively of any changes in gait. It also requires additional tests to evaluate and compare the performance of different control strategies [94].

2.6.3 Additional trends in development of controlled prosthetic feet

Development of advanced prosthetic feet is a multidisciplinary area in which the following trends are being observed.

- It is now a common understanding that the advanced prosthetic foot will improve the gait performance if it is capable of replicating the dynamic characteristics of the biological limb [34, 77, 92]. Development of controlled

prosthetic feet will be further supported by experimental and theoretical biomechanical research on both non-amputee and amputee gait.

- Another trend in the development of advanced prosthetic feet is the utilization of kinematic and electromyography signals measured from the users' movement for recognition of gait and detection of gait events. Data measurement techniques and interpretation algorithms applied to gait analysis for able bodied will be extended to generate trigger signals for control mechanism for the ankle devices [70, 98, 99].
- There will be more studies on contraction of the residual muscles and the relationship between their contraction profiles and the gait. These studies hold out promise and are likely to motivate the use of signals from residual muscles to control the prosthetic foot [68, 100].
- Combination of the mechanical control and biological-based signal monitoring and interpretation will result in hierarchical prosthetic control structures [94]. Fundamental control loops such as impedance, position, and torque controls which are specifically designed for each gait mode will incorporate supervisory control that can interpret the gait and switch between different gait modes. The resulting control structure will be capable of detecting gait change and providing required ankle stiffness, movement, and power.
- Finally, performance of advanced prosthetic feet will be evaluated by quantitative performance indices such as the deviation of the joint ankle from the desired trajectory, mechanical energy, metabolic energy consumption [3, 93, 101], etc.

2.7 Framework of the experimental gait study

In this dissertation, the shortcomings identified in the previous subsections will first be addressed through the development of a portable gait analysis system. The detail of the device and the experimental setup are discussed below. This framework is used subsequently in Chapter 3 to Chapter 6.

2.7.1 Criteria for subject selection

Subjects for the experimental studies are recruited from the amputee populations who live in the state of Oklahoma for at least 6 months following unilateral below-knee amputation surgery. All subjects are between 18-64 years of age and capable of walking independently without using any other assistive devices except their own prosthetic feet. All subjects are free of medical conditions such as cardio-respiratory, peripheral vascular, neuromuscular, inflammation, diabetes, and open wound on the residuum. All the selected subjects speak English and can independently give written consent to participate in the study. Non-amputee subjects are also recruited for the study to serve as a control group.

2.7.2 Protocol

Several protocols are approved by the Institutional Review Board at the University of Oklahoma Health Sciences Center (OUHSC) for protection of human subjects [40, 41] (IRB# 15948, IRB# 15713). All subjects use their own prosthetic systems (socket and prosthetic foot) during the studies. A certified prosthetist is available onsite to adjust socket alignment and fit. Heart rate, pulse, blood oxygen level, and the Borg index of participants are monitored by a healthcare professional from the College of Allied Health, OUHSC.

2.7.3 Measurement and sensors

Gait parameters

A gait monitoring device called Intelligent Device for Energy Expenditure and Physical Activity (IDEEA®) by MiniSun™ [82] will be used to obtain the gait parameters from the subjects (Figure 2.5). Each subject will wear an IDEEA unit during the gait. Information such as stance time, gait cycle duration, step length and stride length will be determined using the analysis software provided by MiniSun.

Figure 2.5. Intelligent Device for Energy Expenditure and Physical Activity.

RSI force measurement

Residuum socket interface force will be measured inside the prosthetic sockets using ultrathin FlexiForce® A201 piezo-resistive sensors (thickness – 0.208mm; active sensing area – 0.713cm2; force sensitivity range – 20g - 2200kg; response time – 5-20µsec; linearity – <±5%) [102]. The force sensors are secured to the inner wall of the prosthetic socket by medical tapes (Figure 2.6a). With the short response time, wide sensitivity range and small thickness, these sensors enable non-intrusive and real-time loading measurement without affecting the comfort and mobility of the subjects during gait. The amount of applied force on each sensor can be converted into the voltage by

an amplifying circuit similar to Figure 2.6b. All force sensors will be calibrated prior to the data collection.

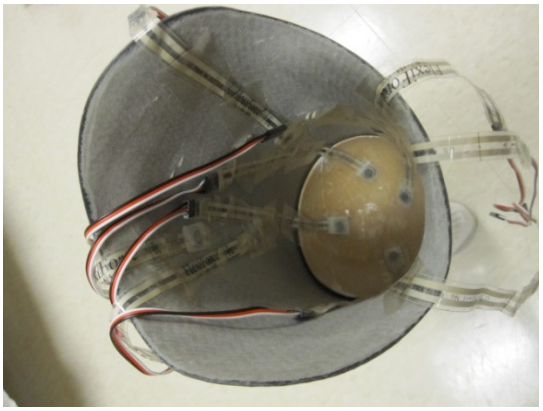

(a)

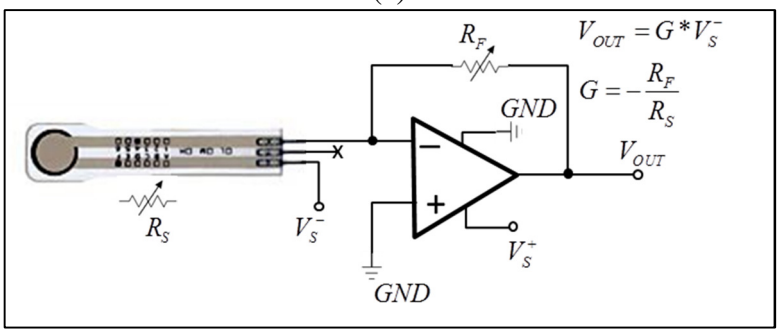

(b)

Figure 2.6. (a) Placement of FlexiForce® sensors inside the socket; (b) Force-to-voltage signal converter.

Electromyography

Electromyography signals generated by muscle activities will be measured using disposable surface stimulating and recording Ag/AgCl electrodes (square, sensing area of 1.44cm^2) [103]. For each muscle, a pair of electrodes will be placed 2.5cm apart longitudinally along the muscle (Figure 2.7a). Skin surface at the selected location will be shaved and cleaned with alcohol and conductivity gel will be applied before placement of the EMG electrodes. Since the magnitude of the electromyography signal is very small, a differential amplifying circuit (Figure 2.7b) will be used to increase the signal magnitude to a measurable level.

(a)

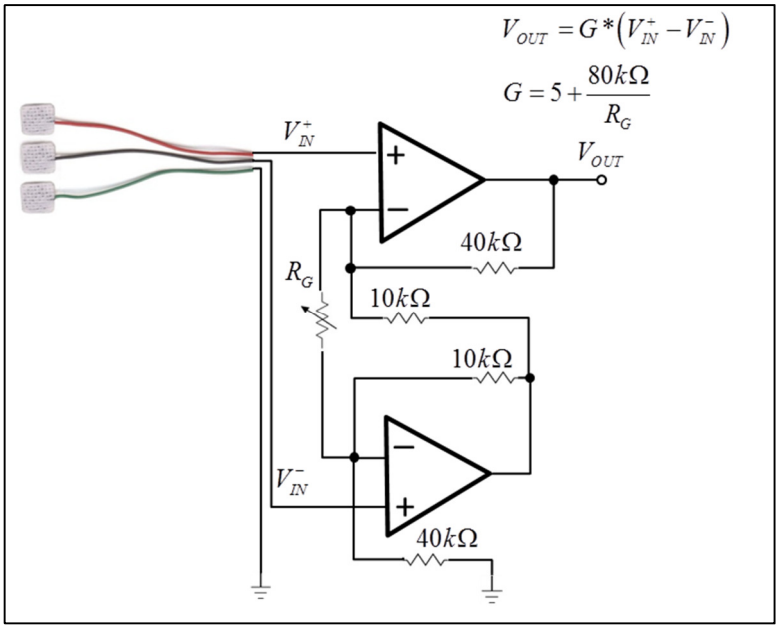

(b)

Figure 2.7. (a) Placement of EMG electrodes on the muscles; (b) Differential amplifying circuit for EMG signals.

2.7.4 Data acquisition

Two versions of data acquisition systems will be used for the experimental studies. The first version, which is designed to be used in the experimental study in Chapter 4, is shown in Figure 2.8a. This system includes a Mobile Demand© tablet computer (CPU U25000 – 1.20GHz, 1.99GB RAM) which is equipped with a 12-bit data acquisition and control board PC-CARD-DAS16/12 AO (Measurement Computing©) and a customized signal conditioning box. Matlab®, Simulink® and Real-time Windows Target™ (Mathworks®) will be used to develop an embedded application which

sampled, collected, and organized the experimental data. Signals are sampled at the rate of 500Hz. During the test, the signal conditioning box will be strapped to the subject's thigh and the tablet computer will be placed inside a backpack and carried by the individual (Figure 2.8b).

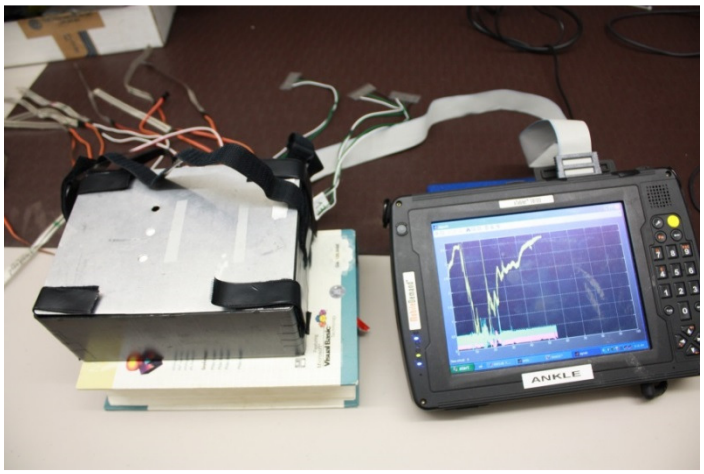

(a)

(b)

Figure 2.8. (a) Data acquisition unit – version 1; (b) An individual wearing the data acquisition unit during gait.

The second version which is named OUPAM (University of Oklahoma Prosthetic Activity Monitor, [23]) will be used for experimental studies in Chapter 3, Chapter 5, and Chapter 6. This unit includes a box containing the signal conditioning circuits and data acquisition boards and two tubes which house the cables for capturing the signals from the prosthetic socket on the amputated side and muscles on both sides of the subjects (Figure 2.9a). OUPAM is equipped with an Atmel® development board STK525 (with 8-bit micro-controller AT90USBxxxx) and an Atmel® extension board ATEVK525 with SD card slot for data acquisition [104]. OUPAM can acquire data at the rate of 1000Hz which is sufficient to capture all variations of the EMG signals in real time. Both customized signal conditioning circuits and Atmel® boards will be placed inside a box which is carried by the subjects during the gait (Figure 2.9b).

(a) (b)

Figure 2.9. (a) Data acquisition unit – OUPAM; (b) An individual wearing OUPAM during gait.

It is important to note that the developed gait acquisition systems allow the subjects to walk freely on various terrain during the study. Dependence on laboratory setup is

therefore eliminated and data is collected while the subject walks under normal conditions.

2.7.5 Data analysis

All data analysis and graphical illustrations will be performed in Matlab® environment with its toolboxes including DSP System Toolbox™, Statistic Toolbox™, and Neural Network Toolbox™. Customized Matlab scripts will be written for each experimental study.

The next four chapters will present the design and results of the experimental studies carried out in this dissertation. Each chapter is structured into the following parts: **Background** which identifies the need for each study and states the motivation; **Objectives and Hypothesis** of the study; **Methods** including information about subjects, protocol, and data analysis; **Results** of the study; **Discussion of the results**; and **Conclusions** drawn from the study.

Chapter 3: Asymmetry in Gait Parameters and Muscle Activities in People with Unilateral Below-knee Amputation

In the literature, there is little research into the gait performance of people with transtibial osteomyoplastic amputation. Therefore, the investigation of temporal-spatial gait parameters and muscle activities in individuals with TOA is addressed in this chapter. Twenty non-amputee, i.e., intact subjects and fifteen amputee subjects are recruited under an IRB protocol designed to study the effect of amputation on the gait and muscle activities of the individuals. Temporal gait parameters (stance time and gait cycle duration), and spatial gait parameters (step length and stride length) will be obtained from both subject groups during 2 minutes walking with self-selected speed on the level ground. Signals from the rectus femoris, a major quadriceps muscle, are captured from both limbs of individuals in each subject group. The data from each subject group will be examined for evidence of asymmetry in gait parameters and dissimilarities in muscle contractions.

3.1 Background

During the late stance phase (*Pre-swing*), active contraction of the healthy gastrocnemius muscle allows the ankle joint to generate more propulsion power than it stores during the early stance phase (*Loading Response*) of the gait. The ankle joint performs approximately 50% of the work required during locomotion while the hip and knee joints contribute the remainder [105]. While energy storage and return feet are designed to store energy during the loading phase and return it to the body during the *Pre-swing* phase of the gait, these designs are yet to match the performance of the biological ankle joint [92]. Such mismatch causes excessive strain on the residual joints

and muscles and is one of the causes of long-term deterioration in the health of the individual. Some of the effects of inadequate prostheses are discussed below.

Persons with below-knee amputation tend to have lower self-selected walking speed and asymmetric gait with shorter stance time and longer step length on the amputated side compared to the sound side [13, 14]. In [106] where all subjects wore PTB socket with solid ankle cushion heel feet, such asymmetry was attributed to the stiffness of the prosthesis ankle. The lack of trust on the prosthetic feet also forced the users to quickly transfer weight onto the sound limb during gait [13, 14]. Users also had shorter stance time on the affected limb to subconsciously protect the soft tissue at the bottom of the residual limb from damage. Although the asymmetry in temporal and spatial gait parameters might not necessarily be the best metrics for assessment of quality of gait or performance of prostheses [3], gait asymmetry is one of the indicators of long-term secondary complications such as mandatory osteoarthritis of the knee and/or hip joints of the intact limb [17].

The second consequence of the amputation is the excessive demands on the quadriceps muscles in the amputated limb during gait. In order to satisfy the dual requirements for gait stability and forward progression [107], the quadriceps muscles on the amputated side of unilateral below-knee amputees have been observed to be active for a longer duration at a higher amplitude compared to the same muscles on the intact side. The additional effort of the quadriceps muscles on the amputated side is supposed to compensate for the loss of plantarflexion of the ankle joint [15, 65, 66]. The stiffness of the prosthetic ankle joint corresponds to the amount of returned energy in the period before *Toe Off* and affects the activity of the quadriceps muscles on the amputated side

[108]. Such interaction results in almost 25% increase in energy cost during gait compared to people without below-knee amputation [16].

The temporal-spatial gait parameters and the contraction of a major quadriceps muscle, rectus femoris (RF), during the gait of individuals with unilateral TOA are investigated in this chapter. It is known through gait analysis that the contraction profile of the rectus femoris muscle is related to the movements of the joints/limbs during gait [25, 28]. First, the muscle is active before and during the early stance phase (*Loading Response*) to absorb the shock of *Heel Strike* and remains active until early *Mid-stance* for controlling the extension of the knee. Then during late stance phase (*Pre-swing*), this muscle is active again to restrain excessive passive knee flexion. Finally, it contracts during *Initial Swing* to assist hip flexion and to lift the foot for limb advancement [25]. Therefore in the subsequent section, activities of the rectus femoris muscle at specific sub-windows that covering these gait durations will be extracted for study.

It is noted that experimental study in this chapter is designed so that the subjects can select their preferred walking speeds and are not limited by any specific types of prosthetic feet. Therefore, consideration of different prosthetic components on gait parameters and muscle contractions are out of the scope of this chapter. To the best of our knowledge, this is the first comprehensive study of the gait parameters and muscle activities in amputees with unilateral TOA.

3.2 Objectives and hypotheses

The overall goal of this study is to investigate temporal-spatial gait parameters and activities of the rectus femoris muscle in persons with unilateral below-knee amputation

in order to examine the effect of below-knee amputation. The specific objectives and hypotheses of this investigation are as follows.

Objective O3A: Study the temporal-spatial gait parameters and gait asymmetry in individuals with unilateral TOA during walking on level ground with self-selected speed. ***Hypothesis H3a*** states that there will be significant differences between the gait parameters measured from the amputated side and intact side of the subjects. Hypothesis H3a will be verified by comparing the stance time, gait cycle duration, step length and stride length between the amputated leg and the intact leg. Support of hypothesis H3a will indicate gait asymmetry.

Objective O3B: Study the activities of the rectus femoris muscles in subjects with unilateral TOA during walking on level ground. In order to achieve this objective, ***Hypothesis H3b*** states that the activation levels of the rectus femoris muscle on the amputated side will be significant higher compared to the intact side. EMG data from rectus femoris muscles on amputated side and intact side during specific durations of the gait cycle will be compared to see whether H3b is supported.

3.3 Methods

3.3.1 Subjects

Fifteen subjects with unilateral below-knee amputation participated in this study. They were otherwise healthy and capable of walking for long duration without dependence on any walking assistive devices except their own prostheses. The subjects wore their own prosthetic socket and foot during this study. Twenty subjects without amputation (control subjects) also participated as references. All participants gave formal consent to participate in this study. Information about the subject is shown in Table 3.1.

Table 3.1. Subject information

	Control subjects	Subjects with amputation
Number of subject	20	15
Age (year)	30.2±10.1	39.8±11.1
Weight (kg)	84.2±16.2	95.7±17.1
Height (m)	1.79±0.09	1.81±0.07
Walking speed (m/s)	1.28±0.12	1.27±0.13
Amputation side	NA	8 Left 7 Right

3.3.2 Protocol

The following protocol was approved by the Institutional Review Board at the University of Oklahoma Health Sciences Center for protection of human subjects.

Gait: During the study, each subject performed a two-minute walking on level ground with self-selected walking speed.

Measurements: Temporal gait parameters (stance time and gait cycle duration) and spatial gait parameters (step length and stride length) were obtained from the Minisun™ Intelligent Device for Energy Expenditure and Activity (IDEEA®, Section 2.7.3) [82] which was worn by each subject during the gait. Signals from rectus femoris muscle from both sides (amputated side and intact side of subjects with amputation, and left and right in control subjects) were capture by two pairs of disposable EMG electrodes (Ag/AgCl electrodes, square shape, sensing area of 1.44 cm^2). Placement of the EMG electrodes followed the procedure described in Section 2.7.3. EMG signals were captured by the portable gait monitoring device OUPAM (Section 2.7.4) and stored to a SD card. The EMG signals were sampled at the rate of 1000 samples per second.

3.3.3 Data analysis

Preprocessing: Temporal and spatial gait parameters were obtained from an analysis software provided by IDEEA®. EMG signals from rectus femoris muscles were

preprocessed by a linear envelope (full-wave rectifier + low pass filter with a cut-off frequency of 8Hz) following by a symmetry moving window averager of 150ms (±75ms). For each muscle of each subject, multiple curves which corresponded to multiple gait cycles were obtained. Magnitudes of signals from each muscle were normalized by the peak value of the same muscle during the gait while the durations of the signals were also normalized by the gait cycle duration. The normalized curves then had the range [0, 1] and constituted [0-100%] of the gait cycle. The average contraction profile for each muscle of each subject was obtained by superimposing and averaging multiple curves captured during the two-minute walking.

Calculation: From the average curve of each muscle of each subject, the following sub-windows which corresponded to specified durations of the gait cycle were considered.

Sub-window 1: from *Heel Strike* (HS) to 15% of the gait cycle (GC) after *Heel Strike* ([HS] → [HS + 15%GC]), which covered the duration of *Loading Response*.

Sub-window 2: from 15% of the gait cycle prior to *Toe Off* (TO) to *Toe Off* ([TO-15%GC] → [TO]), which covered the duration of *Pre-swing*.

Sub-window 3: from *Toe Off* to 15% of the gait cycle after *Toe Off* ([TO] → [TO+15%GC]), which covered the duration of *Initial Swing*.

These sub-windows were selected in order to cover the specific durations in which the rectus femoris was active as analyzed in Section 3.1. Root Mean Square (RMS) values were then calculated from each sub-window to represent the activation level of the muscle in the interested durations of the gait. Figure 3.1 shows the selection of sub-windows from a typical rectus femoris activation profile during a complete gait cycle.

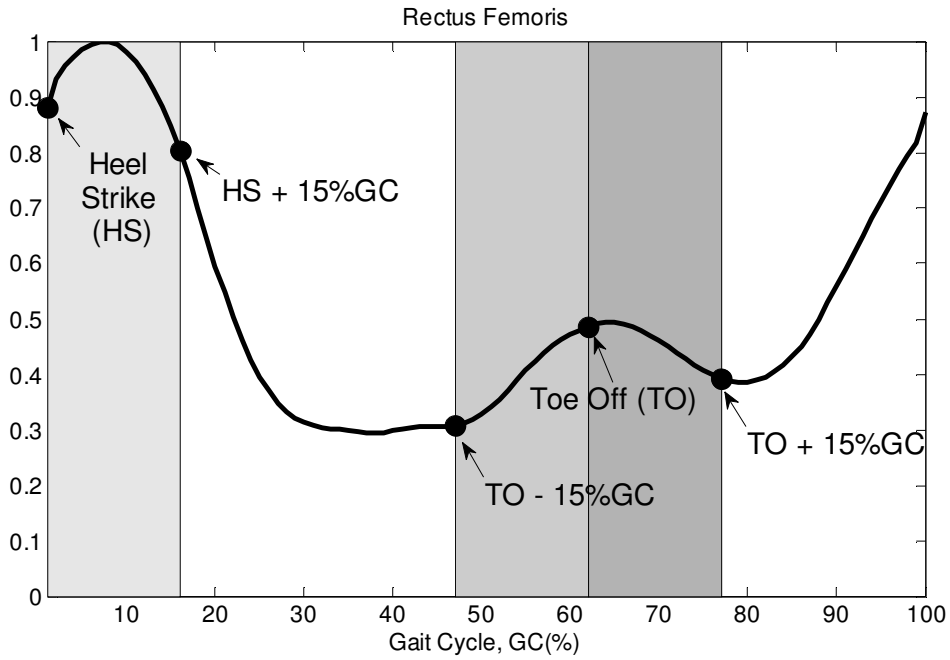

Figure 3.1. Sub-windows from a typical contraction profile of the rectus femoris.

Statistical analysis:

For evaluation of the hypothesis H3a for the gait parameters, stance time, gait cycle duration, step length, and stride length from the amputated side and intact side were compared by statistical t-tests (paired, alpha = 0.05).

It was hypothesized in the experiment (H3b) that during the level ground walking with self-selected speed, the contraction levels of the rectus femoris muscle on the amputated are higher than the rectus femoris muscle on the intact side as a strategy to compensate for the lack of ankle movement. Such compensation and resulting imbalance in muscle activity are not expected in the control subjects. In order to compare between rectus femoris muscle activities from two sides of each subject group, paired t-tests (significant level alpha = 0.05) were carried out to compare between RMS values calculated from the corresponding sub-windows. For individuals with amputation, RMS

values from each sub-window of the RF muscle on the amputated side were compared to the RMS values from the same sub-window of the RF muscle on the intact side. Similarly, RMS values from each sub-window of the RF on the left side of the control subjects were compared to the RMS values obtained from the same sub-window of the RF muscle on the right side.

3.4 Results

Temporal-spatial gait parameters: All the subjects were able to finish the experiment while maintaining their preferred walking speed without any difficulty. Individuals with below-knee amputation walked slightly slower than the non-amputee groups as seen in the Table 3.1 (1.27±0.13m/s compared to 1.28±0.12m/s). No significant difference was found in any of the considered gait parameters between the amputated side and intact side (hypothesis H3a was rejected).

Stance time on the amputated side of the individuals with amputation was not significant shorter compared to the sound side. In this group, the temporal parameters between two sides were less symmetric compared to the group of control subjects. Differences between temporal parameters from two sides were higher in the subjects with amputation (Table 3.3) compared to the other (Table 3.2).

Table 3.2. Gait parameters from control subjects.

	Left side	Right side	Difference
Stance time (s)	0.698±0.046	0.696±0.048	0.007±0.007
Gait duration (s)	1.118±0.067	1.118±0.066	0.001±0.003
Step length (m)	0.644±0.060	0.674±0.078	0.039±0.032
Stride length (m)	1.305±0.134	1.316±0.132	0.016±0.013

In subjects with amputation, step length on the amputated side seemed to be longer than the intact side while difference in the stride length between two sides was minor.

Table 3.3. Gait parameters from subjects with amputation.

	Amputated side	Intact side	Difference
Stance time (s)	0.783±0.107	0.781±0.119	0.075±0.042
Gait duration (s)	1.177±0.123	1.190±0.118	0.026±0.039
Step length (m)	0.755±0.226	0.659±0.154	0.251±0.153
Stride length (m)	1.445±0.325	1.376±0.255	0.139±0.209

Electromyography: Figure 3.2 shows the activation profile of the rectus femoris muscles from left and right side of the control subjects (top plots) as well as from the amputated side and intact side of persons with amputation (bottom plots). Standard deviations at each data point of the normalized curve are presented by the shaded area around the mean curve.

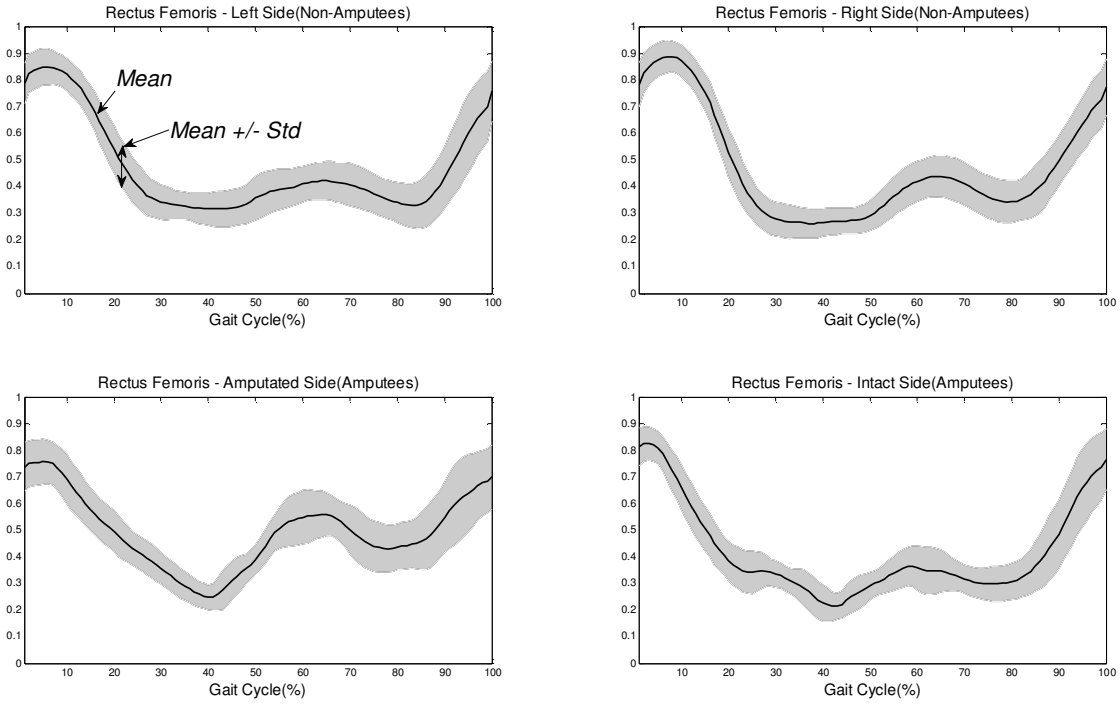

Figure 3.2. Rectus femoris muscle contraction from two subject groups.

Root Mean Square values calculated from the selected sub-windows and the corresponding statistical test results are shown for both groups in Table 3.4 and Table 3.5. At all of the selected sub-windows, the left and right rectus femoris of the control subjects contracted at the similar levels. In amputees, during the first sub-window ([HS] → [HS + 15%GC]) which covered the duration of *Loading Response*, rectus femoris on the amputated side and intact side contracted similarly. However, amputated side rectus femoris contracted significantly stronger than the intact side RF during the second sub-window ([TO – 15%GC] → [TO], p-value = 0.011) and the third sub-window ([TO] → [TO + 15%GC], p-value = 0.028)

Table 3.4. Root mean square values from sub-windows of rectus femoris muscles of the control subjects

Sub-window	Left side	Right side
[HS] → [HS + 15%GC]	0.82±0.132	0.85±0.087
[TO-15%GC] → [TO]	0.39±0.234	0.38±0.217
[TO] → [TO + 15%GC]	0.40±0.220	0.40±0.213

Table 3.5. Root mean square values from sub-windows of rectus femoris muscles of subjects with amputation

Sub-window	Amputated side	Intact side
[HS] → [HS + 15%GC]	0.72±0.202	0.73±0.210
[TO-15%GC] → [TO]	0.53±0.273	0.32±0.203
[TO] → [TO + 15%GC]	0.50±0.276	0.32±0.223

The shaded boxes indicate the support of H3b

3.5 Discussion of the results

3.5.1 Temporal-spatial gait parameters

First, individuals with unilateral below-knee amputation in this study seemed to have a lower self-selected walking speed compared to the control subjects, which was in

agreement with other studies [13, 14]. However, the difference between two groups was not significant. The difference between stance duration on intact and amputated side was larger than the difference between two sides of non-amputees. For the amputee subjects, the stance durations between two sides were different, but not significant. These results differentiated from studies in which subjects had undergone traditional transtibial amputation [13]. In those studies, the decreased time spent on the amputated leg was the result of an effort to protect the soft issue of the residual limb. In conventional amputation, such area was not suitable for weight-bearing because of the pain, discomfort, and instability inside the socket [109]. The significant difference was reported in a group of persons who wore SACH foot and patellar tendon bearing socket with which very little weight-bearing was distributed to the distal end of the residual limb [110]. In this study, all subjects had transtibial osteomyoplastic amputation (Section 2.2) and wore total surface bearing socket which allowed significant amount of weight-bearing at the residuum end. With that additional body support and the flexibility in selecting preferred walking speed, the subjects might have gained the trust on their prostheses and developed a more balance weight transfer between two legs during the gait.

Observations on the spatial gait parameters from subjects with amputation in this study agreed with the review in [3]. While the stride lengths were similar between two sides, the step length on the amputated side was slightly longer than the intact side. These outcomes are in agreement with other works in the literature and might relate to the stability of the prosthesis or function of the prosthetic ankle/foot system [3, 14].

3.5.2 Muscles activities

No significant difference was observed between the left and right rectus femoris muscles in the control group in all of the considered sub-windows. This result was expected since the control subjects in this study were healthy and free of any muscular problems.

In [15], the author reported the increased activities of the rectus femoris muscle on the amputated side compared to the intact side during the braking phase (0 – 50% of stance phase) of level ground walking with speeds of 0.9 m/s, 1.2 m/s, and 1.5 m/s. It was explained that the individuals tented to contract their amputated side quadriceps muscles more in order to provide additional body support and absorb the ground reaction force. Such observations were not seen in our data. Indeed, during the first sub-window which covered the *Loading Response* phase as well as first 50% of the stance phase, there was no significant difference between the rectus femoris activities on the two sides. It is important to note that different from the protocol used in [15], participants with amputation in this study wore total surface bearing sockets after undergoing the TOA procedure and they also had flexibility in choosing their preferred walking speeds. The TOA and TSB were expected to provide additional body support by allowing users to put more weight on the distal end of the residual limb. In addition, the co-contraction of the residual muscles below the knee [111] might have helped in stiffening the limb inside the socket to reduce the impact due to ground reaction and stabilize the gait.

During the second sub-window which covered the *Pre-swing* phase, significant higher activities were observed from the rectus femoris on the amputated side compared to the

intact side. Besides playing its natural role in restrain excessive passive knee flexion [25, 72], the increased activities on the residual leg rectus femoris muscles indicate the individuals' attempt to compensate for the lack of active ankle joint movements which are needed for the advancement of the residual limb.

Finally, during the *Initial Swing* which was covered by the third sub-window, rectus femoris on the amputated side contracted significantly higher than the intact side. In the individual without amputation of the lower limb, lifting the foot and ankle and providing swing clearance are the responsibilities of the pretibial muscles and long toe extensors [72]. Since the biological ankle and foot were missing in individuals with below-knee amputation, the rectus femoris would contract stronger to lift and create clearance for swinging of the residual limb.

3.6 Conclusions

In this chapter, temporal-spatial gait parameters and muscle activities of individuals who had undergone the transtibial osteomyoplastic amputation procedure and wore the total surface bearing socket during level ground walking with self-selected speed were investigated. There were evidences of gait asymmetry in the subjects with amputation. However, such asymmetry was not statistically significant in comparison to results in literature where subjects had undergone traditional amputation and wore patellar tendon bearing sockets and classical solid ankle-based prosthetic feet. The lack of proper plantarflexion of the prostheses used also linked to higher contraction levels of the rectus femoris on the amputated side compared to the intact side. Such additional contraction could be a result of the effort needed to advance the movement and provide swing clearance for the residual limb. Results of this chapter motivates the development

of highly functional prosthetic feet that can replicate the human ankle joint to possibly improve the gait symmetry and preserve energy expenditure during gait of users with unilateral below-knee amputation

Chapter 4: Effect of Prosthetic Foot on Residuum Socket Interface Force and Gait Characteristics

The dependence of the residuum socket interface force and gait parameters of individuals with TOA procedure on the type of prosthetic feet has not been studied in the literature. Among the prosthetic feet that are fitted for individuals with below-knee amputation, Renegade Foot® (Freedom Innovations©), Venture Foot™ (College Park©), and Proprio Foot® (Össur®) are 3 of the most common prostheses. Therefore, the effect of these feet on the RSI force of an individual with unilateral TOA will be elucidated in this chapter. Gait activities include level ground walking with normal and fast speed, walking up and down a staircase, and walking up and down a ramp. Contact forces will be measured from six locations inside the socket including the distal (end-bearing) anterior, middle posterior, and four proximal locations. Gait parameters will be extracted from the load distribution. Statistical analysis will be carried out to examine the dependence of the RSI forces and gait parameters on the changes in gait and prosthetic foot.

It is anticipated that during gait activities, significant force will be observed at distal area (end-bearing) of the residual limb (under the bony bridge which stabilized the residual limb anatomy) as well as middle posterior point (where the length-tension relationship of the residual gastrocnemius muscle was retrieved). Moreover, such TOA procedure allows the persons with below-knee amputation to wear a TSB socket which

will lead to uniform force distributions at four proximal locations (anterior, posterior, lateral, and medial)[1].

4.1 Background

Unlike traditional transtibial amputation techniques, proponents of the transtibial osteomyoplastic amputation procedure (as described in Section 2.2) contend that the TOA allows the functional restoration of the residual limb extremity by providing weight bearing capability at the distal area of the residuum and restoring the length-tension relationship of the residual muscles [38, 40]. Such an end-bearing limb can theoretically stimulate the skin and deep tissue and minimize atrophy of the residuum due to disuse. End-bearing is also expected to reduce pain, improve sensation and blood flow, and improve walking ability and prosthetic wear. Although several studies have examined force distribution inside the TTA prosthetic socket with a wide variety of prosthetic alignment [54, 112], socket material [113], type of socket [45, 46, 114, 115], or type of gait activity [56, 62], there was little reported research on the effect of different prosthetic feet on force distribution inside the socket of amputees with TOA. In this chapter, distribution of the RSI force inside the prosthetic socket of an otherwise healthy individual with TOA and its relationship to the type of prosthetic foot will be investigated.

[1] This chapter is adapted from [A. Mai, S. Commuri, C. P. Dionne, J. Day, W. J. J. Ertl, and J. L. Regens, "Effect of prosthetic foot on residuum-socket interface pressure and gait characteristics in an otherwise healthy man with transtibial osteomyoplastic amputation," *Journal of Prosthetics and Orthotics*, vol. 24, pp. 211-220, 2012].

4.2 Objectives and hypotheses

The primary purpose of this experimental study is to investigate the effect of different prosthetic feet on RSI force and temporal gait parameters of a healthy man with unilateral TOA. The specific objectives and hypotheses are as follows.

Objective O4A: As the TOA procedure allows loading at the distal residuum, this study aims to quantify and compare the forces at the distal location to forces at other locations inside the socket during different gait activities. ***Hypothesis H4a*** states that during the same gait activity with the same prosthetic foot, there will be significant amount of forces detected at the distal area of the residuum. Hypothesis H4a will be examined by comparing the mean forces measured at the distal locations to the maximal mean forces at other locations during each gait activity.

Objective O4B: Examine the effect of different prosthetic feet on RSI force distributions and temporal gait parameters. In order to achieve this objective, ***Hypothesis H4b*** states that between any two prosthetic feet, the peak (mean) forces observed at the same socket location during the same gait activity will be different. Support of the hypothesis H4b will suggest the effects of prosthetic feet on the RSI force distribution and their contributions in achieving desired socket loading profiles.

4.3 Methods

4.3.1 Subject

The subject was a 43 year-old man (height – 1.91m, weight – 109.1 kg) with left TOA due to a traumatic event. He was otherwise healthy without comorbidity and gave informed consent to be a participant in this study. Following amputation and provision

of a prosthesis system, the subject returned to walking on various terrains without an assistive device.

4.3.2 Protocol

Gait: In this study, the subject performed the following six gait activities: walking forward on level ground with self-selected pace (FOR – *Forward*), walking on level ground with fast pace (FOB – *Forward brisk*), ascending and descending a staircase (UPS – *Stair-up* and DOS – *Stair-down*, 53^{o} – 24 steps), and ascending and descending a ramp (UPR – *Ramp-up* and DOR – *Ramp-down*) designed for wheel chair access (8^{o} inclination).

Prosthesis: The subject's prosthesis had an end-bearing, modified total surface bearing socket with 6mm Alpha™ Locking liner and Bulldog™ Lock. The feet studied were the Renegade Foot® (Freedom Innovations© [116]), Venture Foot™ (College Park© [117]), and Proprio Foot® (Össur [18]), all of the size 27cm. The Renegade Foot had a deformable carbon fiber spring-type keel to absorb shock and provide dynamic response. The Venture Foot provided significant energy return and had a multi-axial configuration that allowed maximal terrain compliance. Finally, the Proprio Foot was an advanced design with the ability to detect the walking terrain and automatically adjust the ankle angular position. During the study, the subject wore his own prosthetic socket for consistent RSI fit. All prosthetic feet were aligned by a certified prosthetist for consistency in fit and function. There were 3 trials in the study. In each trial, the subject wore one of three prosthetic feet and performed all gait activities.

Measurement: Ultra-thin force resistive sensors (FlexiForce® A201, Section 2.7.3) were placed inside the socket to measure RSI force at the distal anterior (DA) point

under the residuum, middle posterior (MP) point at the middle level, and four points at the proximal level including proximal anterior (PA), proximal posterior (PP), proximal lateral (PL), and proximal medial (PM) of the residual limb (Figure 4.1). During each trial, voltage signals that represented the applied force values were captured by a data acquisition unit described in Section 2.7.4 (Figure 2.8).

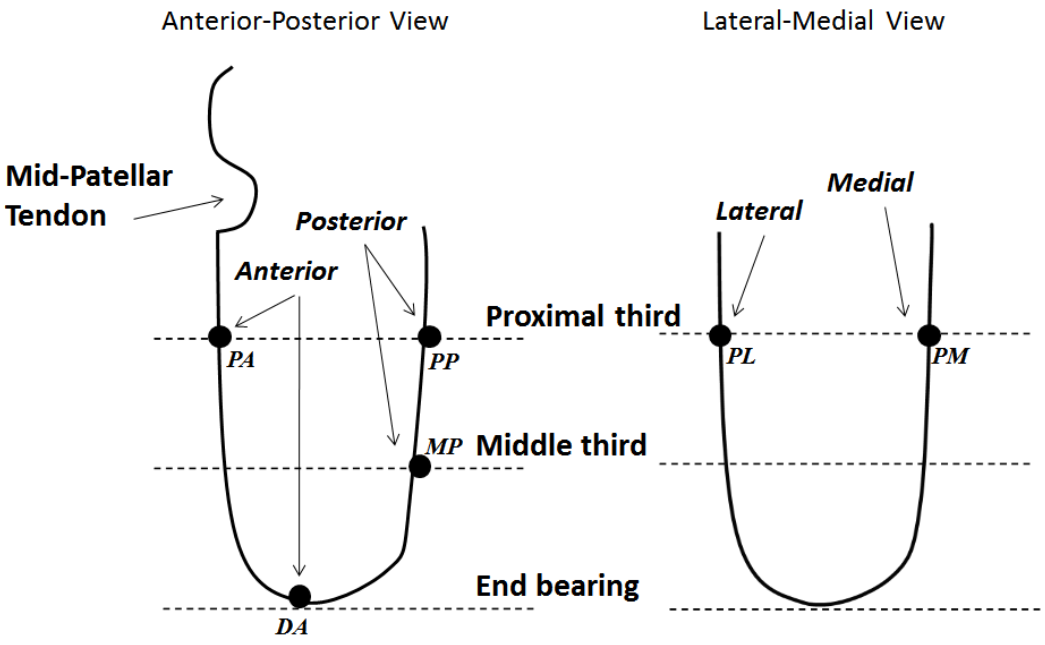

Figure 4.1. Placement of force sensors inside the prosthetic socket.

4.3.3 Data analysis

Preprocessing: Signals representing the applied forces were converted into force values, filtered by a low pass filter with the cut-off frequency of 3Hz, and normalized to 100% of the gait cycle. For each activity, the gait cycle was divided into stance phase when there was loading on the residual limb, and swing phase when the amount of loading was negligible.

Calculation: The peak force, mean force, and mean sustained force MF_{80+} (i.e., average of all force values above 80% of the peak force) at each measured location over the stance phase were calculated. The mean sustained force MF_{80+} represented the sub-maximal tissue loadings [54, 56]. For each measured location, the coefficient of variations of MF_{80+} was calculated from the MF_{80+} values of all six gait activities to quantify the variations of the sustained sub-maximal loading.

Statistical analysis: Testing of hypotheses H4a and H4b was performed as follows.

Hypothesis H4a was tested for 18 cases (6 gaits × 3 prosthetic feet) by two-sample, both tailed t-tests (alpha = 0.05). Results of these statistical tests would help evaluate the significance of the end-bearing capability at the distal residuum.

Similarly, there were totally 216 cases (6 gaits × 2 parameters × 3 prosthetic feet = 36 cases at each of 6 locations) two-sample, two-tailed t-tests (alpha = 0.05) for the hypothesis H4b. Hypothesis H4b was performed between peak (mean) force calculated from any two prosthetic feet at the same location during the same gait activity.

4.4 Results

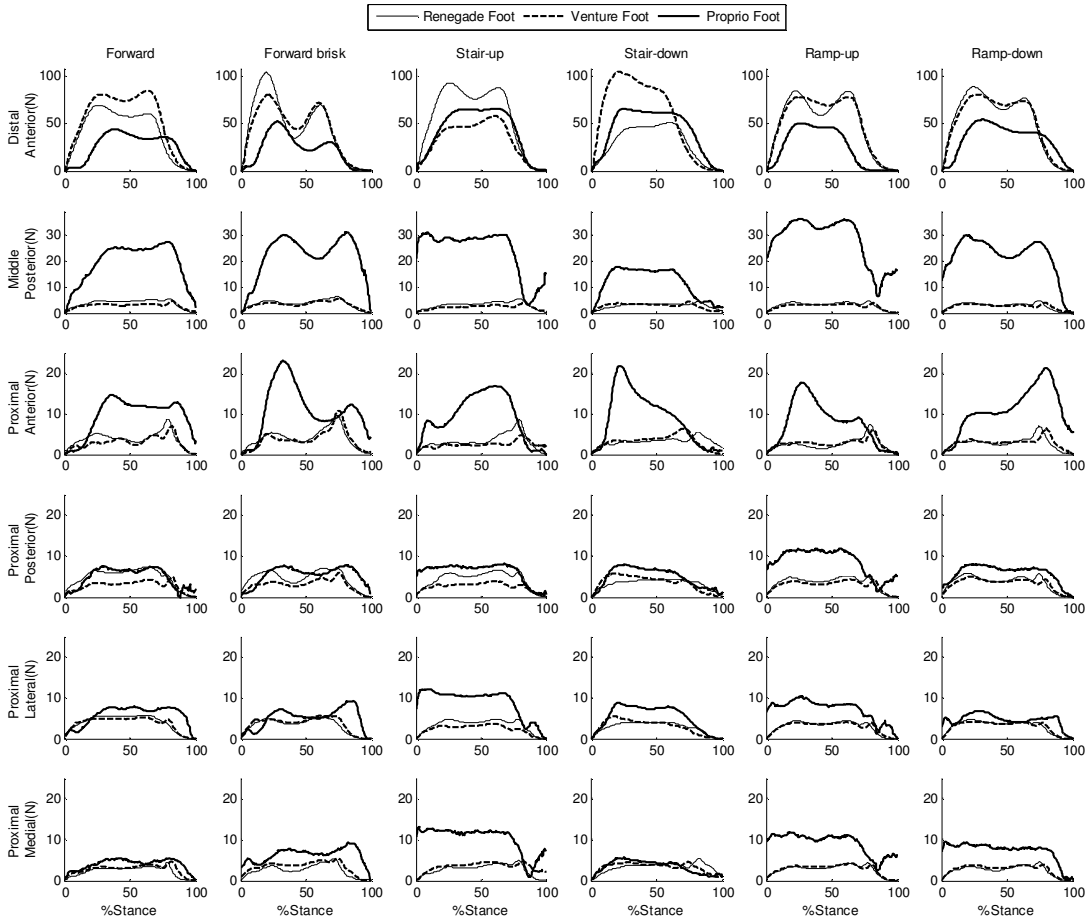

Figure 4.2. Residuum socket interface forces.

Figure 4.2 shows average forces recorded at each of the sensor locations during the gait activities. The duration of each force curve was normalized to represent the corresponding stance phase. Swing phases are not shown since there was no contact during that duration.

The mean sustained forces MF_{80+} at distal anterior and middle posterior locations during six gait activities are shown in Figure 4.3. In each column, the MF_{80+} at the distal anterior end-bearing location is represented by the light vertical bar while the dark vertical bar represents the MF_{80+} at the middle posterior. Across different gait activities,

MF_{80+} at the distal sensor averaged at 74.8±17.2, 74.4±13.8, and 51.6±9.1 for Renegade, Venture, and Proprio foot, respectively. These measures at the middle posterior were 4.9±0.6, 4.1±0.7, and 27.4±5.6 for the three feet.

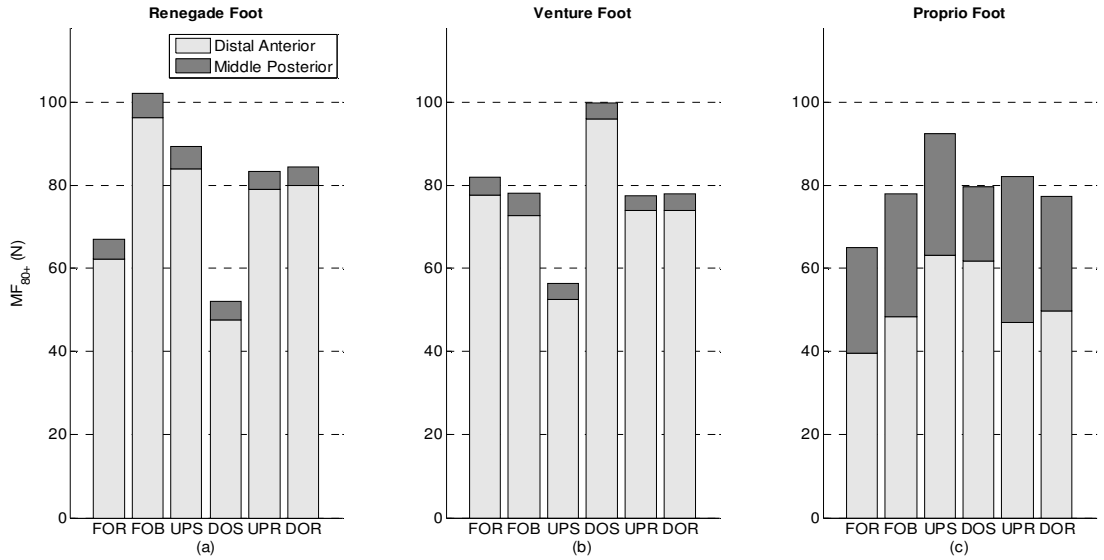

Figure 4.3. Mean sustained force MF_{80+} observed at distal anterior and middle posterior locations.

Figure 4.4 shows the mean sustained force MF_{80+} at four proximal sensor locations. At the proximal anterior location, the mean sustained force MF_{80+} across all gait activities were 7.7±1.2, 6.9±2, 18.1±3.1 for Renegade, Venture, and Proprio foot, respectively. Similarly, the average MF_{80+} of other three proximal sensors (proximal posterior, proximal lateral, and proximal medial) were 5±0.9 (Renegade), 4.5±0.7 (Venture), and 8.7±2.1 (Proprio).

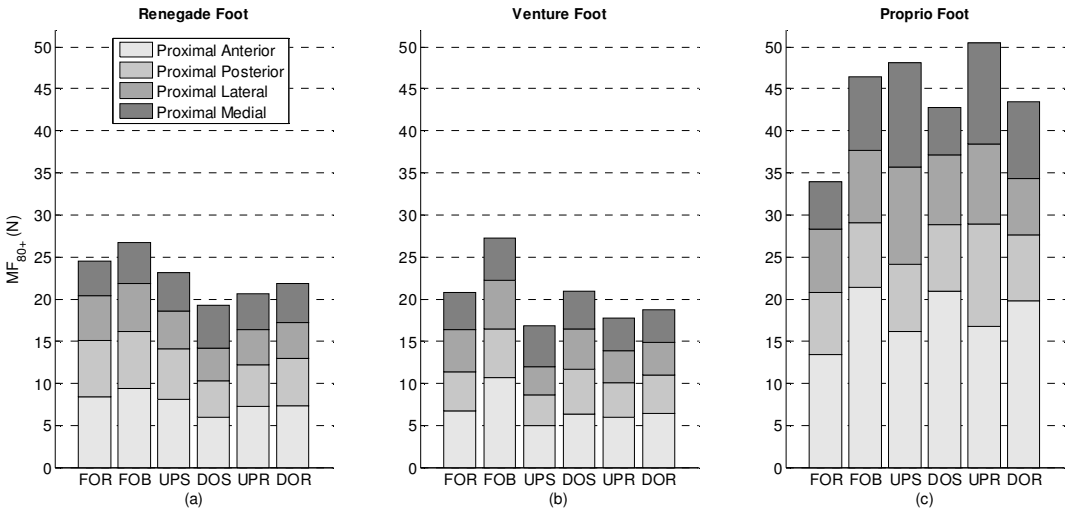

Figure 4.4. Mean sustained force MF_{80+} observed at four proximal locations.

The mean forces at the distal anterior location were significantly higher than the maximum of mean forces at other locations (in 17 out of 18 cases, except with Proprio Foot during walking up a ramp, Table 4.1).

Table 4.1. Mean forces (N) at distal anterior location and maximum of mean forces at other locations

Gait activity	Renegade Foot	Venture Foot	Proprio Foot
Forward	42.4±1.1 (4.9±0.1)	53.9±1.1 (4±0.2)	26.7±0.9 (19.9±1.2)
Forward brisk	46.8±2.6 (4.7±0.1)	44.4±0.9 (4.1±0.2)	25.4±1.4 (22.2±1.2)
Stair-up	57.9±1.3 (4.5±0.2)	34.1±1.7 (3.5±0.2)	44.2±1.3 (24.8±3)
Stair-down	31.2±1.6 (3.8±0.3)	60.7±2.3 (3.9±0.2)	45±1.7 (12.6±2.1)
Ramp-up	51.7±2.9 (3.7±0.2)	52±1.1 (3.2±0.1)	30.3±3 (29.3±1.3)
Ramp-down	54.1±1.9 (3.9±0.2)	52.3±1.5 (3.5±0.1)	34.8±1.5 (22.7±6.6)

Maximum of mean forces at other locations are inside the parentheses

At the distal anterior location, the peak forces were significantly different between any two feet in each gait activity (Hypothesis H4b was supported in all 18 cases). The mean forces were also significantly different in 15 out of 18 cases when the subject wore different feet (except between Renegade Foot and Venture Foot during forward brisk, walking up and down a ramp, Table 4.2).

Table 4.2. Peak and mean forces (N) at distal anterior location

Gait activity	Peak force			Mean force		
	Renegade Foot	Venture Foot	Proprio Foot	Renegade Foot	Venture Foot	Proprio Foot
Forward	69.5±1.9	84.4±1.1	44±1.4	42.4±1.1	53.9±1.1	26.7±0.9
Forward brisk	104±6.2	80.6±2.8	52.2±3.1	46.8±2.6	44.4±0.9	25.4±1.4
Stair-up	92.6±2.8	58±3.1	66±1.9	57.9±1.3	34.1±1.7	44.2±1.3
Stair-down	52.5±3.3	104.3±6.1	66.1±3.6	31.2±1.6	60.7±2.3	45±1.7
Ramp-up	86.4±5.1	79.5±2.4	50.9±3.2	51.7±2.9	52±1.1	30.7±3.2
Ramp-down	88.7±4	80.8±2.5	54.3±2.5	54.1±1.9	52.3±1.5	34.8±1.5

The shaded boxes indicate the rejection of H4b.

At the middle posterior location (Table 4.3), both peak and mean forces were significantly changed when the subject changed his feet (except between Renegade and Venture Foot during walking down a staircase).

Table 4.3. Peak and mean forces (N) at middle posterior location

Gait activity	Peak force			Mean force		
	Renegade Foot	Venture Foot	Proprio Foot	Renegade Foot	Venture Foot	Proprio Foot
Forward	5.8±0.2	4.7±0.2	28.3±1.5	3.7±0.1	2.8±0.3	19.9±1.2
Forward brisk	6.6±0.2	6.1±0.2	32.8±4.6	3.7±0.2	3.3±0.1	22.2±1.2
Stair-up	5.9±0.2	4.2±0.5	32.8±3.8	3.1±0.2	2.2±0.3	24.8±3
Stair-down	5±0.5	4.5±0.2	20±3.1	2.9±0.2	2.7±0.2	12.6±2.1
Ramp-up	5±0.2	4.1±0.2	38.9±3	3.1±0.2	2.6±0.1	29±1.6
Ramp-down	5.1±0.2	4.4±0.1	30.7±7.4	2.8±0.1	2.6±0.1	22.7±6.6

The shaded boxes indicate the rejection of H4b.

Similarly, Table 4.4 – Table 4.7 show the peak and mean forces at four proximal locations. At this level, different feet led to significant difference in peak forces (61 out of 72 cases) and mean forces (54 out of 72 cases).

Table 4.4. Peak and mean forces (N) at proximal anterior location

	Peak force			Mean force		
Gait activity	Renegade Foot	Venture Foot	Proprio Foot	Renegade Foot	Venture Foot	Proprio Foot
Forward	9.2±0.3	7.3±0.2	15.1±0.8	3.9±0.3	3±0.1	9.6±0.4
Forward brisk	10.2±0.3	11.7±0.3	23±1.7	4.1±0.3	3.9±0.3	11±0.6
Stair-up	8.9±0.7	5.4±0.8	17.6±2	3.4±0.4	2.5±0.6	9.9±1.2
Stair-down	6.5±1.3	6.9±0.2	22.8±2.3	3.3±0.6	3.4±0.3	9.8±1
Ramp-up	7.8±0.4	6.5±0.2	18.2±2	2.6±0.4	2.7±0.2	8.4±1.4
Ramp-down	7.9±0.3	7±0.4	21.8±4.9	3±0.2	3±0.3	11.1±1

The shaded boxes indicate the rejection of H4b.

Table 4.5. Peak and mean forces (N) at proximal posterior location

	Peak force			Mean force		
Gait activity	Renegade Foot	Venture Foot	Proprio Foot	Renegade Foot	Venture Foot	Proprio Foot
Forward	7.4±0.3	5.2±0.1	8.5±0.7	4.9±0.1	2.9±0.2	5.3±0.6
Forward brisk	7.8±0.3	6.4±0.3	9±0.8	4.7±0.1	3.2±0.1	5.6±0.6
Stair-up	6.8±0.3	4.1±0.5	9.1±1.2	4.5±0.2	2.8±0.4	6.5±0.9
Stair-down	4.7±0.6	5.8±0.3	8.8±0.8	3.4±0.5	3.8±0.2	5.3±0.6
Ramp-up	5.6±0.3	4.6±0.1	13.7±1.1	3.7±0.2	3.1±0.1	9.2±0.7
Ramp-down	6.4±0.3	5±0.2	8.9±2.1	3.9±0.2	3.4±0.2	6.2±1.9

The shaded boxes indicate the rejection of H4b.

Table 4.6. Peak and mean forces (N) at proximal lateral location

	Peak force			Mean force		
Gait activity	Renegade Foot	Venture Foot	Proprio Foot	Renegade Foot	Venture Foot	Proprio Foot
Forward	5.8±0.2	5.4±0.2	8.6±0.7	4±0.2	4±0.2	5.7±0.5
Forward brisk	6.4±0.4	6.6±0.4	9.4±1	3.7±0.1	3.9±0.3	5.2±0.4
Stair-up	5.1±0.3	3.6±0.3	13.2±1	3.4±0.2	2.5±0.1	9.9±0.9
Stair-down	4.3±0.3	5.3±0.4	9.5±0.8	3±0.2	3.2±0.2	6.2±0.8
Ramp-up	4.7±0.3	4.4±0.3	10.7±1.9	3.2±0.2	3±0.2	7.8±1.4
Ramp-down	4.9±0.5	4.5±0.3	7.5±2.7	3.3±0.3	3.2±0.3	4.9±2.4

The shaded boxes indicate the rejection of H4b.

Table 4.7. Peak and mean forces (N) at proximal medial location

	Peak force			Mean force		
Gait activity	Renegade Foot	Venture Foot	Proprio Foot	Renegade Foot	Venture Foot	Proprio Foot
Forward	4.6±0.3	5±0.2	6.4±0.5	2.4±0.2	2.8±0.2	4.1±0.5
Forward brisk	5.6±0.4	5.6±0.2	9.9±0.8	2.7±0.2	3.5±0.2	6.4±0.9
Stair-up	5.1±0.1	5.5±0.4	14.1±1.3	2.9±0.2	3.5±0.2	10.5±0.9
Stair-down	5.6±0.3	5.2±0.4	6.3±0.8	3.4±0.4	3.5±0.2	3.6±0.4
Ramp-up	4.9±0.3	4.3±0.3	13.7±1.9	2.8±0.3	3±0.3	9.5±0.7
Ramp-down	5.1±0.2	4.3±0.3	10.5±2.9	2.7±0.2	2.9±0.2	7.6±2.5

The shaded boxes indicate the rejection of H4b.

Finally, Table 4.8 shows the stance and gait cycle durations during the gait activities. For each gait activity, the coefficient of variations of the stance duration was calculated as the ratio of the standard deviation of stance durations from three feet to their mean values. Similar calculation was used for the variations of the gait cycle durations.

Table 4.8. Temporal gait parameters of each gait activity and each prosthetic foot

Gait activity	Stance duration (s)			Stance time CV (%)	Gait cycle duration (s)			Gait cycle CV (%)
	Renegade Foot	Venture Foot	Proprio Foot		Renegade Foot	Venture Foot	Proprio Foot	
Forward	0.84	0.86	0.71	10.1%	1.20	1.21	1.13	3.7%
Forward brisk	0.70	0.72	0.62	7.8%	0.96	1.00	0.99	2.1%
Stair-up	0.81	0.75	0.76	4.2%	1.14	1.13	1.12	0.9%
Stair-down	0.72	0.65	0.64	6.5%	1.07	1.01	1.04	2.9%
Ramp-up	0.78	0.77	0.78	0.7%	1.11	1.14	1.08	2.7%
Ramp-down	0.78	0.78	0.68	7.7%	1.08	1.11	1.10	1.4%
Average				6.2%				2.3%

4.5 Discussion of the results

4.5.1 Effect of prosthetic feet on distal anterior force

First of all, significant forces which were recorded at the distal anterior location during all gait activities verified that end-bearing occurred with the TOA procedure. This result emphasized the outcome of the TOA procedure in allowing persons with below-knee

amputation to wear total surface bearing socket and bear significant amount of the body weight at the distal end of the residual limb. Such phenomena was not observed in persons with traditional transtibial amputation and patellar tendon bearing socket in which the body weight was mainly distributed around the knee joint [2, 113]. As seen in Figure 4.2, the RSI forces at the distal anterior sensor measured were greater compared to other locations. This was seen with all prosthetic feet during all gait activities. Figure 4.3 and Figure 4.4 show that the mean sustained force MF_{80+} was also higher at the distal anterior location compared to any other studied locations inside the socket. Moreover, such end-bearing was not only affected by the type of gait activities but also to some extend dependent on the type of prosthetic feet.

Table 4.1 shows the mean forces measured by the distal anterior sensor and test results of hypothesis H4a. Hypothesis H4a was supported in 17 out of 18 cases except during walking up a ramp with the Proprio Foot, when the mean forces at the distal anterior location was similar to the greatest mean force recorded at other locations in the socket (30.3±3 and 29.3±1.3). As shown in Table 4.2, during the gait *Forward*, different mean forces were observed when using different prosthetic feet. However, no appreciable differences were observed between Renegade Foot and Venture Foot during *Forward brisk*, *Ramp-up*, and *Ramp-down* gait activities. All failed cases involved the comparison between Renegade and Venture feet while the statistical tests involving Proprio Foot were supported. These results might be due to the adaptation nature of the Proprio Foot, which placed it in a different configuration at the *Heel Strike* moment compared to other feet.

4.5.2 Effect of prosthetic feet on middle posterior force

The RSI forces at the middle posterior location were similar in the tests conducted when the subject was using the Renegade Foot and the Venture Foot, but significantly higher when using the Proprio Foot (Figure 4.2, Figure 4.3). This effect of Proprio Foot on middle posterior location was in agreement with the results reported by Wolf et.al.,[20]. The peak and mean forces observed at this location (Table 4.3) were both characteristics of the foot used and validated hypothesis H4b, i.e., the observed values when the subject wore the Proprio Foot were distinct from those seen when either the Renegade or the Venture Foot was used. Even when Renegade and the Venture Foot were compared, the observed forces at the middle posterior location on the RSI were distinct in a majority of the test cases and the hypothesis H4b was validated in all but two instances when the subject was descending the stairs (*Stair-down*). Similar to hypothesis tests at the distal anterior location, failed statistical tests (H4b was rejected) at the middle posterior did not involve Proprio Foot. Again, the adaptation mechanism of the Proprio Foot might have had a distinct effect on the force observed at this location. Additionally, there was less variations in mean sustained force (CV= 12.1%) using the Renegade Foot than the Proprio Foot (CV = 20.5%) when the gait activities were switched.

4.5.3 Effect of prosthetic feet on the force at the proximal locations

During all gait activities with each of the feet considered in this study, the observed forces at the proximal level were similar for all locations with slightly higher values in the proximal anterior point (Figure 4.2 and Figure 4.4). When testing for different peak forces at the proximal locations, hypothesis H4b was rejected in fewer cases compared

to when testing for different mean forces. Between any two prosthetic feet, significantly different peak forces were detected in 61 out of 72 cases, while significantly different mean forces were detected in 54 out of 72 cases (Table 4.4 – Table 4.7). These observations suggested that while different prosthetic feet produced similar mean forces at the proximal level during the entire stance phase, they still had different effects on the peak forces. Greater instances of failed statistical tests were observed using data from the proximal level (anterior: 5 cases; posterior: 3 cases; lateral: 13 cases; medial: 8 cases) compared to data from distal anterior (3 cases) and middle posterior (2 cases). Furthermore, at the proximal level, failed tests also involved Proprio Foot, which was in contrast to the outcomes of the hypothesis tests using data from other sensors (middle and distal). This implied that the adaptation mechanism in the Proprio Foot had less effect on the proximal contact forces than the forces at distal anterior end-bearing and middle posterior locations. The difference in prosthesis mechanism might also have more effect on the force distribution along the anterior-posterior direction than the lateral-medial direction. There was greater number of failed tests along the lateral-medial direction (proximal lateral: 13 cases; proximal medial: 8 cases) than failed tests along the anterior-posterior direction (proximal anterior: 5 cases; proximal posterior: 3 cases).

4.5.4 Effect of prosthetic feet on temporal gait parameters

In general, differences in prosthetic feet had more effect on the stance duration than on the gait cycle durations. During walking on level ground with normal speed (*Forward*), while the gait cycle durations of three feet varied only by 3.7%, the stance duration variation was 10.7% (Table 4.8). By taking the average of all gait activities, different

prosthetic feet varied the stance durations by 6.2% while the gait cycle durations changed by only 2.3% (Table 4.8). This implied that wearing different prosthetic feet could alter the tissue loading time of the residual limb with little changes on the gait cycle.

During walking on the level ground (*Forward* and *Forward brisk*) with the Proprio Foot, the stance phase was shorter compared to when using the Renegade or Venture Foot (Table 4.8). The stance/gait ratio of the Proprio Foot was also closed to the gait of typical non-amputees (~62%) while that ratio of Renegade or Venture Foot was higher (~71%). This might be beneficial from the dorsiflexion of the controlled ankle joint during the swing phase to create toe clearance and plantarflexion before ground contact [118].

When walking on stairs, the stance duration was higher with the Renegade Foot compared to the others (Table 4.8). It was possible that the multi-axis functions of the Venture Foot and Proprio Foot provided the participant with more flexibility to walk on an unconventional terrain as stairs.

Finally when walking up a ramp, differences in prosthetic feet did not affect the stance or gait cycle durations. On the other hand, active plantarflexion of the ankle joint of the Proprio Foot before ground contact might have contributed to the shorter stance time during ramp descending.

4.6 Conclusions

The study reported in this chapter provided evidence that the choice of prosthetic feet impacted force distributions inside the socket during six gait activities in an otherwise

healthy person who had undergone a TOA procedure. Significant end-bearing, which is an expected outcome of the TOA procedure, was observed in all gait activities.

While nominal forces were observed in the proximal locations, greater forces were observed at the distal anterior location of the socket (supported by 17 out of 18 statistical t-tests). Furthermore, at the same socket location during the same gait activity, different peak (mean) forces were observed between any two prosthetic feet (182 out of 216 statistical t-tests confirmed). Each prosthetic foot also uniquely affected the temporal gait parameters. This experimental study showed that the residuum socket interface force, which related to the comfort and long-term health of amputees, and the gait parameters were the function of the prosthetic feet.

Results of this study provides credence to the principles motivating the design of prosthetic feet, as well as the role of the dynamic response characteristics of these feet in generating desired distribution of force inside the socket. Taken as a whole, these results indicate that for the same socket design, loading characteristics inside the socket vary with changes in both the selected gait and the type of prosthetic feet used by the subject. Although this study was restricted to one individual, the results highlight the important role of prosthesis design in modifying the loading response and providing desired residuum socket interface force distributions.

Chapter 5: Contraction of Residual Muscles in Individuals with Below-knee Amputation

The relationships between the contraction of the residual below-knee muscles and the variations of the residuum socket interface forces in individuals with transtibial osteomyoplastic amputation during gait have not been addressed. In this chapter, an investigation into the restoration of the residual tibialis anterior and gastrocnemius muscles in persons with unilateral TOA will be presented. Ten subjects will perform three gait activities including 2-minute level ground walking with self-selected speed, 2-minute level ground walking with fast speed, and 25-feet level ground walking while carrying an additional weighted box. Statistical analysis will be carried out to examine the relationships between activities of the considered muscles to the gait cycle and the contact forces inside the prosthetic socket[2].

5.1 Background

As the expected outcome of the TOA procedure, individuals with TOA can put more body weight on the distal area (end-bearing) of the residuum and actively contract their residual muscles voluntarily and during gait activities. To the best of our knowledge, the relationships between the contraction of the residual below-knee muscles and the variations of the RSI forces in individuals with TOA during gait have not been addressed.

Studies on the relationships between residual muscle activities and residuum socket interface force in the literature were limited to people with above-knee amputation

[2] This chapter is adapted from [A. Mai, S. Commuri, C. P. Dionne, J. Day, W. J. J. Ertl, and J. L. Regens, "Residual muscle contraction and residuum socket interface force in men with transtibial osteomyoplastic amputation," *Journal of Prosthetics and Orthotics*, vol. 25, pp. 151-158, 2013].

[119]. Most studies on gaits of people with below-knee amputation investigated the activities of proximal muscles above the knee (e.g., vastus medialis and biceps femoris) [15, 106, 108]. There was only a few studies on the activation of residual below-knee muscles (e.g., tibialis anterior and gastrocnemius) during gait [69, 120, 121]. Furthermore, recent trends of using electromyography signals from residual muscles in recognition of locomotion modes [70] and in control of active prostheses [100] motivated the effort to retrieve and understand the contraction of these muscles.

In this chapter, the contraction of the residual muscles and their relationships with the RSI force variations in a group of otherwise healthy individuals who had undergone the transtibial osteomyoplastic amputation procedure are investigated. Motivated by the desired outcomes of the TOA procedure namely limb stabilization, end-bearing, and restoration of residual muscle contraction, this study aims at quantitative verification of the effectiveness of the TOA procedure.

5.2 Objectives and hypotheses

This study investigates the similarities between the contraction profiles of the residual tibialis anterior and residual gastrocnemius muscles of the residual limb and the same muscles from persons without below-knee amputation. The following objectives and hypotheses are developed.

Objective O5A: Investigate whether the residual tibialis anterior and residual gastrocnemius muscles are active during the gait of subjects with TOA. ***Hypothesis H5a*** states as there will be significant difference between the maximum and the minimum contraction levels from each muscle. If hypothesis H5a is supported for both

residual muscles, the expected outcomes of the TOA procedure in reestablishment of the length-tension relationship in these muscles will be confirmed.

Objective O5B: Investigate whether the residual tibialis anterior and gastrocnemius muscles contract at the designated gait phases as compared to non-amputee subjects. The relationships between gait phases and the RSI force were observed in previous studies [42, 122]. Therefore, the correspondence between residual muscle contraction and gait phases will be determined by studying how the muscle signals related to the RSI force. ***Hypothesis H5b1*** states that the residual tibialis anterior muscle will contract more when the distal RSI force shows the highest variations (early and late stance) than when the distal RSI force shows the lowest variations (*Mid-stance*). On the other hand, ***Hypothesis H5b2*** states that the residual gastrocnemius muscle will contract less when the distal RSI force shows the highest variations (early and late stance) than when the distal RSI force shows the lowest variations (*Mid-stance*). Specifically, contraction profiles of the residual tibialis anterior and gastrocnemius muscles in individuals with unilateral TOA will be similar to these muscles from non-amputees if the hypotheses H5b1 and H5b2 are respectively supported.

5.3 Methods

5.3.1 Subjects

Experimental protocol was approved by the Institutional Review Board at the University of Oklahoma Health Sciences Center for protection of human subjects. Ten otherwise healthy men with unilateral transtibial osteomyoplastic amputation consented to participate in this study (Table 5.1). All subjects wore their own prosthetic systems

(socket and prosthetic foot) during the tests, therefore the distal RSI force and muscle activities quantified in this study would be similar to their values during daily activities. A certified prosthetist was available onsite to assure socket alignment and fit.

Table 5.1. Subject information

Subject	Amputation side	Age (year)	Height (m)	Weight (kg)	Length of residual limb (cm)	Years since amputation
S1	L	40	1.78	97.1	22	1.5
S2	L	55	1.78	93.0	13	2
S3	R	50	1.80	111.1	18	3
S4	L	38	1.83	79.4	16	3.5
S5	L	50	1.83	122.5	18	7.5
S6	L	53	1.75	72.6	16	1.5
S7	R	27	1.83	90.7	20	1
S8	R	53	1.75	72.6	16	6
S9	L	30	1.88	93.9	24	3
S10	R	45	1.70	89.8	27	7
Mean		44.1	1.79	92.3	18.9	
Std.		10.0	0.051	15.8	4.3	

5.3.2 Protocol

Gait: During the study, the participants performed common work-related gait activities including 2-minute level ground walking with self-selected speed (*Forward*), 2-minute level ground walking with fast speed (*Forward brisk*), and 25-feet level ground walking while carrying a box with weight at capacity (*Weight carrying*).

RSI force measurement: Residuum socket interface force at the distal residuum was measured using 4 ultra-thin FlexiForce® A201 piezo-resistive sensors (Section 2.7.3). These sensors were placed at anterior, posterior, medial, and lateral locations at the distal end of the prosthetic socket of each individual (Figure 5.1a). Placement and calibration of these force sensors followed the procedure described in Section 2.7.3.

Contact forces captured by these four distal sensors were used to confirm the presence of distal loading as the result of the TOA procedure.

Electromyography: Activities of the tibialis anterior and gastrocnemius muscles in both amputated and intact limb of the subjects were measured using disposable surface stimulating and recording Ag/AgCl electrodes (square, sensing area of 1.44cm^2) [103]. A pair of EMG electrodes was placed on each muscle (Figure 5.1b) as described in Section 2.7.3.

Signals representing the applied forces and muscle activities were captured by the gait monitoring device OUPAM (Section 2.7.4) at the rate of 1000 Hz. During the tests, each subject also wore a gait monitoring device called Intelligent Device for Energy Expenditure and Physical Activity (IDEEA®) by MiniSun™ [82] (Section 2.7.3). Gait parameters obtained by the IDEEA® system were used to validate the stance and swing phases of the gait detected using distal RSI force measurements.

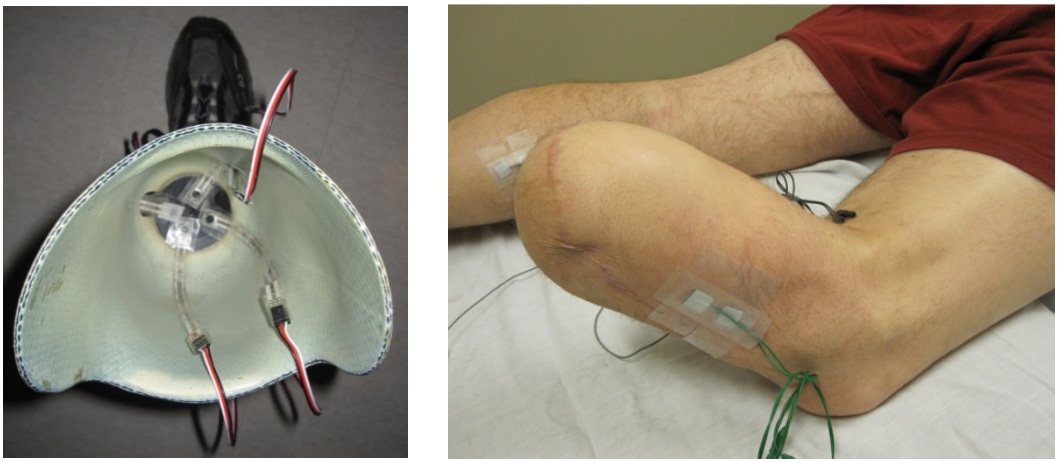

(a) (b)

Figure 5.1. (a) Placement of force sensors inside the socket; (b) Placement of EMG electrodes on residual tibialis anterior muscle.

5.3.3 Data analysis

During the stance phase, positive forces were observed at the distal RSI, whereas negligible forces were recorded during the swing phase of the gait. The duration of the stance phase was then normalized in time domain and represented by 120 data points. Stance phase was further divided into 10 equal segments with each segment contained 12 data points and corresponded to 10% of the stance phase [123].

Distal residuum socket interface force: Signals representing the applied forces were filtered using a first-order low pass filter with the cut-off frequency of 3Hz to eliminate high frequency noises without affecting the signal content. The total distal RSI force was generated by adding up the forces measured at four locations (i.e., anterior, posterior, medial, lateral) at the bottom of the residual limb (Figure 5.1a). The distal force curve was then normalized to represent 100% of the stance phase with 120 data points used. For each segment as defined above, the variation of the distal RSI force, $F_{VAR}(\%)$, was calculated as the percentage between the standard deviation and the mean value of 12 data points contained in that segment. Higher F_{VAR} value in a particular segment implied larger variations in the force transferred between the socket and the distal end of the residual limb.

Electromyography: Each EMG signal was processed through a linear envelope constructed with a full-wave rectifier followed by a low pass filter with the cut-off frequency of 8Hz [28]. The Root Mean Square curve of the filtered signal, E_{RMS}, was then obtained using a symmetric moving window averager of 150ms wide (±75ms) and normalized to represent the stance phase (with 120 data points). For each subject, the EMG curve of each muscle during each gait activity was normalized by the maximal

E_{RMS} value obtained from the same muscle of the same subject throughout the study. The resulted signal was then divided into 10 equal segments with each segment corresponded to 10% of the stance phase (12 data points in each segment) [123]. Activation level of each muscle in each segment was represented as the average of the 12 data points. For each subject and during each gait activity, 10 values of normalized E_{RMS} in 10 segments (i.e., one E_{RMS} value in each segment) were calculated.

Statistical analysis: Hypothesis H5a was tested by two-sample *t*-tests (two-tailed, paired, alpha = 0.05) which looked for significant difference between the maximum and minimum E_{RMS} values of each residual muscle. In addition, maximum and minimum values of the distal RSI force variation F_{VAR} were obtained for each subject during each gait activity. Hypotheses ***H5b1*** and ***H5b2*** were then tested by two-sample *t*-tests (one-tailed, alpha = 0.05) using the residual tibialis anterior and gastrocnemius E_{RMS} values which were obtained from the segments where the maximum and minimum F_{VAR} were observed.

5.4 Results

Variations in residuum socket interface force: Average normalized distal RSI forces are shown in the top 3 plots in Figure 5.2. Each curve was normalized by the maximum distal RSI force observed throughout three tests. Table 5.2 reports the minimum and maximum RSI force variations F_{VAR} and the time durations when they occurred.

Table 5.2. Minimum and maximum distal residuum socket interface force variations F_{VAR}(%)

	Forward				Forward Brisk				Weight Carrying			
	Lowest variation		Highest variation		Lowest variation		Highest variation		Lowest variation		Highest variation	
Subject	F_{VAR} (%)	At (% stance)	F_{VAR} (%)	At (% stance)	F_{VAR} (%)	At (% stance)	F_{VAR} (%)	At (% stance)	F_{VAR} (%)	At (% stance)	F_{VAR} (%)	At (% stance)
S1	1.24	50-60	54.4	80-90	1.27	50-60	77.1	90-100	0.78	50-60	81.7	0-10
S2	2.86	80-90	71.2	0-10	2.58	70-80	65.2	90-100	2.65	20-30	70.8	0-10
S3	3.02	70-80	91.2	90-100	1.64	20-30	77.0	90-100	2.04	30-40	58.9	90-100
S4	2.79	70-80	67.8	90-100	4.94	70-80	78.3	90-100	0.49	50-60	65.0	0-10
S5	0.82	50-60	68.8	0-10	1.17	50-60	66.0	0-10	2.31	30-40	75.4	0-10
S6	2.88	70-80	73.6	90-100	6.61	70-80	81.3	90-100	0.60	30-40	79.4	90-100
S7	3.00	60-70	73.0	0-10	1.34	40-50	69.4	90-100	3.71	60-70	77.2	90-100
S8	7.96	10-20	82.7	0-10	5.57	10-20	77.2	80-90	3.04	20-30	81.4	90-100
S9	1.52	50-60	74.8	90-100	1.64	60-70	78.0	0-10	0.74	60-70	70.6	0-10
S10	1.00	50-60	32.4	90-100	3.11	20-30	49.0	90-100	1.02	30-40	61.9	90-100

During *Forward* gait, the minimum and maximum F_{VAR} were 2.71±2.05% and 69±16%, respectively. During *Forward brisk* gait, F_{VAR} ranged from 2.99±2.01% to 71.8±9.78%. Finally, F_{VAR} varied from 1.74±1.16% to 72.2±8.17% during the *Weight carrying*. For all three gait activities, maximum RSI force variations were observed at either the first 10% or the last 20% of the stance phase. In contrast minimum RSI force variations occurred predominantly (except subject S2 during *Forward* gait) during 10-80% of the stance phase.

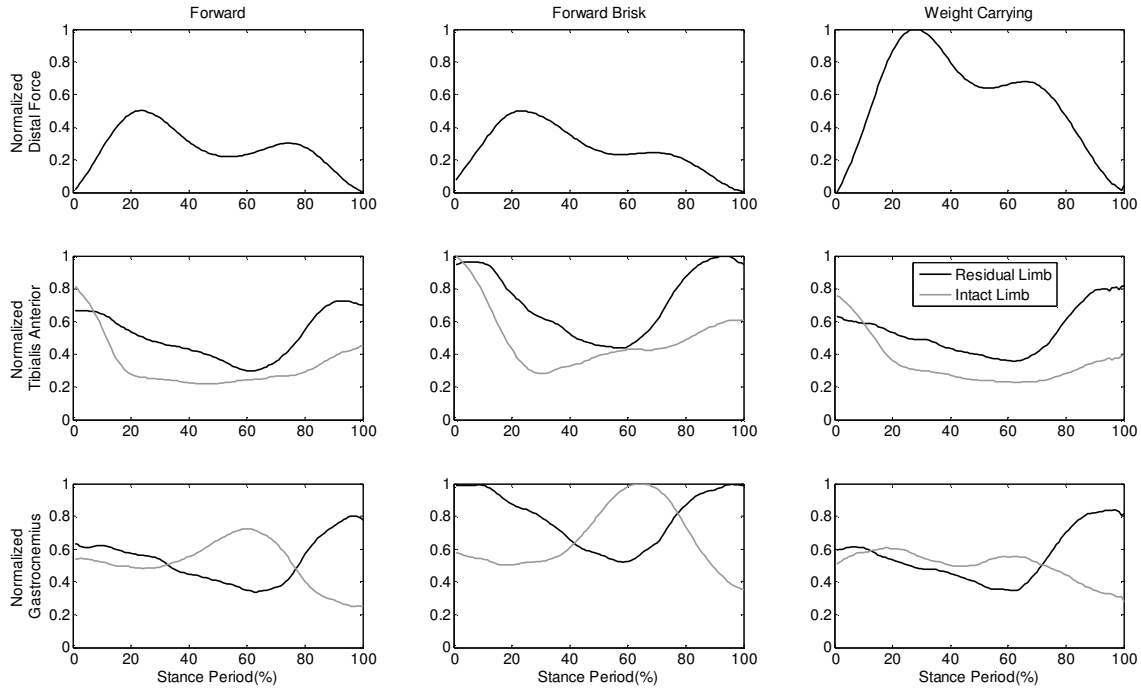

Figure 5.2. Normalized distal residuum socket interface force, tibialis anterior, and gastrocnemius EMG.

Residual muscle activities: The average normalized electromyography signals of the tibialis anterior and gastrocnemius muscles of both amputated side and intact side of participants are shown in bottom 6 plots in Figure 5.2. It can be seen that for the subjects in this study, tibialis anterior and gastrocnemius muscles of both limbs contracted at the highest levels during the *Forward brisk* gait. There were significant differences between the maximum E_{RMS} and the minimum E_{RMS} of the residual TA muscle (Table 5.3): 0.94±0.046 compared to 0.04±0.035 (p(H5a was rejected) < 0.001), 0.96±0.027 compared to 0.014±0.005 (p(H5a was rejected) < 0.001), and 0.91±0.079 compared to 0.033±0.021 (p(H5a was rejected) < 0.001) for *Forward*, *Forward brisk*, and *Weight carrying*, respectively. Also from Table 5.3, there were significant differences between the maximum and minimum E_{RMS} of the residual GAS muscle

during the gaits *Forward* (0.93±0.058 compared to 0.05±0.032; p(H5a was rejected) < 0.001), *Forward brisk* (0.97±0.031 compared to 0.028±0.029; p(H5a was rejected) < 0.001), and *Weight carrying* (0.90±0.061 compared to 0.031±0.032; p(H5a was rejected) < 0.001).

Table 5.3. Normalized tibialis anterior and gastrocnemius E_{RMS}

Residual tibialis anterior			
Gait	Minimum E_{RMS}	Maximum E_{RMS}	p(H5a was rejected)
Forward	0.04±0.035	0.94±0.046	<0.001
Forward brisk	0.014±0.005	0.96±0.027	<0.001
Weight carrying	0.033±0.021	0.91±0.079	<0.001
Residual gastrocnemius			
Gait	Minimum E_{RMS}	Maximum E_{RMS}	p(H5a was rejected)
Forward	0.05±0.032	0.93±0.058	<0.001
Forward brisk	0.028±0.029	0.97±0.031	<0.001
Weight carrying	0.031±0.032	0.90±0.061	<0.001

Relationship between the residual muscle activities and RSI force variations: Table 5.4 reports the results of testing hypotheses H5b1 and H5b2 for the relationships between E_{RMS} values at instances corresponding to the lowest and highest RSI force variations. When the RSI force variation was maximum (highest F_{VAR}), the residual TA muscle E_{RMS} was 0.84±0.14, 0.72±0.18, and 0.7±0.217 compared to 0.19±0.23 (p(H5b1 was rejected)<0.001, *Forward*), 0.4±0.39 (p(H5b1 was rejected)≈0.0187, *Forward brisk*), and 0.30±0.269 (p(H5b1 was rejected)≈0.001, *Weight carrying*) when the lowest F_{VAR} occurred. On the other hand, hypothesis H5b2 was not supported in any of gait activities considered in this study. The probability of rejecting the hypothesis H5b2 was high for all three walking conditions. Especially during the *Forward* gait, the hypothesis H5b2 was completely rejected.

Table 5.4. Normalized tibialis anterior and gastrocnemius E_{RMS} at the lowest and highest variation F_{VAR}

Residual tibialis anterior			
Gait	E_{RMS} at lowest F_{VAR}	E_{RMS} at highest F_{VAR}	p(H5b1 was rejected)
Forward	0.19±0.23	0.84±0.14	<0.001
Forward brisk	0.4±0.39	0.72±0.18	0.0187
Weight carrying	0.30±0.269	0.7±0.217	0.001
Residual gastrocnemius			
Gait	E_{RMS} at lowest F_{VAR}	E_{RMS} at highest F_{VAR}	p(H5b2 was rejected)
Forward	0.20±0.16	0.79±0.2	1
Forward brisk	0.36±0.35	0.61±0.268	0.958
Weight carrying	0.25±0.27	0.60±0.261	0.9956

5.5 Discussion of the results

5.5.1 Distal residuum socket interface force variations

In general, the distal RSI forces had the highest variation during the first 10% of the stance phase (early stance) and the last 20% of the stance phase (late stance) whereas the lowest variation was observed during 20-80% of the stance phase (*Mid-stance*). The only exception occurred with subject S2 where the distal RSI force did not increase in the late stance phase of the *Forward* gait. As can be observed from Table 5.1, subject S2 had the shortest residuum limb as well as the smallest residuum-limb/body-height ratio among all subjects in this study.

The stance and gait durations extracted from the distal RSI forces agreed with the temporal gait parameters obtained by footswitches placed under the prosthetic foot. Data collected independently using the gait monitoring system IDEEA® (MiniSun™) [82] validated the stance and the gait events. For the subjects in this study, the temporal differences between the two systems (OU-PAM and IDEEA®) were 0.051±0.029s and 0.037±0.024s for the stance phase and gait cycle durations, respectively. This implied that the RSI force could distinguish the stance and swing durations, therefore related to

the phases of the gait. For that reason, contraction profiles of the residual tibialis anterior and gastrocnemius muscles during the gait cycle could be analyzed through the relationships with the distal RSI force.

5.5.2 Residual muscle contraction

Contraction profiles of residual TA and GAS muscles (Figure 5.2) were in agreement with the preliminary results in [120, 121], which confirmed contraction of these muscles following a myoplasty procedure. Through investigation of hypotheses H5a (Table 5.3), the contractions of residual TA and GAS muscles were confirmed, even though the activation profile of the residual GAS muscle was not similar to that of the GAS muscle from the intact limb.

5.5.3 Residual tibialis anterior activation profile

The residual tibialis anterior was more active during early and late stance (when the RSI force showed highest variation) compared to *Mid-stance* (when the RSI force showed lowest variation) (Table 5.4). These relationships indicated the correspondence of the residual TA muscle activity to the phases of the gait cycle. This result supported the expectation of the TOA procedure in restoration of residual muscle contraction [38].

5.5.4 Residual gastrocnemius activation profile

Although the residual GAS muscle was active and its contraction was measureable (Figure 5.2 and Table 5.3), its activation profile was not similar to the intact limb GAS muscle (Figure 5.2) or GAS muscles from non-amputee subjects (as seen in Figure 2.3). This implied that the residual GAS muscle activities did not relate to the RSI force variations and gait phases in an expected manner. Instead, the residual GAS muscle tended to contract in a manner similar to the residual TA muscle which was more active

during early and late stance and less active during *Mid-stance* of the gait. This might be due to the co-contraction of the residual TA and GAS muscles in an effort to stiffen the limb inside the prosthetic socket. These co-contractions could be individuals' effort to enhance the stability of the gait, as observed in the literature [69].

5.6 Conclusions

In this chapter, the contraction of residual tibialis anterior and gastrocnemius muscles during work-related gaits in subjects with unilateral transtibial osteomyoplastic amputation was examined. Analysis of experimental data confirmed the presence of loading at the bottom of the residual limb and restoration of length-tension relationship of residual muscles. Both of these outcomes were expected results attributable to the TOA procedure. Furthermore, it was shown that the contraction of residual tibialis anterior related to the phases of the gait through the variations in distal RSI forces. Such relationships were not observed in the residual gastrocnemius muscle activities. Instead, there were evidences of the co-contractions of the tibialis anterior and gastrocnemius muscles on the residual limb. Further research along this line would be beneficial to the design of prosthetic sockets and establishment of possible exercise regimen during rehabilitation [124].

Chapter 6: Potential of Residuum Socket Interface Forces and Residual Muscle Activities in Recognition of Amputee Gait

In order to properly control the prosthetic feet to adapt to the changing gait, it is necessary to recognize the characteristics such as gait type, walking speed, and terrain. The problem of identification of the type of gait of individuals with below-knee amputation using the RSI force and EMG signals captured from the residual muscles will be presented in this chapter.

A group of nine subjects with unilateral TOA will perform 3 level ground walking gaits with preferred slow, normal, and fast speeds. Contact forces and residual muscle activities will be measured from the individuals during the gait. Statistical analysis will be carried out to examine the effect of changing walking speeds on the RSI force and residual muscle activities. An artificial neural network (ANN) will then be trained with the parameters calculated from the RSI force and residual muscles to recognize the gait with different walking speeds. It is anticipated that the RSI forces and residual muscle activities will vary as the walking speed changes and therefore can be used for identification of the gait of the individuals.

6.1 Background

In the development of advanced below-knee prosthetic feet, there is a common trend in replicating the biomechanical characteristics and specifically the stiffness profile and movement of the biological ankle joint [77, 93, 95]. Research on biomechanics of the human ankle joint has indicated that the ankle stiffness profile varies with the changes in walking speed [34]. In addition, activities of the muscles that control the biological ankle joint also depend on the walking speed [125]. Wearing prosthetic feet which

cannot adapt to the users' intent also requires below-knee amputees to develop strategies to compensate for the lack of ankle movement by increasing muscle contractions [15, 65] which lead to additional energy consumption during gait [16]. Therefore, in order to design prosthetic feet which can adapt their behaviors to the gait demands, it is necessary to recognize the gait conditions such as gait type, walking speed, and terrain [77, 126].

Footswitches and kinematic-based sensors have been used in identification of different gait and walking terrain [94] in order to select proper control commands for the prosthetic feet. The general rules for recognition of gait using these measurements usually assume that movements of the amputees' limb during gait are similar to non-amputees. However, the general rules are not guaranteed to be applicable for individuals with different gait characteristics or different level of amputation and activity.

Recently, activities of the residual muscles inside the socket of below-knee amputees have started drawing attention. Residual muscle contraction has been captured in order to recognize the movement of the upper limb [127] or above-knee residuum [128]. It has been shown that the EMG signals can be measured and have potential for used in recognition of gait and control of prosthetic feet [67, 68]. That approach highly depends on the availability, measurability and reliability of the signals from residual muscles. Furthermore, sophisticated measurement devices and careful preparation of the skin surfaces are required in order to obtain good EMG signals from the muscles.

Studies on the dependence of the RSI force and residual muscle activities on walking speeds in persons with unilateral below-knee amputation are very little. Most of the studies on RSI forces aimed at investigating the influence of socket concepts [45, 114,

115], socket fit and alignment [54, 112], or socket materials [113]. Majority of researches on muscle activities in below-knee amputees did not address the variations of residual muscles below the knee (e.g., tibialis anterior and gastrocnemius) when the walking speed changed.

6.2 Objectives and hypotheses

This chapter aims to investigate the dependence of the RSI force and activities of residual muscles inside the prosthetic socket on the walking speed. Objectives and hypotheses of this study are as follows.

Objective O6A: Show that during gait on level ground, the RSI force and residual muscle EMG of subjects with TOA depend on the walking speed. ***Hypothesis H6a*** states that for each subject, changes in walking speed will lead to significant difference in both RSI forces and residual muscle activities. Hypothesis H6a will be verified by multiple comparisons between the parameters calculated from the RSI force (mean force, peak force, force-time integral) during 3 walking speeds (slow, normal, and fast). Similarly, root mean square values and signal-time integral of the residual muscle EMG signals will be compared between 3 gaits. The results will be prerequisites for achievement of the next objective.

Objective O6B: Investigate the potential of using parameters calculated from the RSI force and residual muscle EMG in recognition of gaits with different walking speeds. Selected parameters which are calculated from the RSI force or EMG signals will be used to train an artificial neural network to recognize the type of gait of each participant.

6.3 Methods

6.3.1 Subjects

This study included nine male subjects with unilateral transtibial osteomyoplastic amputation (age: 40±12years; weight: 94.5±15.5kg.; height: 1.83±0.05m) with at least 6 months following amputation surgery and had active lifestyles (Table 6.1). All subjects were capable of walking independently without using any assistive walking devices. They wore total surface bearing socket and their own prostheses during the study. The following protocol was approved by the Institutional Review Board at the University of Oklahoma Health Sciences Center for protection of human subjects. Formal consent was obtained from each subject prior to the study.

6.3.2 Protocol

Gait: In order to assess the dependence of the RSI force and EMG activity on the walking speed, each subject performed three gaits labeled slow, normal, and fast along a hallway for 2 minutes. Each subject could select comfortable and safe walking speeds.

Measurement: RSI forces were measured from the participated subjects using ultrathin force sensors (FlexiForce® A201, [102], Section 2.7.3) which were placed inside the prosthetic socket at 10 locations allocated in 3 levels: end-bearing distal level (anterior, medial, posterior, lateral), middle level (anterior, medial, posterior, lateral), and proximal level (anterior, posterior) (Figure 6.1). EMG signals were collected from residual tibialis anterior and gastrocnemius muscles of the residual limb by placing disposable surface electrodes [103] on the corresponding muscle compartments of each subject. For each muscle, a pair of electrodes was placed ~2.5cm apart from each other along the muscles' belly (Figure 6.1 and Section 2.7.3). Signals representing the applied

RSI force and muscle contractions were captured at the rate of 1000Hz. Signal conditionings such as amplification and filtering were done by a portable gait monitoring device worn by subjects during gait (OUPAM, Section 2.7.4).

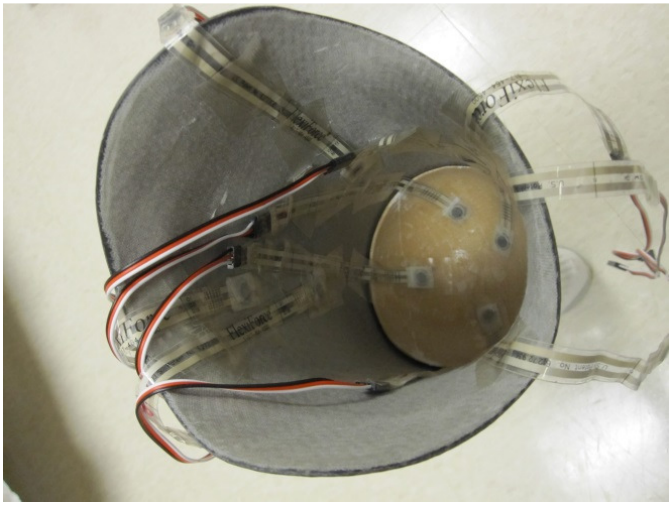

(a)

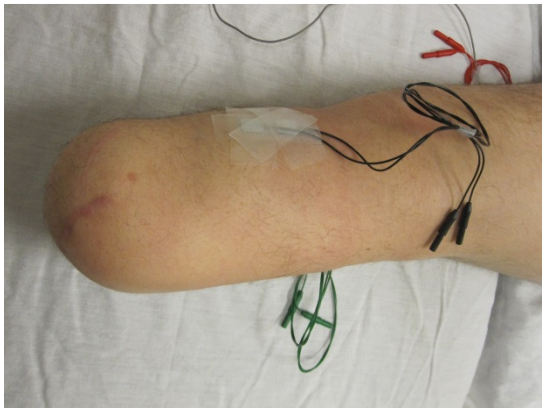

(b) (c)

Figure 6.1. (a) Locations of force sensors inside the socket; (b) EMG electrodes on the residual tibialis anterior and (c) gastrocnemius muscles.

6.3.3 Data analysis

Preprocessing: Low-pass filters with cut-off frequency of 3Hz were applied to signals representing the applied forces to remove the noises generated by the electronics components and motion artifacts. The amplified EMG signals were preprocessed by a linear envelope (full-wave rectifier and low-pass filter, with cut-off frequency of 8Hz) and a symmetric moving window averager (±75 milliseconds). For each subject, the RSI force and muscle EMG curves were normalized by the corresponding maximal values observed from 3 walking gaits.

Calculation: From the normalized RSI forces, m_F – the mean force during each gait cycle, p_F – the peak force during each gait cycle, and a_F – the force-time integral during each gait cycle, were calculated. For each normalized muscle signal, the following parameters were calculated: m_E – root mean square of the signal during each gait cycle, and a_E – the signal-time integral during each gait cycle.

Statistical analysis: Since the RSI forces were measured at 10 locations inside the socket and EMG signals were measured from 2 residual muscles, each walking speed was represented by 34 parameters (10 RSI locations × 3 parameter-per-RSI-location + 2 muscles × 2 parameter-per-muscle). A multiple comparison routine (significant level alpha of 0.05) provided by The Mathworks® Statistical Toolbox™ [129] was executed to compare parameters from different walking speeds and thereby verifying the hypothesis H6a. Results from the multiple comparisons would help determine whether a particular parameter was significantly dependent on the walking speed.

6.4 Results

Significant differences were found between walking speeds of the slow gait (0.90±0.08m/s), normal gait (1.31±0.14m/s), and fast gait (1.73±0.21m/s) as shown in Table 6.1.

Table 6.1. Subject information and walking speeds

Subject	Age (year)	Weight (kg)	Height (m)	Walking speed (m/s)		
				Slow	Normal	Fast
S1	56	93.0	1.77	0.97	1.19	1.69
S2	39	86.2	1.82	0.94	1.17	1.46
S3	47	111.1	1.93	1.00	1.34	1.82
S4	51	124.7	1.82	0.79	1.34	1.76
S5	54	72.6	1.77	0.88	1.24	1.64
S6	31	94.3	1.87	0.96	1.53	2.00
S7	25	93.0	1.82	0.94	1.37	1.91
S8	32	93.9	1.82	0.77	1.11	1.36
S9	29	81.6	1.82	0.83	1.46	1.90
Mean±Std	40±12	94.5±15.5	1.83±0.05	0.90±0.08	1.31±0.14	1.73±0.21

Typical normalized RSI forces and residual muscle EMG signals during gaits with different walking speeds are shown in Figure 6.2 and Figure 6.3 respectively.

Results of the multiple comparisons further illustrated the dependence of the RSI forces on the walking speed at 4 to 10 locations inside the socket. When the walking speed changed, number of locations at which significantly different force parameters were observed varied from 9 to 10 locations (2 subjects S4, S6), 6 to 7 locations (5 subjects S1, S3, S5, S8, S9), and at 4 locations (2 subjects S2, S7) (Table 6.2).

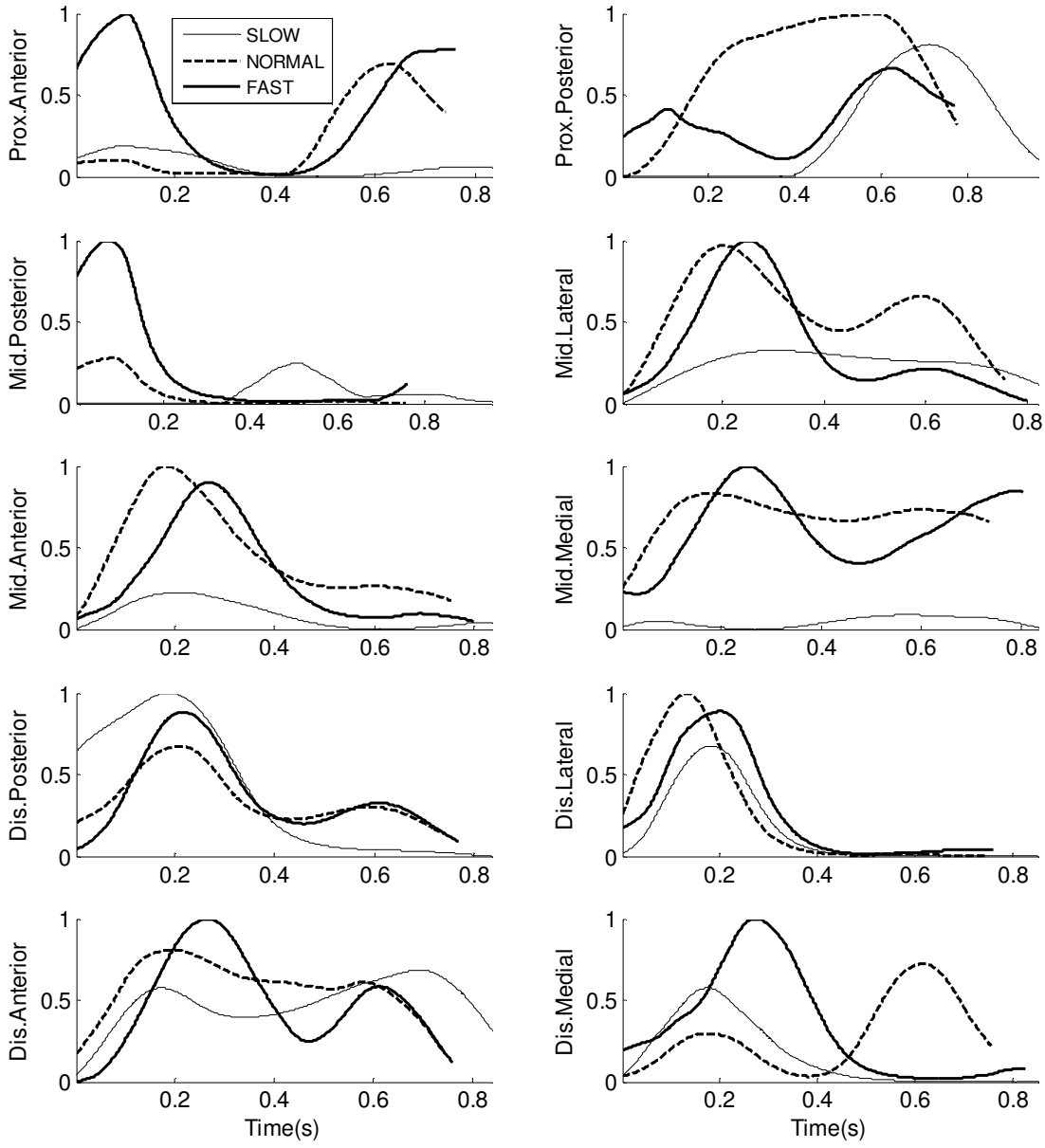

Figure 6.2. Typical normalized RSI forces during slow, normal, and fast gaits.

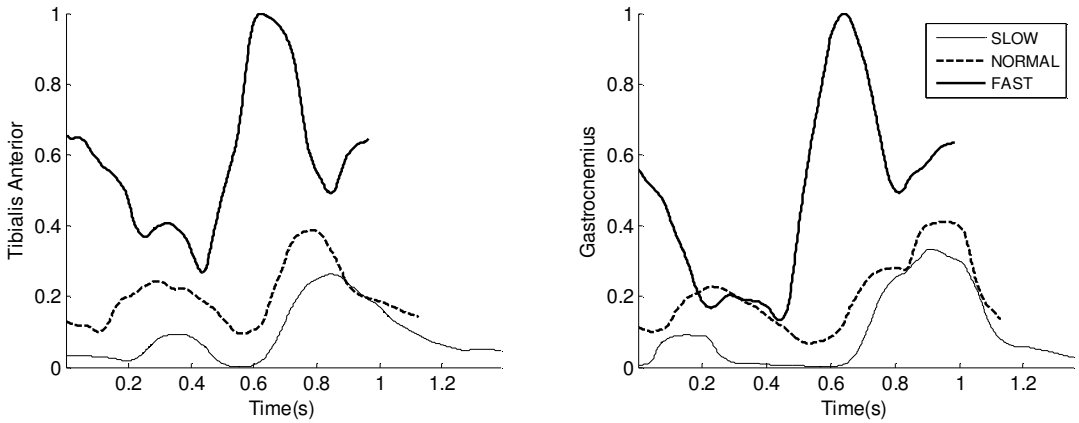

Figure 6.3. Typical normalized EMG signals during slow, normal, and fast gaits.

Similarly, multiple comparisons between parameters from the residual muscle EMG signals showed their dependence on the walking speed. Significantly different activation levels were seen at the residual tibialis anterior of all 9 subjects as the walking speed changed. Residual gastrocnemius muscle in 7 out of 9 subjects showed the dependence on walking speed (Table 6.2).

Table 6.2. Residuum socket interface locations and residual muscles whose measurements were significantly dependent on the walking speed

Subject	RSI location (max = 10)	Residual muscles (max = 2)
S1	7 (DA, DM, DL, MA, MM, ML, PP)	1 (TA)
S2	4 (DP, ML, PA, PP)	2 (TA, GAS)
S3	7 (DA, DM, MA, MP, ML, PA, PP)	2 (TA, GAS)
S4	10 (DA, DM, DP, DL, MA, MM, MP, ML, PA, PP)	2 (TA, GAS)
S5	6 (DL, MA, MM, ML, PA, PP)	2 (TA, GAS)
S6	9 (DA, DM, DP, DL, MA, MM, ML, PA, PP)	2 (TA, GAS)
S7	4 (DA, DP, MM, ML)	2 (TA, GAS)
S8	7 (DA, DP, MM, MP, ML, PA, PP)	2 (TA, GAS)
S9	6 (DM, DP, MA, MM, ML, PA)	1 (TA)

DA,DM,DP,DL – Distal (anterior, medial, posterior, lateral)
MA,MM,MP,ML – Middle (anterior, medial, posterior, lateral)
PA, PP – Proximal (Anterior, posterior)
TA – Tibialis anterior; GAS – Gastrocnemius

ANN-based gait recognition: The dependence of the RSI forces and residual muscle EMG signals on the walking speed motivated the use of these measurements in recognition of gait with different paces. Parameters (m_F, p_F, a_F) calculated from the distal RSI force (anterior, medial, posterior, and lateral) and (m_E, a_E) from residual tibialis anterior and gastrocnemius EMG were used for recognition of gaits with different walking speeds. Only distal RSI locations were chosen because the force sensors were easily embedded at the bottom of the prosthetic socket and shifting of the sensors was minimum compared to force sensors at the middle and proximal levels.

Accuracy of gait recognition: The percentages of correct recognition were 98.48%, 98.39%, and 97.25% respectively for 3 gaits when features from both distal RSI forces and residual muscle EMG signals were used to train the ANN. By using only the parameters from the distal forces, the percentages of correct gait recognition were 95.74%, 92.40%, and 90.78% for 3 gaits slow, normal, and fast, respectively (Table 6.3).

Table 6.3. Confusion matrices of the gait recognition.

	Use features from distal socket force and residual muscles			*Use features from only distal socket force*		
	Slow (predict)	Normal (predict)	Fast (predict)	Slow (predict)	Normal (predict)	Fast (predict)
Slow (actual)	98.48%	1.52%	0.00%	95.74%	1.82%	2.43%
Normal (actual)	0.46%	98.39%	1.15%	1.61%	92.40%	5.99%
Fast (actual)	1.18%	1.57%	97.25%	4.51%	4.71%	90.78%

6.5 Discussion of the results

In this study, RSI forces and residual muscle activities were simultaneously measured from inside the prosthetic socket of subjects with unilateral transtibial osteomyoplastic amputation. By using ultrathin force and EMG sensors and allowing the subjects to select their preferred walking speeds, the captured signals were similar to what would be observed under conditions of daily activities. These factors were different from [67, 68] in which subjects wore thicker electrodes (~5mm) and walked on a treadmill. Since each subject had a unique residual limb geometry and personal preference in choosing walking speeds, subject-specific analysis for each individual was performed.

6.5.1 Effect of walking speeds on in-socket measurement

First, there was no general rule applied for all subjects regarding the influence of the walking speed on the RSI forces measured inside the socket (Table 6.2). At the distal level of all 9 individuals, different walking speeds significantly influenced the RSI force parameters of at least 1 location. The significant differences were also found at 2 distal locations of 4 subjects, 3 distal locations of 1 subject and all 4 distal locations of 2 subjects. RSI force at the middle levels was also significantly affected by the changes in walking speeds. Different gaits led to differences in at least 1 middle location of all 9 subjects, 2 locations of 1 subject, 3 middle locations of 6 subjects and all 4 middle locations of 1 subject. Finally, RSI force parameters at 2 proximal locations of 6 individuals and at least 1 proximal location of 8 subjects were significantly different as the walking speed changed.

Four subjects S1, S3, S6, S8 showed significantly different force parameters at about half (~17 out of 30) of the total 30 parameters (10 locations × 3 parameter-per-location).

Less than half (~10 out of 30) force parameters of subjects S2, S5, S7, and S9 were significantly dependent on the walking speed. Subject S4 showed more than half (25 out of 30) significantly different force parameters. Although no general rule was applied, the results illustrated the dependence of RSI force of each individual on the walking speed as the combined outcomes of the geometry of the residual limb, socket alignment, socket fit, and prosthesis used.

On the other hand, although each subject had unique residual limb and prosthesis characteristics, dependence of the residual muscle activities on walking speed seemed to be more general. At least one residual muscle of all 9 subjects was significantly depended on the walking speed. Different walking speeds also led to significant changes in both residual tibialis anterior and gastrocnemius muscles in 7 out of 9 individuals. Majority of the subjects (except S1 and S9) showed significant differences at all of the 4 EMG parameters (2 locations × 2 parameter-per-location).

6.5.2 Gait recognition with parameters from in-socket measurement

As seen in Table 6.3, gaits with different walking speeds could be recognized with high accuracy (~98%) when both distal RSI forces and residual muscle EMG signals were used to train the artificial neural network. However, using electromyography signals required placement of the EMG electrodes on a carefully prepared skin surface. Furthermore, the EMG electrodes could be shifted during the gait therefore affecting the reliability of the muscle signals. It would be desirable to use the sensor type that had less restriction while still providing accurate recognition capability. In fact, fairly high correct percentage (~93%) in Table 6.3 indicated that the ANN which was trained by only distal RSI forces still yielded good recognition results compared to when the

muscle EMG [70] or kinematic sensors [73] were used. The ultra-thin force sensors can be easily embedded inside the prosthetic socket to provide real-time force measurement without affecting the mobility and gait of the subjects. Placement of the sensors at the bottom of the socket also decreases the chance of sensor shifting which might lead to inaccuracy in recognition of gait. In addition, distal RSI forces not only perform the task of gait recognition but also allow real-time monitoring of the tissue loading inside the socket.

6.6 Conclusions

Results of the gait analysis in this chapter indicated that the RSI forces and residual muscle EMG signals in individuals with TOA were significantly dependent on the walking speed. As the walking speed changed, all subjects showed significant differences in at least 4 out of 10 force locations and at least 1 out of 2 residual muscles. Significant differences in more than half of the force locations and both residual muscles were also seen in the majority of the subjects (7 out of 9). An average correct recognition percentage of ~98% was obtained when the ANN was trained with features from both end-bearing distal force and residual muscle EMG. When only the distal RSI force was used to train the ANN, the performance was still good with the correct recognition percentage of ~93%. Real-time monitoring of RSI force/muscle EMG therefore could be beneficial to both control of prosthetic feet and analysis of the gait of individuals with below-knee amputation.

Chapter 7: Framework for Modeling and Control of a Prosthetic Ankle Joint

A framework that is based on modeling and simulation of the prosthetic devices will benefit the studying of the effectiveness of prostheses on kinematic behaviors and other aspects of the gait without posing a risk of injury due to prosthetic malfunctions when testing on human subjects. In this chapter, the framework in which the dynamics of the prosthetic ankle joint during gait are described and the ankle control algorithms are implemented will be presented. First, the link-segment representation will be used to describe the dynamics of the prosthetic ankle in the interaction with the biological knee and hip joints of the residual leg as well as effects of foot-ground interaction and the upper part of the body. The goal for control of the prosthetic ankle joint will then be formulated as a tracking control problem. Necessary conditions for implementation of the control algorithms are also discussed.

7.1 Gait modeling and control of prosthetic ankle joint

Mathematical models and experimental data can be effectively combined to study normal and pathological gaits [130-133]. Figure 7.1 shows the diagram of the control-based approach which concentrates on generating suitable control signals to drive the model dynamics along desired trajectories obtained from the analysis of human gait [134]. In this approach, different methods of generating the joint torque can be analytically evaluated and the overall performance can be improved by feedback modification. Similarly, simulation approaches which combine mathematical gait models and experimental data can be used to study the effect of prostheses on kinematic behaviors and other aspects of the gait [135, 136] without posing a risk of injury due to

prosthetic malfunctions when testing on human subjects [137]. Such frameworks enable a quick evaluation of the performance of prosthetic devices under different operating conditions and extend the understanding of the prosthetic ankle-foot systems [4]. Modeling and control of the prosthetic devices could also be beneficial from the approaches used in robotics systems as they are sharing some common characteristics [138]. Modeling and control approaches not only provide useful insight into the contribution of muscles and prostheses in walking mechanism of people with below-knee amputation [139] but also can aid the development and functional evaluation of future prosthetics devices [135, 140].

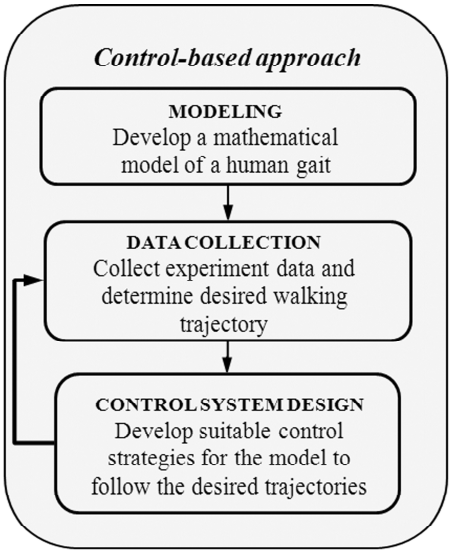

Figure 7.1. Control-based approach to the modeling and control of human gait.

Next generation prosthetic feet are likely to be equipped with controlled actuators to provide continuous displacement of the artificial ankle joint and help achieve desired gait performance [77]. However, control of the ankle prosthesis to replicate the

movement of a healthy ankle by tracking a displacement profile during gait is a difficult task. The reasons are

a) The ideal ankle displacement profile depends on several factors such as user gait (e.g., stance time, swing time, step length, and stride length), selected walking speed, inclination of the terrain, and type of activity (e.g., walking on level ground, ascending/descending stairs), etc. Due to changes in gait and terrain and unknown intent of the user, the ideal ankle displacement profile cannot be specified a priori.

b) During gait, the movement of the prosthetic foot is influenced by the reaction force due to the interaction with the terrain. This ground reaction force (GRF) plays a critical role in supporting the body weight, ensuring stability, and providing the propulsion for the gait [25]. GRF causes a reaction torque at the joint that has to be compensated for proper tracking behavior. However, GRF is usually computed using motion tracking systems and force plates in a laboratory setting [28] which is not applicable for the prosthetic control purpose.

c) The dynamics of the foot are affected by the nonlinear coupling effects between the prosthetic ankle joint and the biological knee and hip joints of the individuals with below-knee amputation. These effects not only depend on anthropometric measurements of the human body but also vary with gait. Neglecting these interactions will lead to larger tracking errors for a specified ankle displacement profile.

A framework for modeling and control of the prosthetic ankle joint will be developed to overcome those difficulties. In this framework, the following steps will be implemented.

a) First, the dynamic representation of movement of the leg on the amputated side of an individual with unilateral below-knee amputation will be modeled by a link-segment diagram in the sagittal plane using the Euler-Lagrange approach. The resulted mathematical model will be comprised of the biological knee and biological hip joints of which the movements are assumed to be controlled by the residual leg, and the prosthetic ankle joint which is controlled by an external actuator.

b) Then the dynamics of the prosthetic ankle joint will be extracted from the full gait model. The ankle dynamics itself and the reflected dynamics from the knee and hip joints contribute to the unknown ankle dynamics during gait. The ankle dynamical model will also include the disturbance torque from the Head-Arm-Trunk as well as effect of the ground reaction torque.

c) The control goal for the prosthetic ankle joint will be formulated as the tracking control problem of a desired (ideal) ankle joint trajectory.

d) However, the ideal joint profile is not available due to unknown users' intent and changes in walking terrain. Gait data measured from the amputees will aid in recognizing the gait type and detecting the gait events. Then a desired ankle joint displacement profile will be generated correspondingly to the recognized gait type and used in the development of control algorithms.

e) Since the actual ground reaction torque is not available, the gait-based ground reaction torque will be generated based on the recognized gait and the actual ground reaction will be compensated by an empirical viscoelastic contact model describing the foot-ground interaction during gait.

f) Boundary conditions which are required for implementation of the control algorithms will also be discussed. These conditions include the bounds on the gait-based ankle trajectory, gait-based ground reaction torque and the disturbance torques.

g) Error dynamic representation of the prosthetic ankle joint will be described to illustrate the relationship between the control torque and the ankle joint tracking error.

h) Finally, two learning-based control approaches with the use of multi-layer neural networks will be implemented. In the first approach, a neural network is trained to learn the unknown ankle dynamics and used for computation of the ankle torque. The second approach involves the optimization of a gait-related performance index and generation of an optimal torque for the ankle joint. The control torque is computed online to adapt to the change in gait of an individual.

The remaining of this chapter will describe all the steps above except the last step of control algorithm implementations. In Chapter 8 and Chapter 9, the multi-layer neural network-based ankle torque control strategies will be described in more details.

7.2 Framework for modeling of the prosthetic ankle joint during gait

In this section, the leg on the amputated side of a person with unilateral below-knee amputation is modeled by a link-segment diagram in the sagittal plane where most of the ankle joint movements occur during gait. This representation includes a biological knee joint, a biological hip joint, and a prosthetic ankle joint on the prosthetic foot. Euler-Lagrange approach is used to derive the dynamics of this representation. By

assuming the total human control of the biological joints, this section then concentrates on dynamics and control of the ankle joint.

7.2.1 Link-segment diagram

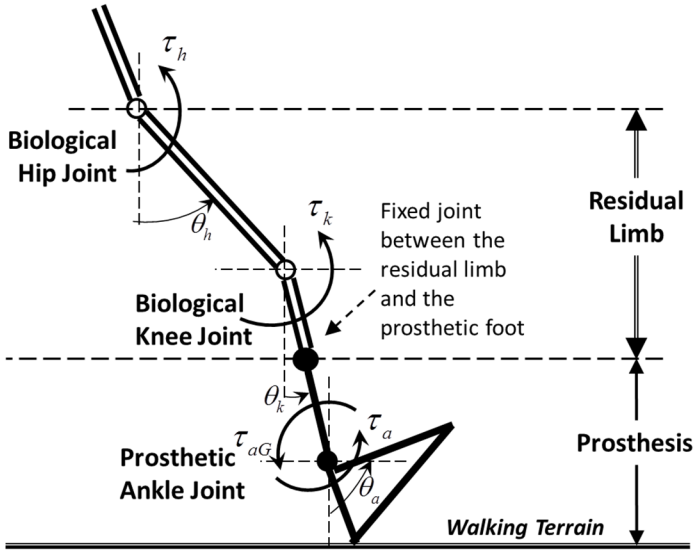

Figure 7.2. Link-segment diagram of the residual limb and prosthetic foot.

Figure 7.2 represents the link-segment diagram of the leg on the amputated side of an individual in the sagittal plane. The dynamics of this diagram can be obtained using the Euler-Lagrange approach [28, 141] and presented as follows:

$$M(\theta)\ddot{\theta}+V(\theta,\dot{\theta})\dot{\theta}+G(\theta)+\tau_d=\tau, \tag{7.1}$$

with the time-dependent joint variable θ(rad), input torque τ (Nm) and disturbance torque τ_d (Nm). The joint variable $\theta(t)=\begin{bmatrix}\theta_a(t) & \theta_k(t) & \theta_h(t)\end{bmatrix}^T \in \mathbb{R}^3$ represents the angular position of the prosthetic ankle joint, the biological knee joint, and the biological hip joint. Input torque to the model is $\tau(t)=\begin{bmatrix}\tau_a+\tau_{aG} & \tau_k & \tau_h\end{bmatrix}^T$ with $\tau_a(t)$ is the external torque generated by the actuator at the prosthetic ankle joint; $\tau_{aG}(t)$ is the ground reaction torque (GRT) and caused by the interaction between the prosthetic

foot and the ground during gait; $\tau_k(t)$ and $\tau_h(t)$ describe the internal torques generated by the biological knee and hip joints, respectively. The additional component $\tau_d(t) = [\tau_{ad} \quad \tau_{kd} \quad \tau_{hd}]^T$ represents the disturbance torque which is generated by the movement of the Head-Arm-Trunk (HAT), i.e., upper body, during gait. It is important to note that total human control is assumed at the biological knee joint and biological hip joint [28]. Therefore, knee torque $\tau_k(t)$ and hip torque $\tau_h(t)$ are purposely generated by the user to compensate for the coupling effects from the ankle joint, effect of ground reaction, and disturbance torque from the HAT. Finally, nonlinear terms in (7.1) include the inertia matrix $M(\theta)$, the vector of Coriolis and Centripetal forces $V(\theta,\dot{\theta})\dot{\theta}$, and the vector representing gravitational forces $G(\theta)$. Detailed dynamical equations and the parameters of the model are given in Appendix A1.

7.2.2 Ankle joint dynamics

Since total human control is assumed at the biological knee joint and the biological hip joint of the residual limb, this dissertation focuses on the dynamics and control of the ankle prosthesis. Dynamics of the prosthetic ankle joint can be extracted from (7.1) as follows:

$$\underbrace{\underbrace{M_{aa}\ddot{\theta}_a + V_{aa}\dot{\theta}_a + G_a}_{\text{independent ankle dynamics}} + \underbrace{M_{ak}\ddot{\theta}_k + V_{ak}\dot{\theta}_k}_{\text{reflected dynamics of knee joint}} + \underbrace{M_{ah}\ddot{\theta}_h + V_{ah}\dot{\theta}_h}_{\text{refected dynamics of hip joint}}}_{\textit{UNKNOWN ANKLE DYNAMICS}} + \underbrace{\tau_{ad}}_{\substack{\text{disturbance} \\ \text{from the HAT}}} = \underbrace{\tau_a}_{\substack{\text{control} \\ \text{torque}}} + \underbrace{\tau_{aG}}_{\substack{\text{ground reaction} \\ \text{torque}}}. \tag{7.2}$$

Unknown dynamics of the prosthetic ankle joint (7.2) include the dynamics that depend only on the ankle angular position and its derivatives $\left(M_{aa}\ddot{\theta}_a + V_{aa}\dot{\theta}_a + G_a\right)$, the coupling between the ankle joint and the biological knee joint $\left(M_{ak}\ddot{\theta}_k + V_{ak}\dot{\theta}_k\right)$, and the coupling

between the ankle joint and the biological hip joint $\left(M_{ah}\ddot{\theta}_h + V_{ah}\dot{\theta}_h\right)$. The components M_{aa}, V_{aa}, G_a, M_{ak}, V_{ak}, M_{ah} and V_{ah} are nonlinear functions of the joint angles as listed in the Appendix A1. Ankle dynamics are also affected by the ground reaction torque τ_{aG} and the HAT disturbance torque τ_{ad}.

7.3 Framework for control of the prosthetic ankle joint

Commonly used approaches in control of prosthetic feet treat the unknown dynamics in (7.2) as disturbances and ignore them, thereby degrading the performance and efficiency of the device. These devices are based on linearized dynamics and use proportional-derivative control with fixed control parameters. While these controllers guarantee local stability, their performance might deteriorate quickly in the presence of unmodeled system dynamics and measurement noises. The use of these systems will require prior validation on a large number of subjects under different gait and terrain conditions [41].

In this framework, the goal for control of the prosthetic ankle joint is to track a desired ankle displacement profile during gait. Effectiveness of this control is measured by the deviation of the actual ankle joint angular position from the desired trajectory [134]. That desired, gait-based trajectory is specifically generated for the type of gait which can be recognized by continuous measurement and interpretation of the gait data captured from the persons with below-knee amputation. Control torque τ_a is then computed by different control algorithms for manipulating the movement of the prosthetic ankle joint to follow the gait-based ankle displacement profile. The detailed control framework and problem formulation are discussed in the next section.

7.3.1 Goals for the prosthetic ankle control

As described earlier in Section 2.1, the prosthetic ankle is controlled by a torque generated by an external actuator to follow a displacement profile similar to that of a natural ankle (Figure 2.2). The control system of the prosthetic ankle joint is therefore required to overcome the challenges described in Section 2.6.2 and summarized in Section 7.1. The goals for the control system of the prosthetic ankle joint are listed below:

- Recognize the type of gait and detect the gait events in real time using actual gait data measured from the users
- Determine an ankle joint displacement profile corresponding to the selected gait of users
- Compensate the effect of ground reaction τ_{aG}
- Implement a control algorithm to generate a control torque τ_a that provides guaranteed tracking performance

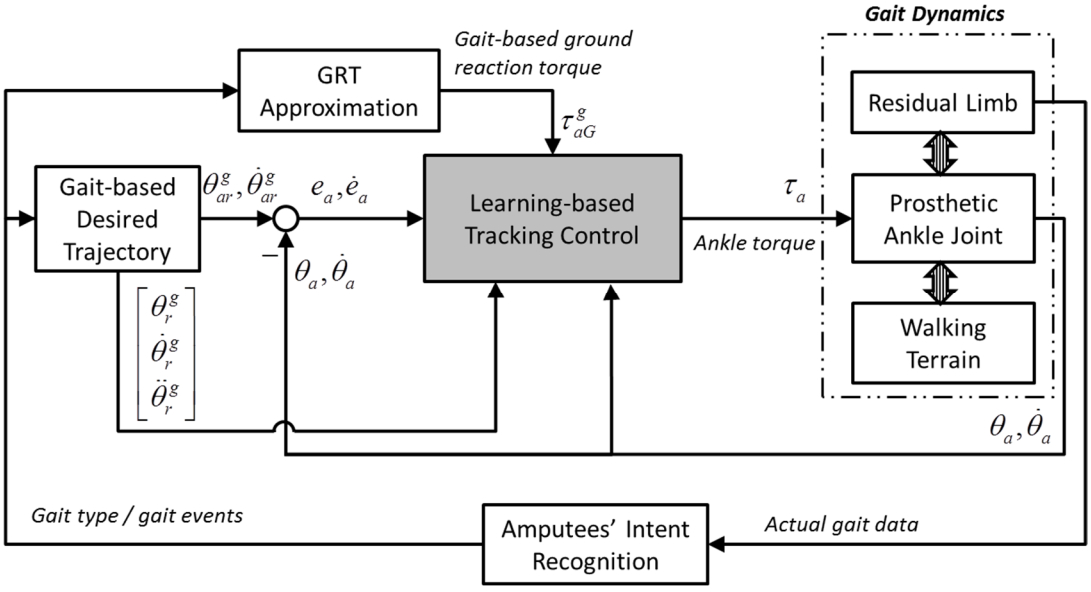

Figure 7.3. Block diagram of the learning-based control structure of the prosthetic ankle joint.

7.3.2 Recognition of gait and detection of gait events

Recognition of gait and detection of gait events can be done using actual gait data such as residuum socket interface force measured from the prosthetic socket of individuals with below-knee amputation. RSI forces that the residual limb applies on the prosthetic socket during gait can be captured by ultra-thin FlexiForce® sensors [102] and a gait monitoring device as seen in Figure 2.9 [23]. These sensors (Figure 6.1) can be embedded inside the socket to provide non-intrusive force measurement in real time and during daily activities outside the laboratory setup.

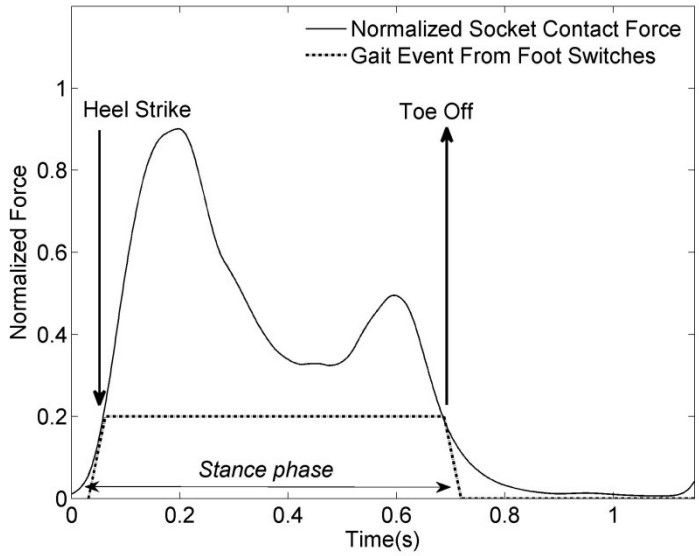

Figure 7.4. Normalized socket contact force and gait events from foot switches.

It has been shown that the recorded RSI forces relate to the gait [122] and can be used to distinguish between different gait types (e.g., normal self-paced walk, brisk walk, ascending/descending stairs, walking on a ramp), and detect gait parameters (*Heel Strike*, *Mid-stance*, *Toe Off* , stance time, etc.) for each detected gait [142]. Comparison of RSI forces with gait events measured using foot switches is shown in Figure 7.4. The

typical double peak shape of the loading profile in Figure 7.4 also confirms that the mechanisms of the weight transferred between the prosthetic side and the intact side of persons with unilateral below-knee amputation have common characteristics with subjects without amputation of the lower limb.

As in Chapter 6, features extracted from the RSI force measured from the distal end-bearing locations inside the prosthetic sockets of a group of subjects with transtibial osteomyoplastic amputation can be used to distinguish the gaits with different walking speeds and provide promising results (Table 6.3).

Based on the recognized gait type and detected gait events, the updated gait-based kinematic references and approximated ground reaction torque are then specifically generated for the recognized gait type and are activated at the moment when ground contact (*Heel Strike*) is observed. Then, the proposed control approach uses these gait-based quantities to calculate an appropriate control torque for the recognized gait.

7.3.3 Gait-based displacement profile

In traditional control, the tracking error is computed as the error between the ideal and actual displacement of the joint. In the case of prosthetic ankle control, the ideal joint profile is not available due to unknown users' intent and changes in walking terrain. Therefore, as the first step, an approximated ankle joint displacement profile is generated based on the gait detected in real time.

Figure 7.3 shows the block diagram of the controlled 'residual limb–prosthetic foot' system. During the gait, the *Amputees' Intent Recognition* block (Figure 7.3) recognizes the intent of users using the actual gait data measured from the prosthetic socket and the *Residual Limb* [142]. Then, the corresponding gait-based kinematic references

$$
\begin{aligned}
\underline{\theta}_r^g &= \left[\theta_r^{g^T} \quad \dot{\theta}_r^{g^T} \quad \ddot{\theta}_r^{g^T} \right]^T \\
\theta_r^g(t) &= \left[\theta_{ar}^g(t) \quad \theta_{kr}^g(t) \quad \theta_{hr}^g(t) \right]^T \\
\dot{\theta}_r^g(t) &= \left[\dot{\theta}_{ar}^g(t) \quad \dot{\theta}_{kr}^g(t) \quad \dot{\theta}_{hr}^g(t) \right]^T \\
\ddot{\theta}_r^g(t) &= \left[\ddot{\theta}_{ar}^g(t) \quad \ddot{\theta}_{kr}^g(t) \quad \ddot{\theta}_{hr}^g(t) \right]^T
\end{aligned}
\tag{7.3}
$$

are generated specifically for the recognized gait. The superscript $(.)^g$ indicates that these profiles are generated based on the determination of the type of gait. Let $\underline{\theta}_r = \left[\theta_r^T \quad \dot{\theta}_r^T \quad \ddot{\theta}_r^T \right]^T$ denotes the ideal kinematic profiles which are not available to the computation of the control input τ_a. Then, the difference between the ideal kinematic references and the gait-based references are defined as

$$
\begin{aligned}
\underline{\tilde{\theta}}_r &= \left[\tilde{\theta}_r^T \quad \dot{\tilde{\theta}}_r^T \quad \ddot{\tilde{\theta}}_r^T \right]^T \\
\tilde{\theta}_r &= \theta_r - \theta_r^g \\
\dot{\tilde{\theta}}_r &= \dot{\theta}_r - \dot{\theta}_r^g \\
\ddot{\tilde{\theta}}_r &= \ddot{\theta}_r - \ddot{\theta}_r^g .
\end{aligned}
\tag{7.4}
$$

7.3.4 Gait-based ground reaction torque

Calculation of the ground reaction torque τ_{aG} during gait requires kinematic tracking systems and force plates in the laboratory environments [28, 71]. Therefore under normal gait conditions, τ_{aG} is not available for the calculation of the control input τ_a. In the control scheme shown in Figure 7.3, the gait-based ground reaction torque τ_{aG}^g is generated based on the recognized gait and an empirical model describing the foot-ground contact. The gait-based torque τ_{aG}^g is then included into the control computation

to compensate for the actual τ_{aG}. The difference between the gait-based τ_{aG}^{g} and the actual ground reaction torque τ_{aG} at the prosthetic ankle joint is defined as

$$\tilde{\tau}_{aG} = \tau_{aG} - \tau_{aG}^{g}. \tag{7.5}$$

The actual ground reaction torque τ_{aG} (Figure 7.2) is approximated by

$$\tau_{aG}^{g}(t) = d_{aZ}(t) F_X(t) + d_{aX}(t) F_Z(t), \tag{7.6}$$

where t is the gait time, $F_X(\mathrm{N})$, $F_Z(\mathrm{N})$ are the horizontal and vertical ground reaction forces, and $d_{aX}(\mathrm{m})$, $d_{aZ}(\mathrm{m})$ are the horizontal and vertical distances between ankle joint and the center of pressure (contact point) during gait. These quantities depend on the height and weight of the individual, as well as the terrain and type of gait.

During gait on level ground, ground reaction forces F_X, F_Z can be modeled by a combination of a spring and a position-dependent damper as follows [130, 131, 143]:

$$F_Z = \bar{k}\left(\bar{z}_{PEN}\right)^{\bar{e}} + \bar{c}_d \dot{\bar{z}}_{PEN} \tag{7.7}$$

$$F_X = \bar{\mu} F_Z \operatorname{sgn}\left(\dot{\bar{x}}_P\right), \tag{7.8}$$

in which $\bar{z}_{PEN}(\mathrm{m})$, $\dot{\bar{z}}_{PEN}(\mathrm{m/s})$ are the penetration and penetration rate of the foot into the ground; $\bar{k}(\mathrm{N/m}), \bar{e}$ are spring coefficient and spring exponent; $\bar{c}_d(\mathrm{N/(m/s)})$ is the damping coefficient; $\bar{\mu}$ is the friction coefficient; $\dot{\bar{x}}_P(\mathrm{m/s})$ is the horizontal velocity of the contact point with respect to the ground, and $\operatorname{sgn}(.)$ is the sign function. These parameters can be obtained using experiments similar to the works in [131] and [143].

The distances d_{aX}, d_{aZ} depend on the gait-based references $\underline{\theta}_r^g$, temporal gait parameters, and the contact profiles assumed for the prosthetic feet.

7.3.5 Boundary conditions

This section discusses the boundary conditions which are necessary for implementation of the control algorithms in Chapter 8 and Chapter 9.

Bound on the gait-based kinematic references and the reference error

The gait-based kinematic references $\underline{\theta}_r^g$ satisfying the bound condition $\left\|\underline{\theta}_r^g\right\| \le B_{\theta_r^g} \in \mathbb{R}$ can be generated for each gait type. Since the human gait and joint movements are cyclic in nature, the gait-based kinematic references can be generated using Fourier series as follows [131]

$$\theta_r^g(t) = a_g^0 + \sum_{k_g=1}^{5} a_g^{k_g} \cos\left(k_g w_g t\right) + b_g^{k_g} \sin\left(k_g w_g t\right), \tag{7.9}$$

where t denotes gait time and the parameters $\left(a_g^0, a_g^{k_g}, b_g^{k_g}, w_g\right)$ can be obtained for specific gait types. Since the sine and cosine functions in (7.9) are bounded, the gait-based kinematic patterns $\underline{\theta}_r^g$ are also bounded. The ideal kinematic references $\underline{\theta}_r$ are also bounded, i.e., $\left\|\underline{\theta}_r\right\| \le B_{\theta_r} \in \mathbb{R}$ due to the cyclic nature of gait and the human control of the movement of the residual limb to follow specific joint patterns which help minimize the metabolic energy consumption during gait [30]. Finally, the kinematic reference error $\underline{\tilde{\theta}}_r$ is also bounded because $\underline{\theta}_r, \underline{\theta}_r^g$ are both bounded and $\underline{\tilde{\theta}}_r = \underline{\theta}_r - \underline{\theta}_r^g$.

Bound on the gait-based ground reaction torque

It can be seen that τ_{aG}^g in (7.6) is bounded because F_X, F_Z in (7.7) and (7.8) are modeled by passive mechanical components and finite penetration, and d_{aX}, d_{aZ} are

functions of the bounded kinematic references. The actual ground reaction torque τ_{aG} is also bounded due to its cyclic nature and the finite body weight. Therefore, the difference $\tilde{\tau}_{aG} = \tau_{aG} - \tau_{aG}^{g}$ is bounded.

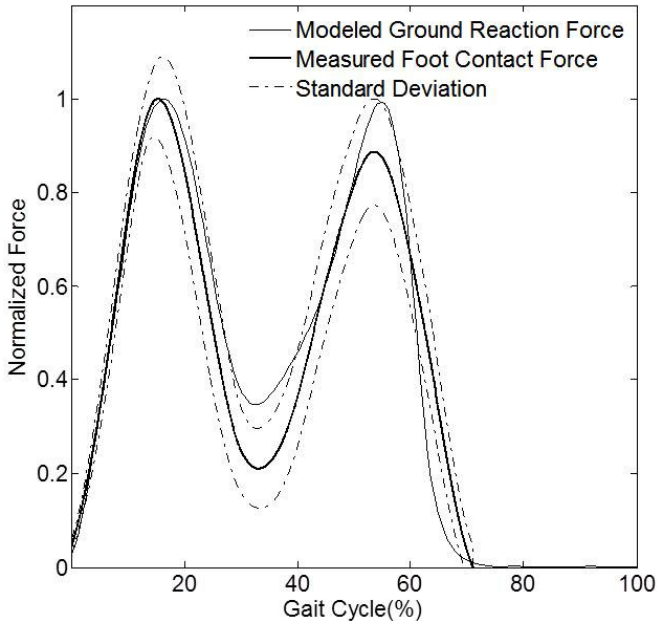

Figure 7.5. Approximated ground reaction force and loading profile from actual foot pressure sensors.

The dependence of the vertical ground reaction force generated by the empirical model on the gait cycle (7.7) is confirmed by the actual foot loading profile during a normal gait on level ground of an able bodied. The normalized foot loading profile in Figure 7.5 is calculated as the summation of the forces measured by force sensors (FlexiForce® A201,[102]) placed under the heel, the outer ball of the foot, and the toe of the foot. The typical double peak shape of the modeled ground reaction force also agrees with ground reaction force captured using force plates as found in the literature [28, 71].

Bound of the disturbance torque

It has been shown that the upper body movement and arm swing during gait are passive and mainly powered by the movement of the lower body [144]. These movements are in fact the human efforts to further stabilize the gait and reduce metabolic energy consumption during gait [145]. Calculation of the Head-Arm-Trunk torque from the quantitative gait data in [28] also confirms that this is a bounded quantity. In the ankle dynamics (7.2), the external disturbance τ_{ad} represents the HAT torque, therefore is bounded.

7.3.6 Error dynamics

The (pseudo) ankle joint tracking error is defined as

$$e_a = \theta_{ar}^g - \theta_a. \tag{7.10}$$

Then the dynamics in (7.2) can be expressed as

$$\begin{aligned} M_{aa}\ddot{e}_a = &-V_{aa}\dot{e}_a + M_{aa}\ddot{\theta}_{ar}^g + V_{aa}\dot{\theta}_{ar}^g + G_a + \\ &+M_{ak}\ddot{\theta}_k + V_{ak}\dot{\theta}_k + M_{ah}\ddot{\theta}_h + V_{ah}\dot{\theta}_h + \tau_{ad} - \tau_a - \tau_{aG}. \end{aligned} \tag{7.11}$$

Unknown terms in (7.11) are grouped into

$$\begin{aligned} f = &\left[M_{aa}\left(\ddot{\theta}_{ar}^g + \lambda\dot{e}_a\right) + V_{aa}\left(\dot{\theta}_{ar}^g + \lambda e_a\right) + G_a\left(\theta_a\right)\right] + \\ &+\left[M_{ak}\ddot{\theta}_k + V_{ak}\dot{\theta}_k \right] + \left[M_{ah}\ddot{\theta}_h + V_{ah}\dot{\theta}_h \right]. \end{aligned} \tag{7.12}$$

Defining the filtered tracking error as

$$r = \dot{e}_a + \lambda e_a, \tag{7.13}$$

with $\lambda > 0$. Then, using (7.11), the closed loop error dynamics can be expressed as

$$M_{aa}\dot{r} = -V_{aa}r + f + \tau_{ad} - \tau_a - \tau_{aG}. \tag{7.14}$$

The actual tracking error of the prosthetic ankle joint is calculated as the difference between the ideal displacement profile θ_{ar} (which is not available to the control computation) and the actual ankle angular position θ_a as follows.

$$e_a^{actual} = \theta_{ar} - \theta_a. \tag{7.15}$$

It is important to note that e_a in (7.10) defines the (pseudo) tracking error similar to the traditional neural network control approach [146].

7.4 Conclusions

In this chapter, a framework for the modeling and control of the prosthetic ankle joint was described. Dynamical model of the ankle joint and its interaction with the unaffected joints of the residual leg and foot-ground interaction were obtained. In the next two chapters, the ankle torque control τ_a in (7.14) will be computed using two different approaches. The control algorithm in Chapter 8 will primary focus on learning the unknown ankle dynamics which are described in (7.12) and reducing the filtered tracking error r as defined in (7.13). In Chapter 9, the control approach aims to minimize a long-term cost function which relates to the tracking performance of the prosthetic ankle joint.

Chapter 8: Neural Network Control of a Prosthetic Ankle Joint

Current active prosthetic feet on the market utilize traditional control approaches which tent to ignore the dynamical interactions between the prosthetic ankle joint and the biological joints and the foot-ground relationship during gait. These factors are treated as disturbances and can quickly degrade the performance of the prostheses when the gait and terrain conditions change. In this chapter, an artificial neural network-based hierarchical controller is implemented to adaptively compensate for the unmodeled dynamics and disturbances for closed loop stability with guaranteed tracking performance. The closed-loop stability will be rigorously analyzed using Lyapunov stability theory and the robustness of the controller will be studied using actual gait data collected from human subjects. Numerical simulations in the presence of noises, uncertainties in terrain interaction, disturbance torques, and changes in gait will be performed to evaluate the tracking performance and robustness of the control approach.

8.1 Approximation of the unknown ankle dynamics

In this section, an artificial neural network will be used to approximate the unknown nonlinear terms (in equation (7.2)) that represent the interaction between the prosthetic ankle joint and the biological knee and hip joints of the residual limb (Figure 7.3). Inputs to the ANN are obtained from the actual angular kinematics of the ankle joint $\left(\theta_a, \dot{\theta}_a\right)$ and the gait-based kinematic references, $\underline{\theta}_r^g$, which are generated specifically for the recognized gait type. It is important to note that, the control structure in Figure 7.3 performs tracking of the gait-based reference θ_{ar}^g instead of the predetermined trajectory θ_{ar} as in a traditional neural network-based control approach.

The physical constraints on the joints imply that $(\theta_a, \theta_k, \theta_h)$ and their derivatives are finite. Therefore, the function f in (7.12) is a real function and is bounded on a compact region in $\mathbb{R}$. Since human gait comprises of multiple gait cycles, f is also a periodic function. Therefore, f can be approximated by an artificial neural network with one hidden layer and ideal target weights $W_f \in \mathbb{R}^{N_h \times 1}$, $V_f \in \mathbb{R}^{N_x \times N_h}$ as follows:

$$f(x) = W_f^T \sigma\left(V_f^T x\right) + \varepsilon, \tag{8.1}$$

in which, $x \in \mathbb{R}^{N_x \times 1}$ is the vector of the neural network inputs, ε is the bounded approximation error, i.e., $\|\varepsilon\| < \varepsilon_B \in \mathbb{R}$, $\sigma(.)$ is a sigmoidal activation function, and N_h is the number of nodes in the hidden layer. The neural network input x is selected as follows:

$$x = \begin{bmatrix} e_a & \dot{e}_a & \theta_{ar}^g & \dot{\theta}_{ar}^g & \ddot{\theta}_{ar}^g & \theta_{kr}^g & \dot{\theta}_{kr}^g & \ddot{\theta}_{kr}^g & \theta_{hr}^g & \dot{\theta}_{hr}^g & \ddot{\theta}_{hr}^g \end{bmatrix}^T. \tag{8.2}$$

The ideal weights W_f, V_f are unknown but they can be approximated by adjustable weights $\hat{W}_f \in \mathbb{R}^{N_h \times 1}$, $\hat{V}_f \in \mathbb{R}^{N_x \times N_h}$ with the network weight errors

$$\begin{aligned} \tilde{W}_f &= W_f - \hat{W}_f \\ \tilde{V}_f &= V_f - \hat{V}_f. \end{aligned} \tag{8.3}$$

Then, the unknown function f is therefore approximated by

$$\hat{f}(x) = \hat{W}_f^T \sigma\left(\hat{V}_f^T x\right), \tag{8.4}$$

with the neural network approximation error given by

$$\tilde{f} = f - \hat{f} = W_f^T \sigma\left(V_f^T x\right) - \hat{W}_f^T \sigma\left(\hat{V}_f^T x\right) + \varepsilon \tag{8.5}$$

Using Taylor series expansion of $\sigma\left(V_f^T x\right)$ around $\left(\hat{V}_f^T x\right)$ for a given x, (8.5) can be expressed as

$$\begin{aligned}\tilde{f} &= W_f^T\left[\sigma\left(\hat{V}_f^T x\right)+\sigma'\left(\hat{V}_f^T x\right)\left(V_f^T x-\hat{V}_f^T x\right)+\left(H.O.T\right)\right]-\hat{W}_f^T\sigma\left(\hat{V}_f^T x\right)+\varepsilon \\ &= W_f^T\left[\hat{\sigma}+\hat{\sigma}'\tilde{V}_f^T x+\left(H.O.T\right)\right]-\hat{W}_f^T\hat{\sigma}+\varepsilon \\ &= \tilde{W}_f^T\hat{\sigma}+W_f^T\hat{\sigma}'\tilde{V}_f^T x+W_f^T\left(H.O.T\right)+\varepsilon,\end{aligned} \tag{8.6}$$

where $\hat{\sigma}=\sigma\left(\hat{V}_f^T x\right)$, $\hat{\sigma}'=\sigma'\left(V_f^T x\right)\Big|_{V_f^T x=\hat{V}_f^T x}$ is the Jacobian matrix of the activation function with respect to its inputs, $\tilde{V}_f^T x=V_f^T x-\hat{V}_f^T x$, and $\left(H.O.T\right)$ represents all high order terms in the Taylor series expansion of $\sigma\left(V_f^T x\right)$.

8.2 Control algorithm

Based on the discussions on the boundary conditions in Section 7.3.5, the following assumptions are made for the stability analysis of the control algorithm.

Assumption 8.2.1
The ideal kinematic references, gait-based kinematic references, and their differences are bounded, i.e., $\left\|\underline{\theta}_r\right\| \le B_{\theta_r} \in \mathbb{R}$, $\left\|\underline{\theta}_r^g\right\| \le B_{\theta_r^g} \in \mathbb{R}$ and $\left\|\underline{\tilde{\theta}}_r\right\| \le B_{\tilde{\theta}_r} \in \mathbb{R}$.

Assumption 8.2.2
The difference between the modeled ground reaction torque and the actual ground reaction torque experienced at the prosthetic ankle joint is bounded, i.e., $\left\|\tilde{\tau}_{aG}\right\| \le B_G \in \mathbb{R}$.

Assumption 8.2.3
The disturbance torque τ_{ad} due to the motion of the Head-Arm-Trunk is bounded, i.e., $\left\|\tau_{ad}\right\| \le B_d \in \mathbb{R}$.

Assumption 8.2.4

Ideal ANN weights are constant for each gait type and bounded, i.e., $\left\|Z_f\right\|_F \le B_Z \in \mathbb{R}$ where $\left\|.\right\|_F$ represents the Frobenius norm and $Z_f = \begin{bmatrix} W_f & \Theta \\ \Theta & V_f \end{bmatrix}$.

Theorem 8.2.1
Given the control structure in Figure 8.1, let the ankle torque be computed as:

$$\tau_a = \hat{f} - \tau_{aG}^g + K_V r - v, \tag{8.7}$$

with

- $\hat{f}$ – approximation of unknown nonlinear function f in (7.12)
- τ_{aG}^g – torque required to compensate for the actual ground reaction torque τ_{aG}
- r – filtered tracking error ($r = \dot{e}_a + \lambda e_a$),

$$K_V r = K_V \left(\dot{e}_a + \lambda e_a\right), \tag{8.8}$$

- and v is the robustifying term

$$v = -K_Z \left(\left\|\hat{Z}_f\right\|_F + B_Z\right) r. \tag{8.9}$$

Further, let the neural network weights be updated according to

$$\dot{\hat{W}}_f = R\hat{\sigma} r - R\hat{\sigma}'\hat{V}_f^T x r - kR\left\|r\right\|\hat{W}_f \tag{8.10}$$

$$\dot{\hat{V}}_f = Qx\left(\hat{\sigma}'\hat{W}_f r\right)^T - kQ\left\|r\right\|\hat{V}_f \tag{8.11}$$

where K_v, R, Q and k are real, positive design parameters. Then, the actual tracking error e_a^{actual} defined in (7.15) and the neural network weight errors $\tilde{W}_f$, $\tilde{V}_f$ are uniformly ultimately bounded.

Structure of the prosthetic ankle control system

The controller proposed in this chapter can be viewed as a hierarchical structure. At the lowest level, the controller is responsible for generating a control torque τ_a which drives the ankle joint to follow a gait-based reference trajectory θ_{ar}^g. This level reduces the tracking error by approximating the unknown ankle dynamics using an ANN and compensating the terrain interaction through the use of the gait-based ground reaction torque τ_{aG}^g. In the higher level of the hierarchy, the *Amputees' Intent Recognition* block (Figure 8.1) processes the gait data measured in real time from the individuals to recognize the type of gait and detect the gait events. Appropriate gait-based kinematic references $\underline{\theta}_r^g$ and ground reaction torque approximation τ_{aG}^g are then generated based on the users' gait.

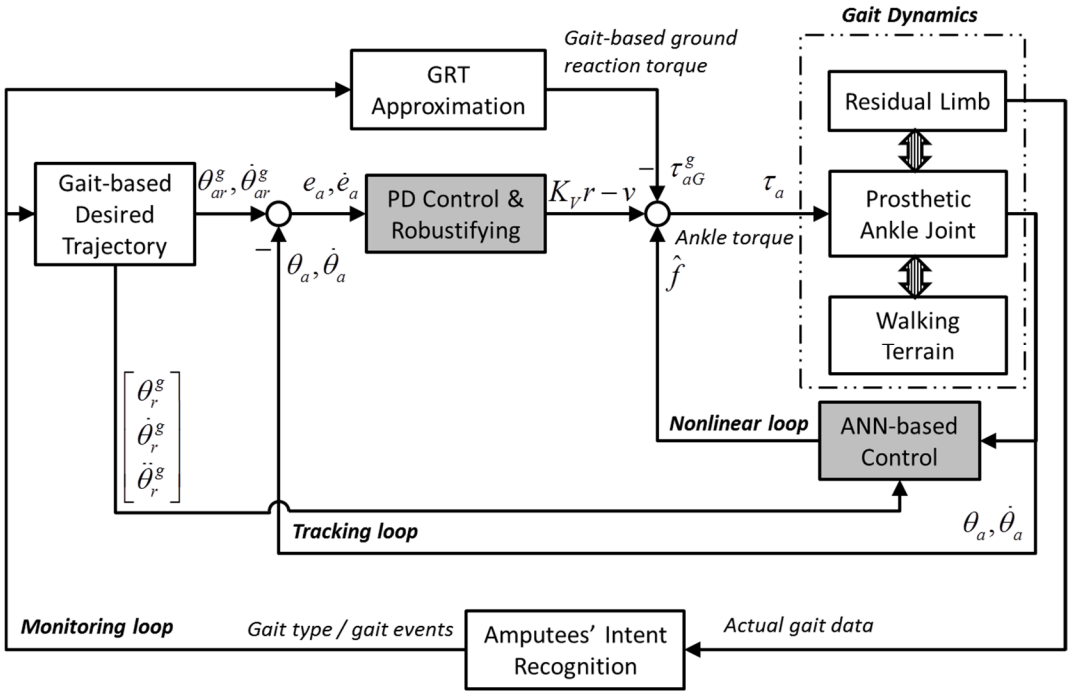

Figure 8.1. Block diagram of the feedback linearization neural network-based control structure of the prosthetic ankle joint.

The control approach in Figure 8.1 can also be viewed as a multi-loop structure. The inner most nonlinear loop comprises of an ANN that is responsible for approximating the unknown ankle dynamics. The outer tracking loop helps reduce the tracking error by comparing actual kinematic feedback $\left(\theta_a,\ \dot{\theta}_a\right)$ with the gait-based references $\left(\theta_{ar}^g,\ \dot{\theta}_{ar}^g\right)$. Finally, the monitoring loop processes the actual measured gait data to recognize the intent of an user. Compared to PD control of a prosthetic foot, this structure requires smaller control gains and is robust to external disturbances and changes in gait.

8.3 Stability analysis

With the control signal (8.7), the closed loop error dynamics (7.14) can be expressed as

$$\begin{aligned} M_{aa}\dot{r} &= -\left(V_{aa}+K_V\right)r + f - \hat{f} + \tau_{ad} - \tau_{aG} + \tau_{aG}^g + v \\ &= -\left(V_{aa}+K_V\right)r + \tilde{f} + \tau_{ad} - \tilde{\tau}_{aG} + v. \end{aligned} \tag{8.12}$$

Substituting $\tilde{f}$ from (8.6), then (8.12) can be written as

$$\begin{aligned} M_{aa}\dot{r} &= -\left(V_{aa}+K_V\right)r + \tilde{W}_f^T\hat{\sigma} + W_f^T\hat{\sigma}'\tilde{V}_f^T x + \left[W_f^T\left(H.O.T\right) + \varepsilon + \tau_{ad} - \tilde{\tau}_{aG} + v\right] \\ &= -\left(V_{aa}+K_V\right)r + \tilde{W}_f^T\hat{\sigma} + \left(\tilde{W}_f^T + \hat{W}_f^T\right)\hat{\sigma}'\tilde{V}_f^T x + \left[\ldots\right] \\ &= -\left(V_{aa}+K_V\right)r + \tilde{W}_f^T\hat{\sigma} + \tilde{W}_f^T\hat{\sigma}'\left(V_f^T - \hat{V}_f^T\right)x + \hat{W}_f^T\hat{\sigma}'\tilde{V}_f^T x + \left[\ldots\right] \\ &= -\left(V_{aa}+K_V\right)r + \tilde{W}_f^T\left(\hat{\sigma} - \hat{\sigma}'\hat{V}_f^T x\right) + \hat{W}_f^T\hat{\sigma}'\tilde{V}_f^T x + \tilde{W}_f^T\hat{\sigma}'V_f^T x + \left[\ldots\right]. \end{aligned} \tag{8.13}$$

Define the total uncertainty δ as

$$\delta = \tilde{W}_f^T\hat{\sigma}'V_f^T x + W_f^T\left(H.O.T\right) + \varepsilon + \tau_{ad} - \tilde{\tau}_{aG}, \tag{8.14}$$

then the closed-loop error dynamics can be simplified as

$$M_{aa}\dot{r} = -\left(V_{aa}+K_V\right)r + \tilde{W}_f^T\left(\hat{\sigma} - \hat{\sigma}'\hat{V}_f^T x\right) + \hat{W}_f^T\hat{\sigma}'\tilde{V}_f^T x + \delta + v. \tag{8.15}$$

Lemma 8.3.1 – Bound on the neural network inputs
The neural network input x is bounded by

$$\|x\| \le C_2 + C_3\|r\|, \tag{8.16}$$

where r is the filtered tracking error defined in (7.13), and C_2, C_3 are positive constants.

Proof: Given in the Appendix A2.

Lemma 8.3.2 – Bound on the high order terms in neural network approximation $(H.O.T)$

The high order terms in the neural network approximation are bounded by

$$\|H.O.T\| \le 1 + C_2 B_\sigma \left\|\tilde{Z}_f^T\right\|_F + C_3 B_\sigma \left\|\tilde{Z}_f^T\right\|_F \|r\|, \tag{8.17}$$

where r is the filtered tracking error, $\tilde{Z}_f = \begin{bmatrix} \tilde{W}_f & \Theta \\ \Theta & \tilde{V}_f \end{bmatrix}$, $\|\hat{\sigma}'\| \le B_\sigma$ and C_2, C_3 are positive constants.

Proof: Given in the Appendix A3.

Lemma 8.3.3 – Bound on the uncertainty δ

The uncertainty term δ is bounded by

$$\|\delta\| \le C_4 + C_5 B_Z \left\|\tilde{Z}_f^T\right\|_F + C_6 B_Z \left\|\tilde{Z}_f^T\right\|_F \|r\|, \tag{8.18}$$

Where r is the filtered tracking error, $\tilde{Z}_f = \begin{bmatrix} \tilde{W}_f & \Theta \\ \Theta & \tilde{V}_f \end{bmatrix}$, $\left\|Z_f\right\|_F \le B_Z$ and C_4, C_5, C_6 are positive constants.

Proof: Given in the Appendix A4.

Proof of Theorem 8.2.1

With the selection of finite neural network input x in (8.2), the ideal neural network $W_f^T \sigma\left(V_f^T x\right)$ can be defined in a compact set $S_x = \{x, \|x\| < B_x\}$ and therefore provides a bounded approximation for the nonlinear function f. The proof of the theorem includes

two parts. First, the boundedness of the (pseudo) tracking error e_a in (7.10) is showed using a procedure inspired by the traditional neural network control approach [146]. Then the actual error e_a^{actual} in (7.15) which describes the movement tracking performance of the prosthetic ankle joint is showed to be bounded due to the triangle inequality of vector norms.

The neural network $\hat{f}(x) = \hat{W}_f^T \sigma\left(\hat{V}_f^T x\right)$ is defined for x on a compact set $S_x = \{x, \|x\| < B_x\}$ to approximate the unknown nonlinear function f in (7.12). From the inequality (8.16), define the compact set $S_r = \{r, \|r\| < B_r\}$ in which $B_r = (B_x - C_2)/C_3$, then the universal approximation property of the neural network holds for all $r \in S_r$.

Now, consider the Lyapunov function

$$\ell = \frac{1}{2} r M_{aa} r + \frac{1}{2} tr\left\{\tilde{W}_f^T R^{-1} \tilde{W}_f\right\} + \frac{1}{2} tr\left\{\tilde{V}_f^T Q^{-1} \tilde{V}_f\right\}, \tag{8.19}$$

with r defined in (7.13), $\tilde{W}_f$, $\tilde{V}_f$ in (8.3), and R, Q in (8.10)-(8.11), respectively.

Taking derivatives of ℓ

$$\dot{\ell} = r M_{aa} \dot{r} + \frac{1}{2} r \dot{M}_{aa} r + tr\left\{\tilde{W}_f^T R^{-1} \dot{\tilde{W}}_f\right\} + tr\left\{\tilde{V}_f^T Q^{-1} \dot{\tilde{V}}_f\right\}, \tag{8.20}$$

then with $M_{aa}\dot{r}$ from (8.15),

$$\begin{aligned} \dot{\ell} = & -r K_V r + \frac{1}{2} r\left(\dot{M}_{aa} - 2V_{aa}\right) r + r\left[\tilde{W}_f^T\left(\hat{\sigma} - \hat{\sigma}'\hat{V}_f^T x\right) + \hat{W}_f^T \hat{\sigma}' \tilde{V}_f^T x + \delta + v\right] \\ & + tr\left\{\tilde{W}_f^T R^{-1} \dot{\tilde{W}}_f\right\} + tr\left\{\tilde{V}_f^T Q^{-1} \dot{\tilde{V}}_f\right\}. \end{aligned} \tag{8.21}$$

The term $r\left(\dot{M}_{aa} - 2V_{aa}\right) r$ vanishes because M_{aa} is a constant and the choice of the reference frame makes $V_{aa} = 0$. Then (8.21) can then be simplified as,

$$\dot{\ell} = -rK_V r + tr\left\{\tilde{W}_f^T\left(R^{-1}\dot{\hat{W}}_f + \hat{\sigma}r - \hat{\sigma}'\hat{V}_f^T xr\right)\right\} + \\ + tr\left\{\tilde{V}_f^T\left(Q^{-1}\dot{\hat{V}}_f + xr\hat{W}_f^T\hat{\sigma}'\right)\right\} + r\left(\delta + v\right) \tag{8.22}$$

Since the ideal neural network weights W_f, V_f are constant, then

$$\dot{\tilde{W}}_f = \dot{W}_f - \dot{\hat{W}}_f = -\dot{\hat{W}}_f = -R\hat{\sigma}r + R\hat{\sigma}'\hat{V}_f^T xr + kR\|r\|\hat{W}_f \tag{8.23}$$

$$\dot{\tilde{V}}_f = V_f - \dot{\hat{V}}_f = -\dot{\hat{V}}_f = -Qx\left(\hat{\sigma}'\hat{W}_f r\right)^T + kQ\|r\|\hat{V}_f, \tag{8.24}$$

and (8.22) becomes,

$$\dot{\ell} = -rK_V r + k\|r\|tr\left\{\tilde{Z}_f^T\left(Z_f - \tilde{Z}_f\right)\right\} + r\left(\delta + v\right). \tag{8.25}$$

Since $tr\left\{\tilde{Z}_f^T\left(Z_f - \tilde{Z}_f\right)\right\} \le \left\|\tilde{Z}_f\right\|_F\left(B_Z - \left\|\tilde{Z}_f\right\|_F\right)$ and δ is bounded as in (8.18), by selecting $K_Z > C_6$, then

$$\dot{\ell} \le -\|r\|\left\{K_V\|r\| - k\left\|\tilde{Z}_f\right\|_F\left(B_Z - \left\|\tilde{Z}_f\right\|_F\right) - C_4 - C_5\left\|\tilde{Z}_f\right\|_F\right\}. \tag{8.26}$$

Defining

$$C_7 = B_Z + \frac{C_5}{k}, \tag{8.27}$$

then (8.26) can be written as:

$$\dot{\ell} \le -\|r\|\left\{K_V\|r\| + k\left[\left\|\tilde{Z}_f\right\|_F - \frac{C_7}{2}\right]^2 - \frac{kC_7^2}{4} - C_4\right\}. \tag{8.28}$$

LaSalle extension of the Lyapunov stability theory [147] states that the filtered tracking error r and the neural network weight error $\tilde{Z}_f$ will be uniformly ultimately bounded (UUB) if $\ell > 0$ in a compact set $S_r = \left\{r, \|r\| < B_r\right\} \subset \mathbb{R}$ and $\dot{\ell} < 0$ outside a smaller compact set contained in S_r.

Then in order to make $\dot{\ell} < 0$, since $k\left[\left\|\tilde{Z}_f\right\|_F - \frac{C_7}{2}\right]^2 > 0$ and $K_V \|r\| > 0$, we need $K_V \|r\| - \frac{kC_7^2}{4} - C_4 > 0$ or $k\left[\left\|\tilde{Z}_f\right\|_F - \frac{C_7}{2}\right]^2 - \frac{kC_7^2}{4} - C_4 > 0$. These conditions imply

$$\|r\| > b_r \equiv \frac{C_4 + kC_7^2/4}{K_V}, \tag{8.29}$$

$$\left\|\tilde{Z}_f\right\|_F > \frac{C_5}{2} + \sqrt{\left(\frac{C_5}{2}\right)^2 + \frac{C_2}{k}}. \tag{8.30}$$

Conditions (8.29)(8.30) define the compact set outside which the derivative of the Lyapunov function $\dot{\ell} < 0$. From (8.29), in order to satisfy $b_r < B_r$, then the control gain K_V has to be selected as

$$K_V > \frac{C_4 + kC_7^2/4}{B_r} = \frac{C_3\left(C_4 + kC_7^2/4\right)}{B_x - C_2}. \tag{8.31}$$

Finally, since r is bounded i.e., $r \in L_\infty$ then $e_a \in L_\infty$ and $\dot{e}_a \in L_\infty$ [148], or the tracking error of prosthetic ankle joint displacement is bounded, i.e., $\|e_a\| \le \varepsilon_a \in \mathbb{R}$.

Since the actual tracking error in (7.15) can be written as $e_a^{actual} = (\theta_{ar} - \theta_a) = (\theta_{ar} - \theta_{ar}^g) + (\theta_{ar}^g - \theta_a)$, then

$$\begin{aligned} \left\|e_a^{actual}\right\| &= \left\|(\theta_{ar} - \theta_{ar}^g) + (\theta_{ar}^g - \theta_a)\right\| \\ &\le \left\|(\theta_{ar} - \theta_{ar}^g)\right\| + \left\|(\theta_{ar}^g - \theta_a)\right\| \\ &\le \left\|\tilde{\theta}_{ar}\right\| + \varepsilon_a \in \mathbb{R}, \end{aligned} \tag{8.32}$$

or the actual tracking error is bounded.

8.4 Numerical simulation

8.4.1 Experimental setup

The performance of the controller designed in the previous section is studied during gait of a person with unilateral below-knee amputation. Performance of the proposed control approach is evaluated through simulation in Matlab/Simulink environment. The simulation model includes the link-segment diagram dynamics (7.1) with both prosthetic ankle joint and biological joints of the residual limb. A fully connected artificial neural network with random initial weights is trained with inputs from the gait-based kinematic references $\underline{\theta}_r^g$ and the pseudo tracking error $\left(e_a, \dot{e}_a\right)$ to approximate the unknown nonlinear ankle dynamics f in (7.12). Tuning rules (8.10), (8.11) update the neural network weights online during the simulation. Gait-based ground reaction torque is generated using (7.6) from the reaction forces (7.7), (7.8). The ankle torque of the ANN+PD approach is then calculated by (8.7). A classical PD-only control

$$\tau_a^{PD} = K_V^{PD}\left(\dot{e}_a + \lambda^{PD} e_a\right) - \tau_{aG}^g \tag{8.33}$$

is also simulated for comparison. Table 8.1 lists the parameters used in the control algorithms.

Table 8.1. Control and neural network parameters

Parameters	Value
Control gain K_V	2
Design parameter λ	5
Number of nodes in input layer N_x	11
Number of nodes in hidden layer N_h	22
Number of nodes in output layer	1

The control approaches are simulated in different simulation scenarios (Table 8.2) under the effect of noisy measurement $\theta_{a,noisy} = \left(1+n_{\theta_a}\right)\theta_a$, noisy control $\tau_{a,noisy} = \left(1+n_{\tau_a}\right)\tau_a$, ground reaction torque compensation error $\tilde{\tau}_{aG}$, disturbance torque τ_{ad}, error in detection of gait event Δt_{HS} which is defined as the difference between the occurrence of the actual *Heel Strike* and the *Heel Strike* detected by the RSI force (Figure 7.4), and changes in the type of gait (changes in walking speed). During walking on level ground, three gait types with different walking speeds are considered.

Table 8.2. Simulation scenarios

Scenario	n_{θ_a}	n_{τ_a}	$\tilde{\tau}_{aG}$	τ_{ad}	Δt_{HS}
S1 – Ideal	0	0	0	0	0
S2 – Noisy	$\pm[5 \div 10]\%$	$\pm[5 \div 10]\%$	0	0	0
S3 – GRT error	0	0	$\pm 20\% \tau_{aG}^{g}$	0	0
S4 – Disturbance torque	0	0	0	+20Nm	0
S5 – HS detection error	0	0	0	0	±20m
S6 – Gait change	0	0	0	Varied	0

The simulation paradigm includes 5 gait cycles of which the first 3 gait cycles are simulated under the ideal condition S1 (Table 8.2). Simulation scenarios S2 – S6 then continue at the beginning of the 4th gait cycle (*Heel Strike*). In the noisy condition S2, magnitudes of the noises n_{θ_a} and n_{τ_a} are between 5% and 10% of the measured ankle angle θ_a and the calculated ankle torque τ_a. In the scenario S3, magnitude of the actual GRT experienced by the prosthetic foot varies within 20% of the GRT estimated by

(7.6). A positive constant torque $\tau_{ad} = 20\text{Nm}$ is added in the scenario S4 to represents the disturbance created by the Head-Arm-Trunk movement during gait. In the scenario S5, the actual *Heel Strike* event might happen before being detected by the measured gait data (late detection with positive detection error +20ms), or the gait data might indicate the *Heel Strike* when that event has yet happened (early detection with negative detection error -20ms). In the scenario S6, the walking speed increases from *Slow* to *Normal* and *Normal* to *Fast*, or decreases from *Fast* to *Normal* and from *Normal* to *Slow*. All those changes occur at the beginning of the 4th gait cycle. Gait-based kinematic references $\underline{\theta}_r^g$ for these walking speeds are adapted from [31] and approximated by Fourier series with adjustable parameters as in (7.9).

8.4.2 Simulation results

The ankle displacements resulted from the ANN+PD and PD-only control approaches in the ideal condition S1 are shown in Figure 8.2. The vertical dashed lines indicate the beginning of each gait cycle (*Heel Strike*). Initially, PD-only control with $K_V^{PD} = 2$ and $\lambda^{PD} = 5$ does not yield stable performance. Parameters for the PD-only control are then increased to $K_V^{PD} = 6$ and $\lambda^{PD} = 20$ so acceptable tracking performance is obtained. These parameters are then used for simulation of the PD-only control algorithm in other scenarios in Table 8.2.

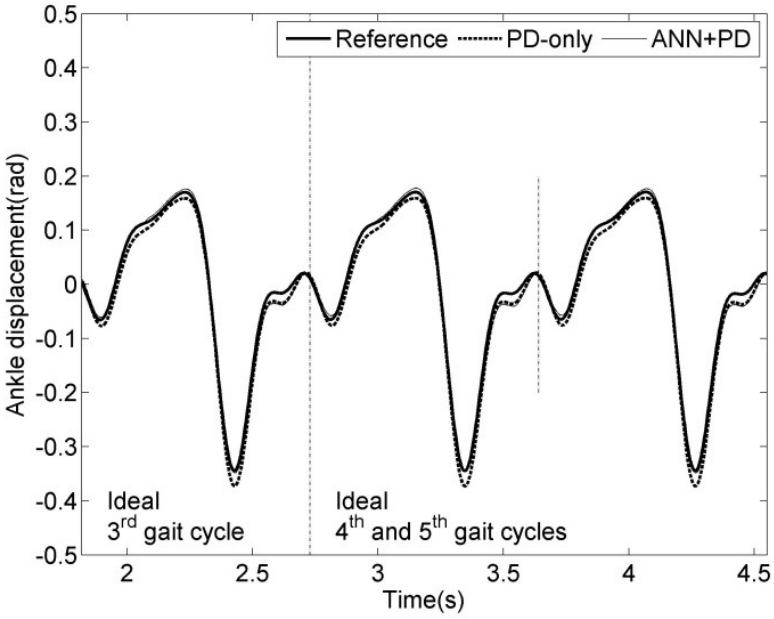

Figure 8.2. Ankle joint displacement in ideal conditions (S1).

Tracking performance of the prosthetic ankle joint of both control approaches in scenarios S2 – S5 are shown in Figure 8.3. The longer vertical dashed line indicates the beginning of the 4th gait cycle when the changes in gait condition occur. The shorter vertical dashed line indicates the beginning of the 5th gait cycle after the neural network-based controller has learned the new dynamics and adapted to the changes. It can be seen that the ANN+PD control outperforms the PD-only control in guaranteeing robust tracking performance in the presence of unmodeled dynamics and unwanted effects on the gait.

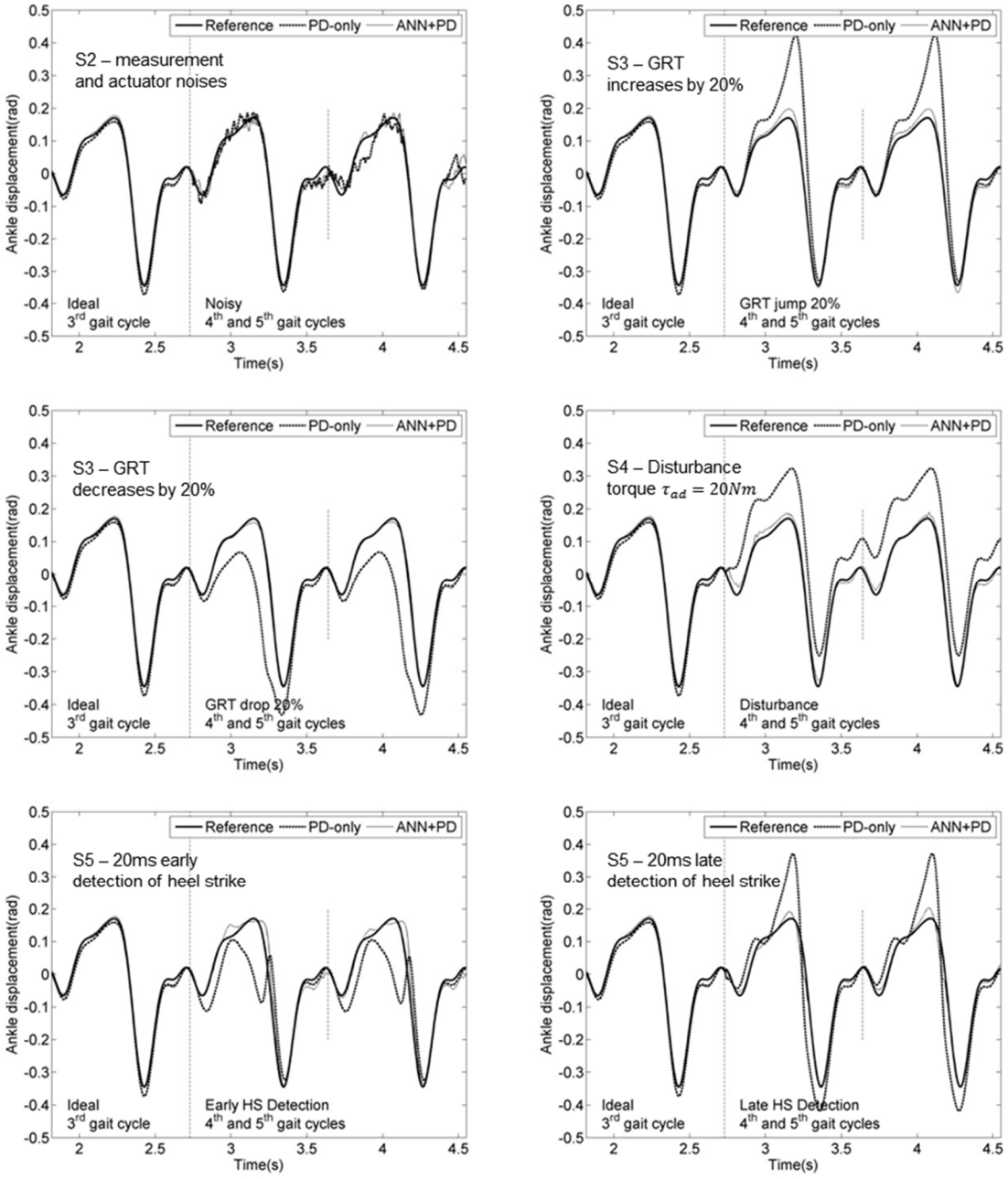

Figure 8.3. Ankle joint displacement under the effects of noises (S2), ground reaction torque error (S3), disturbance torque (S4), and temporal error in detection of *Heel Strike* event (S5)

Finally, when the walking speed changes (scenario S6), the artificial neural network approximates the nonlinear ankle dynamics and adapts to the new gait. Figure 8.4 shows the tracking performance of both control algorithms.

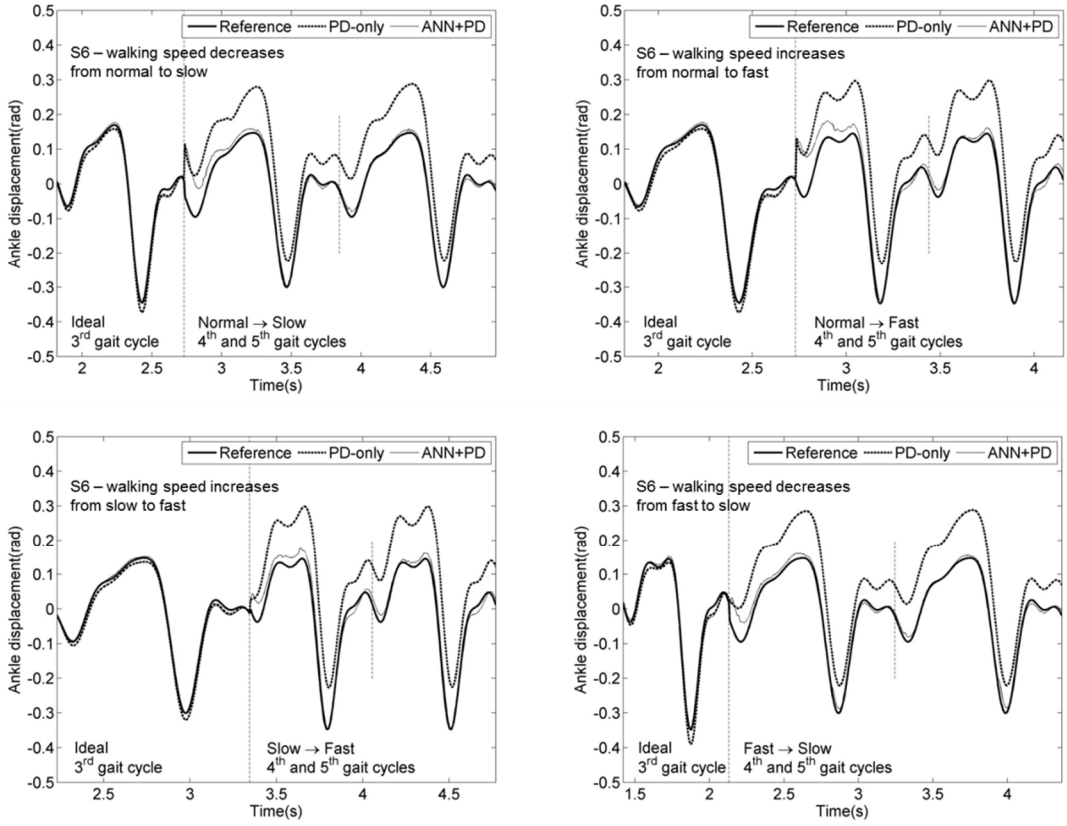

Figure 8.4. Ankle joint displacement with the changes in walking speed (S6)

It is important to note that in all non-ideal conditions (scenarios S2 – S6), the ANN-based control approach needs at most one gait cycle to learn the new dynamics before providing good tracking. The performance of the proposed control structure can be improved by parameterizing and continuously adjusting the parameters used in approximation of the gait-based kinematic references (7.9), real-time estimating of the ground reaction torque (7.6), and increasing the accuracy of the gait recognition and gait event detection.

8.5 Conclusions

A hierarchical control approach which features the adaptation of the prosthetic ankle joint movement to the users' intent during gait was presented in this chapter. The ankle joint displacement reference was specifically generated for the type of movement which

could be recognized by the actual gait data measured from the users. An artificial neural network learnt the varying nonlinear ankle dynamics while the interaction between the foot and the walking terrain was compensated by an empirical model of the ground reaction force. The resulting control torque manipulated the prosthetic ankle joint to follow its displacement reference during the gait.

Simulation results showed that tracking performance was achieved in the presence of measurement/actuator noises, uncertainties in terrain interaction, disturbance torques, variations in gait parameters, and changes in walking speed. Theoretical analysis established the bound of the actual tracking error and neural network weights. The entire system has the multi-level structure which aligns with the current trends in development of highly functional prosthetic feet. Issues such as parameterization of the gait patterns, real-time approximation of ground reaction torque, and performance of this control approach in different walking terrains should be addressed in the future work.

Chapter 9: Optimization-based Control of a Prosthetic Ankle Joint

The optimization principles associated with the synthesis of the movement of human body during locomotion can also be used to not only generate a control torque and synthesize the gaits for people with below-knee amputation but also evaluate the performance of the prosthetic devices. The potential of an adaptive dynamic programming-based control strategy which can adapt in real time to any gait variations in a noisy environment while optimizing a gait-related performance index will be presented in this chapter. A learning-based control strategy including an adaptive dynamic programming-based controller and augmented learning rules will be implemented to generate an ankle torque which drives the prosthetic ankle joint along the designed kinematic patterns. Numerical simulations will be carried out to evaluate the performance of the control approach[3].

9.1 Optimization principle in human gait

Theoretical studies of the human gait have shown that, there exists optimization principles associated with the synthesis of the movement of human body during locomotion [131, 134, 149, 150]. Moreover, these optimization principles can be parameterized [133] and defined by different metrics such as dynamic effort (i.e., integration of squares of all joint torques over time), or deviations of the joint position from a desire trajectory, or metabolic energy [134, 151, 152], etc. The problem can be solved in continuous time domain or by numerical method with the associated constraints by joint angle limits, joint torque limits [134, 153], etc. By optimizing those performance metrics, optimal joint torques are generally obtained to generate the

[3] This chapter is adapted from [A. Mai and S. Commuri, "Adaptive dynamic programming-based control of an ankle prosthetic joint," in *Lecture Note in Electrical Engineering*. vol. 325, ed: Springer, 2015, pp. 91-105].

motion. Several studies have shown that the similar optimization principles can also be extended to not only generate a control torque and synthesize the gaits for people with below-knee amputation [135, 154] but also evaluate performance of the prosthetic devices [101].

In this chapter, a control algorithm which aims at optimizing the performance metric which relates to the deviation of the ankle joint kinematics from its desired profiles for the gait will be presented. Performance and potential of an adaptive dynamic programming-based control structure, named direct neural dynamic programming (DNDP) [155] for control of an active prosthetic ankle joint is demonstrated. DNDP has been shown to be suitable for control of complex nonlinear systems with unknown dynamics and disturbances [156, 157]. Furthermore, this approach also tries to minimize the long-term cost function in the sense of Bellman's principle of optimality. With these properties, DNDP appears to be a good candidate for a challenging task such as control of a prosthetic ankle.

9.2 Direct neural dynamic programming control structure

The DNDP-based control structure comprises of two neural networks: critic network and action network. The critic network is responsible for approximating of the long-term cost function which satisfies the Bellman's principle of optimality. The action network is responsible for generating a control signal which leads to the optimization of the approximated long-term cost (i.e., output of the critic network). Figure 9.1 presents the two-network configuration of the DNDP-based control.

Critic network

From the discussion on the optimization principles of human gait in Section 9.1, it can be hypothesized that there exists a finite optimizable index which indicates the long-term performance of the prosthetic ankle joint in tracking of the desired gait-based trajectory. According to the Bellman's principle of optimality, such long-term performance index is expressed as the weighted sum of the short-term (instantaneous) cost at the subsequent iterations as follows:

$$\begin{aligned} L\big|_{[k-1]} &= S\big|_{[k]} + \alpha\, S\big|_{[k+1]} + \alpha^2\, S\big|_{[k+2]} + \dots \\ &= S\big|_{[k]} + \alpha\, L\big|_{[k]} \end{aligned} \tag{9.1}$$

in which $L\big|_{[k-1]}$ is the long-term performance index at the iteration $k-1$, $S\big|_{[k]}$ is the instantaneous cost at iteration $[k]$ and so on, and $0<\alpha<1$ is the discount factor.

In the direct neural dynamic programming approach, that performance index is approximated by a multilayer neural network (critic network) with ideal weights $W_C \in \mathbb{R}^{N_{hC}\times 1}$ and $V_C \in \mathbb{R}^{N_{xC}\times N_{hC}}$ as

$$L(x_C)\big|_{[k]} = \left[W_C^T \sigma\left(V_C^T x_C\right) + \varepsilon_C\right]\Big|_{[k]} \tag{9.2}$$

in which, $x_C \in \mathbb{R}^{N_{xC}\times 1}$ is the vector of the neural network inputs, ε_C is the bounded approximation error, i.e., $\|\varepsilon_C\| < \varepsilon_{BC} \in \mathbb{R}$, $\sigma(.)$ is a sigmoidal activation function, and N_{hC} is the number of nodes in the hidden layer. For simplifying purpose, the notation of the iteration $\big|_{[k]}$ will be presented only when needed. The ideal weights W_C, V_C in (9.2) are unknown but they can be approximated by adjustable weights $\hat{W}_C \in \mathbb{R}^{N_{hC}\times 1}$ and $\hat{V}_C \in \mathbb{R}^{N_{xC}\times N_{hC}}$ with the network weight errors

$$\begin{aligned}\tilde{W}_C &= W_C - \hat{W}_C \\ \tilde{V}_C &= V_C - \hat{V}_C.\end{aligned} \tag{9.3}$$

As a result, the critic network will generate $J\left(x_C\right)$ which is the approximation of the cost function defined in (9.2):

$$J\left(x_C\right) = \hat{W}_C^T \hat{\sigma}_C\left(\hat{V}_C^T x_C\right) = \sum_{i=1}^{N_{hC}} \hat{W}_C^T\left(1,i\right)\hat{\sigma}_C\left(\sum_{j=1}^{N_{xC}} \hat{V}_C^T\left(i,j\right)x_C\left(j,1\right)\right) \tag{9.4}$$

with N_{hC} is the number of nodes in the hidden layer, and N_{xC} is the number of inputs to the critic network

The backpropagation error of the critic network indicates how closely the approximated long-term cost function J follows the Bellman's principle of optimality and is defined as follows:

$$e_C\big|_{[k]} = \underbrace{\left[J\big|_{[k-1]} - S\big|_{[k]}\right]}_{TARGET} - \underbrace{\alpha J\big|_{[k]}}_{\substack{CURRENT \\ OUTCOME}} \tag{9.5}$$

Action network

The action network is responsible for generating a control action which results in the optimization of the approximated long-term cost function J, i.e., the output of the critic network. During the gait of an individual with below-knee amputation, it is hypothesized that such optimal control signal exists and is formulated as

$$\begin{aligned}u_A &= W_A^T \sigma_A\left(V_A^T x_A\right) + \varepsilon_A \\ &\approx \hat{W}_A^T \hat{\sigma}_A\left(\hat{V}_A^T x_A\right) = \sum_{i=1}^{N_{hA}} \hat{W}_A^T\left(1,i\right)\hat{\sigma}_A\left(\sum_{j=1}^{N_{xA}} \hat{V}_A^T\left(i,j\right)x_A\left(j,1\right)\right)\end{aligned} \tag{9.6}$$

in which $W_A \in \mathbb{R}^{N_{hA}\times 1}$, $V_A \in \mathbb{R}^{N_{xA}\times N_{hA}}$ are ideal network weights, $x_A \in \mathbb{R}^{N_{xA}\times 1}$ is the vector of the neural network inputs, ε_A is the bounded approximation error, i.e.,

$\|\varepsilon_A\| < \varepsilon_{BA} \in \mathbb{R}$, $\sigma(.)$ is a sigmoidal activation function, N_{hA} is the number of nodes in the hidden layer, and N_{xA} is the number of inputs to the action network. The ideal weights W_A, V_A in (9.6) are unknown but they can be approximated by adjustable weights $\hat{W}_A \in \mathbb{R}^{N_{hA} \times 1}$ and $\hat{V}_A \in \mathbb{R}^{N_{xA} \times N_{hA}}$ as in (9.6) with the network weight errors

$$\begin{aligned} \tilde{W}_A &= W_A - \hat{W}_A \\ \tilde{V}_A &= V_A - \hat{V}_A. \end{aligned} \tag{9.7}$$

In order to quantify the performance of the action network in generating a control signal which leads to the optimization of the cost function J, the backpropagation error of the action network is calculated in term of the ultimate control target as follows:

$$e_A\big|_{[k]} = \underbrace{U_C\big|_{[k]}}_{TARGET} - \underbrace{J\big|_{[k]}}_{\substack{CURRENT \\ OUTCOME}} \tag{9.8}$$

where $U_C\big|_{[k]}$ is an ultimate control goal, or the target for the long-term cost approximate $J\big|_{[k]}$.

Performance index

The short-term (i.e., instantaneous) cost is calculated as follows:

$$S = -\frac{1}{2}\left(\frac{\theta_{ar}^g - \theta_a}{\theta_{aM}}\right)^2 - \frac{1}{2}\left(\frac{\dot{\theta}_{ar}^g - \dot{\theta}_a}{\dot{\theta}_{aM}}\right)^2 \tag{9.9}$$

where $\{\theta_a, \dot{\theta}_a\}$, $\{\theta_{ar}^g, \dot{\theta}_{ar}^g\}$ and $\{\theta_{aM}, \dot{\theta}_{aM}\}$ are actual, desired, and maximal values of the ankle joint angular position and velocity. By defining the cost in term of the deviations of the prosthetic ankle joint position and velocity from their desired profiles, the performance measurement is related to the stability of the gait [134]. This selection also relates to the gait efficiency in the way that if the prosthetic ankle joint can perform

as closed as possible to the biological ankle, then the hip and knee joints do not have to perform unnecessary works to compensate for gait degradation. As a result, people with below-knee amputation can walk with no or little unnecessary extra effort/energy consumption. Ultimately, the overall human-prosthetic system can perform a normal gait.

The desire for optimization of the gait efficiency can be expressed as the optimization of the approximated long-term cost function J in the DNDP framework. Since the short-term cost function S is defined in term of tracking errors as in (9.9), the ultimate control goal for J is selected as

$$U_C = 0 \tag{9.10}$$

The learning algorithms for the critic and action networks that are presented in the next section are designed to make the backpropagation errors of the two networks go to zero, i.e., $e_C \to 0$ and $e_A \to 0$. The relationship between the network errors going to zero and the selection of short-term cost function S and the ultimate control goal U_C can be explained as follows.

First, the critic network is trained so that its backpropagation error $e_C \to 0$. As $e_C \to 0$, it can be easily seen from (9.5) that $\alpha J\big|_{[k]} \to \left[J\big|_{[k-1]} - S\big|_{[k]} \right]$ or

$$J_{[k-1]} = S\big|_{[k]} + \alpha J\big|_{[k]} \tag{9.11}$$

By comparing (9.11) to (9.1), it is clear that $J \to L$, i.e., the critic network generates the true approximation of the long-term performance index.

The action network is trained so that its output will make the backpropagation error $e_A \to 0$. Because $e_A = U_C - J$, the output of the critic network J will converge to the ultimate control goal U_C which is 0. If the critic network is trained, then $J \to L$, and this implies that the long-term performance index L also goes to zero, i.e., $L \to 0$. Because L is defined in term of the short-term cost function S as in (9.1) and S is always a negative function as in (9.9), the instantaneous cost S also vanishes, i.e., $S \to 0$. Since S is defined as the sum of the squares of the deviations of the ankle joint kinematics from its desired profiles, $S \to 0$ implies that the ankle joint tracking errors will go to zero, i.e., $e_a \to 0$ and $\dot{e}_a \to 0$.

Finally, as the short-term cost S gets smaller, the smaller target for J in the subsequent iteration will be calculated. The critic network will repeat its training paradigm to generate an output that closely approximates the new target. As a result, the long-term performance index which is approximated by the output of the critic network J will be improved over time. That is the basic idea of adaptive dynamic programming-based controls which incorporate iterating and updating the approximated long-term performance index J over time (i.e., reinforcement learning) and simultaneously satisfying the Bellman's principle of optimality (i.e., dynamic programming).

9.3 Control algorithm

In addition to Assumption 8.2.1 - Assumption 8.2.3, the following assumption is made for the implementation of the DNDP-based control algorithm.

Assumption 9.3.1
Ideal weights of the critic and action networks are constant and bounded, i.e.,

$$\|Z_C\|_F = \left\| \begin{bmatrix} W_C & \Theta \\ \Theta & V_C \end{bmatrix} \right\|_F \leq B_{CZ} \in \mathbb{R} \quad \text{and} \quad \|Z_A\|_F = \left\| \begin{bmatrix} W_A & \Theta \\ \Theta & V_A \end{bmatrix} \right\|_F \leq B_{AZ} \in \mathbb{R} \quad \text{where} \quad \|.\|_F$$

represents the Frobenius norm.

Theorem 9.3.1
Given the control structure in Figure 9.1, the ankle torque can be computed as:

$$\tau_a = u_A - \tau_{aG}^g + K_V r, \tag{9.12}$$

with

- u_A – control signal generated by the action network in (9.6)
- τ_{aG}^g – compensation for the actual ground reaction torque τ_{aG}
- r – filtered tracking error ($r = \dot{e}_a + \lambda e_a$),

$$K_V r = K_V \left(\dot{e}_a + \lambda e_a \right), \tag{9.13}$$

Further, let the critic and action neural network weights be updated according to

$$\Delta W_C = \alpha F_C e_C \hat{\sigma}_C - k_C F_C \left\| e_C \right\|_2 \hat{W}_C \tag{9.14}$$

$$\Delta V_C = \alpha G_C e_C x_C \hat{W}_C^T \hat{\sigma}_C' - k_C G_C \left\| e_C \right\|_2 \hat{V}_C \tag{9.15}$$

$$\Delta W_A = F_A e_A \hat{\sigma}_A \hat{V}_{CA} \hat{\sigma}_C' \hat{W}_C - F_A \hat{\sigma}_A' \hat{V}_A^T x_A r - k_A F_A \left\| e_A \right\|_2 \hat{W}_A \tag{9.16}$$

$$\Delta V_A = G_A e_A x_A \hat{V}_{CA} \hat{\sigma}_C' \hat{W}_C \hat{W}_A^T \hat{\sigma}_A' - k_A G_A \left\| e_A \right\|_2 \hat{V}_A \tag{9.17}$$

in which α is the discount factor, $\hat{V}_{CA}$ is contained in $\hat{V}_C$ to map from $u_A\left(x_A\right)$ to the hidden node outputs of the critic network, $F_C, G_C, k_C, F_A, G_A, k_A$ are real, positive design parameters, $\hat{\sigma}_C'$ and $\hat{\sigma}_A'$ are the Jacobian matrices defined as:

$$\hat{\sigma}_C' = \frac{\partial \hat{\sigma}_C\left(\hat{V}_C^T x_C\right)}{\partial\left(\hat{V}_C^T x_C\right)}$$
$$\hat{\sigma}_A' = \frac{\partial \hat{\sigma}_A\left(\hat{V}_A^T x_A\right)}{\partial\left(\hat{V}_A^T x_A\right)} \tag{9.18}$$

Then, the actual tracking error e_a^{actual} defined in (7.15) and the neural network weights errors $\tilde{W}_C$, $\tilde{V}_C$ in (9.3) and $\tilde{W}_A$, $\tilde{V}_A$ in (9.7) are uniformly ultimately bounded.

Discussions

The DNDP-based control in Figure 9.1 also has a hierarchical structure similar to the feedback linearization neural network-based control in Chapter 8.

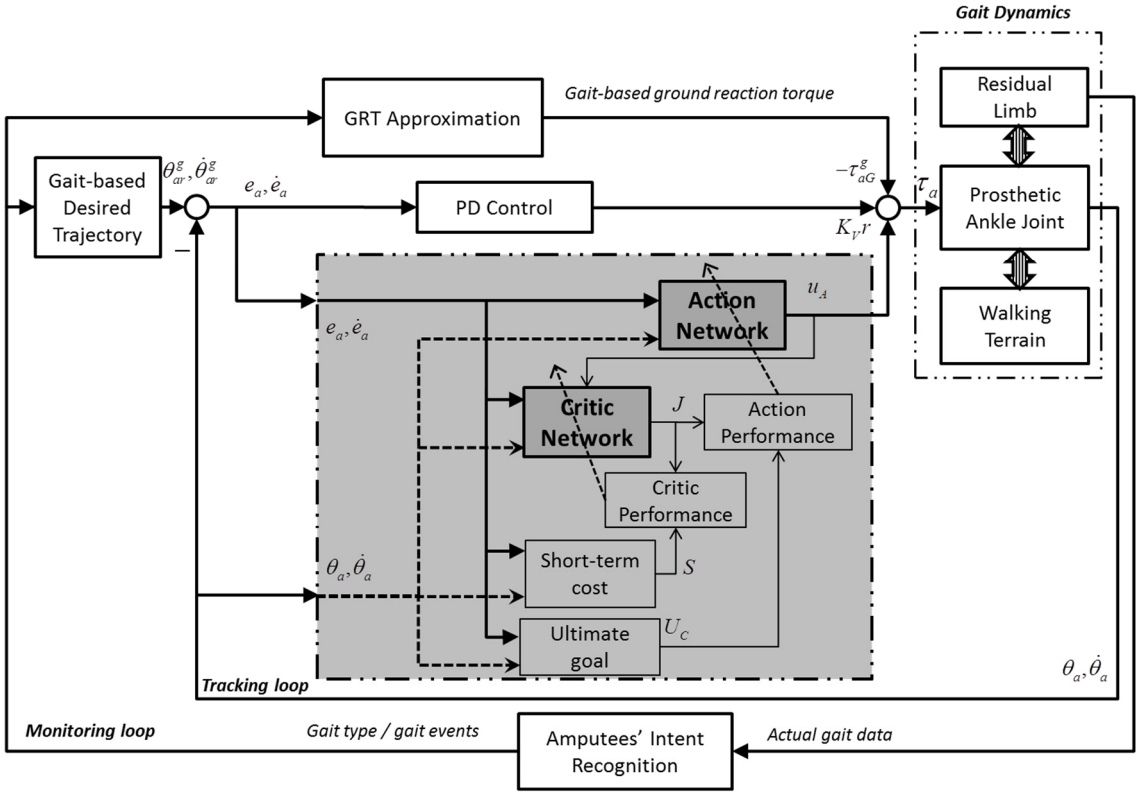

Figure 9.1. Block diagram of the direct neural dynamic programming-based control of the prosthetic ankle joint.

At the supervisory level, the gait data measured from the persons with below-knee amputation is used to recognize the type of gaits, detect the gait events, and generate the corresponding gait-based reference joint patterns. The control level comprises of a learning control algorithm that bases on a critic-action structure, a PD control, and an approximation of the ground reaction torque. This level is responsible for driving the prosthetic ankle joint along the desired gait-based ankle angle profile and improving a gait-related performance index over time.

The monitoring loop and tracking loop of the DNDP-based control in Figure 9.1 perform the tasks similar to the control algorithm in Figure 8.1. However, the most inner loop does not approximate the unknown ankle dynamics. Instead, that loop aims to evaluate the control quality, and calculates a control action that yields an optimized performance.

9.4 Numerical simulation

9.4.1 Experimental setup

Both networks use sigmoid activation functions and are fully connected with randomly initialized weights in the range $[-1,1]$. The critic network and action network weights are updated using (9.14)-(9.15) and (9.16)-(9.17), respectively. Equation (9.9) is used to calculate the short-term cost at each time step. Table 9.1 lists the network and control parameters.

Table 9.1. Direct neural dynamic programming-based control and neural network parameters

Parameters	Value
Control gain K_V	5
Design parameter λ	10
Discount factor α	0.95
Number of nodes in input layer of critic network N_{xC}	5
Number of nodes in hidden layer of critic network N_{hC}	10
Number of nodes in output layer of critic network	1
Number of nodes in input layer of action network N_{xA}	4
Number of nodes in hidden layer of action network N_{hA}	8
Number of nodes in output layer of action network	1

The vector of inputs to the critic network is defined as:

$$x_C = \begin{bmatrix} x_A^T & u_A \end{bmatrix}^T \tag{9.19}$$

in which x_A is the vector of inputs to the action network

$$x_A = \begin{bmatrix} e_a & \dot{e}_a & \theta_a & \dot{\theta}_a \end{bmatrix}^T \tag{9.20}$$

and u_A is the control signal generated by the action network as in (9.6).

Table 9.2 lists the scenarios for simulation of the gait model and the control approaches. These scenarios illustrate the varying noises and gait conditions as follows.

Ideal condition: In this ideal condition, the system is simulated with 20 steps of normal speed without any measurement and actuator noises.

Effect of measurement and actuator noises: Uniformly distributed measurement noises are added to the ankle position and angular velocity. Torque output generated for the ankle joint is also added with uniformly distributed actuator noise as follows:

$$\begin{aligned} \theta_a &= \theta_a + \rho\theta_a \\ \dot{\theta}_a &= \dot{\theta}_a + \rho\dot{\theta}_a \\ \tau_a &= \tau_a + \rho\tau_a \end{aligned} \tag{9.21}$$

where ρ is in the range $[-2\%, 2\%]$ (or $[-5\%, 5\%]$). The system is simulated with 20 steps of normal walking speed and increasing measurement and/or actuator noises. Four simulation scenarios with different levels of measurement noises and actuator noises are summarized in Table 9.2. In all scenarios N1 – N4, the measurement noises and actuator noises are added to the simulation model at the beginning of the 6th step.

Effect of variations in walking speed: Control configurations similar to previous simulation scenarios are repeated here to evaluate the performance of the DNDP-based control in the presence of variations in walking speed. The system is simulated with 5% measurement noise, 5% actuator noise, and 4 different walking setups as shown in Table 9.2. Three gaits labeled *Slow*, *Normal*, and *Fast* indicate different walking speeds.

Table 9.2. Simulation scenarios with noises and changing gaits

Effect of noises	N1	2% measurement noise
	N2	5% measurement noise
	N3	5% measurement noise and 2% actuator noise
	N4	5% measurement noise and 5% actuator noise
Effect of changing gaits	G1	10 normal walking + 10 fast walking
	G2	10 normal walking + 10 slow walking
	G3	10 normal walking + 5 fast walking + 5 slow walking
	G4	10 normal walking + 5 slow walking + 5 fast walking

For the comparison purpose, the simulation is repeated with other types of control at the ankle joint including Proportional-Derivative control (PD) as:

$$\tau_a^{PD} = K_V^{PD}\left(\dot{e}_a + \lambda^{PD} e_a\right) - \tau_{aG}^g \tag{9.22}$$

and feedback linearization neural network-based control (FLNN):

$$\tau_a = \hat{f} - \tau_{aG}^g + K_V r - v, \tag{9.23}$$

in which $\hat{f}$ is the approximation of the unknown ankle dynamics in (7.12), v is the robustifying term to compensate for approximation errors and unknown disturbances. It is noted that the approximation of $\hat{f}$ bases on backpropagation of the tracking errors and does not involve the optimization of the approximated long-term cost $J\left(x_C\right)$ as used in (9.8).

9.4.2 Simulation results

Figure 9.2 shows the tracking performance, short-term cost S and the accumulative cost $A = \Sigma S$ from one step during the *Normal* gait under the ideal condition (no noises, and no gait changes).

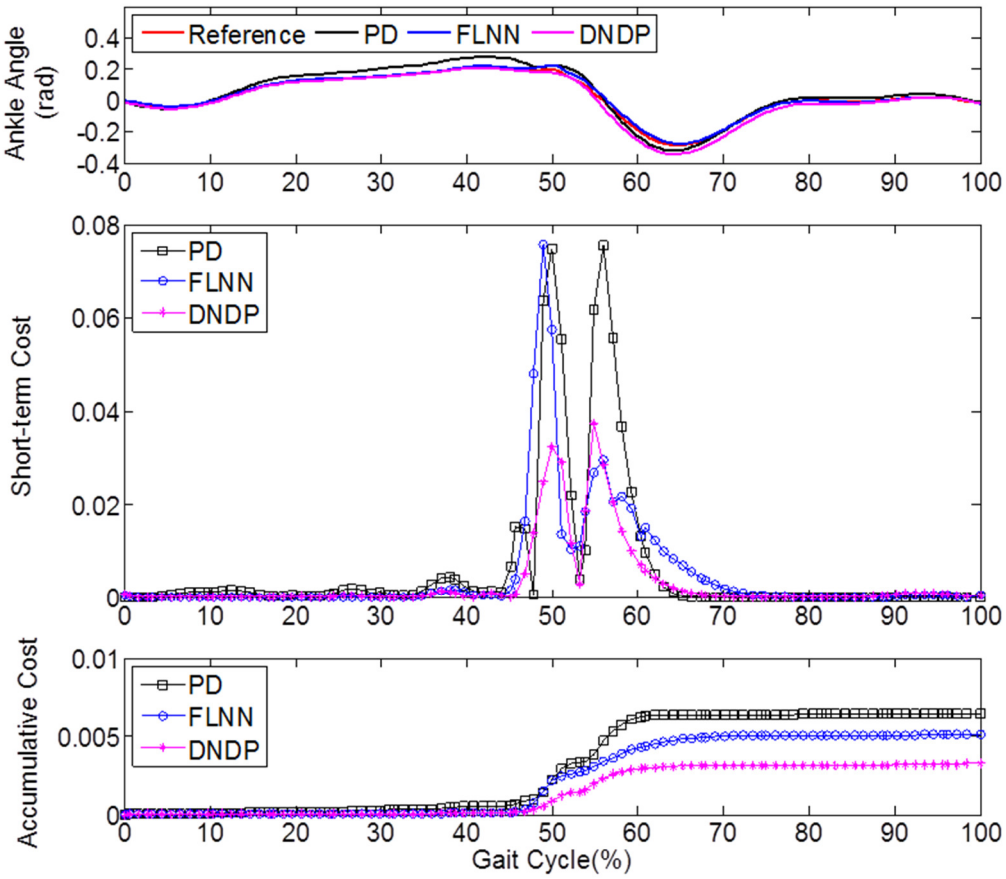

Figure 9.2. Performance of the DNDP-based control during normal gait under ideal conditions.

All the controls can drive the ankle joint along the desired trajectory with a small tracking error. It can be seen that during the gait, although there are instances when the short-term cost S of the DNDP-based control exceeds the short-term cost of the FLNN or PD control, the accumulative cost of the DNDP-based control during the entire gait cycle is lower than the other control algorithms.

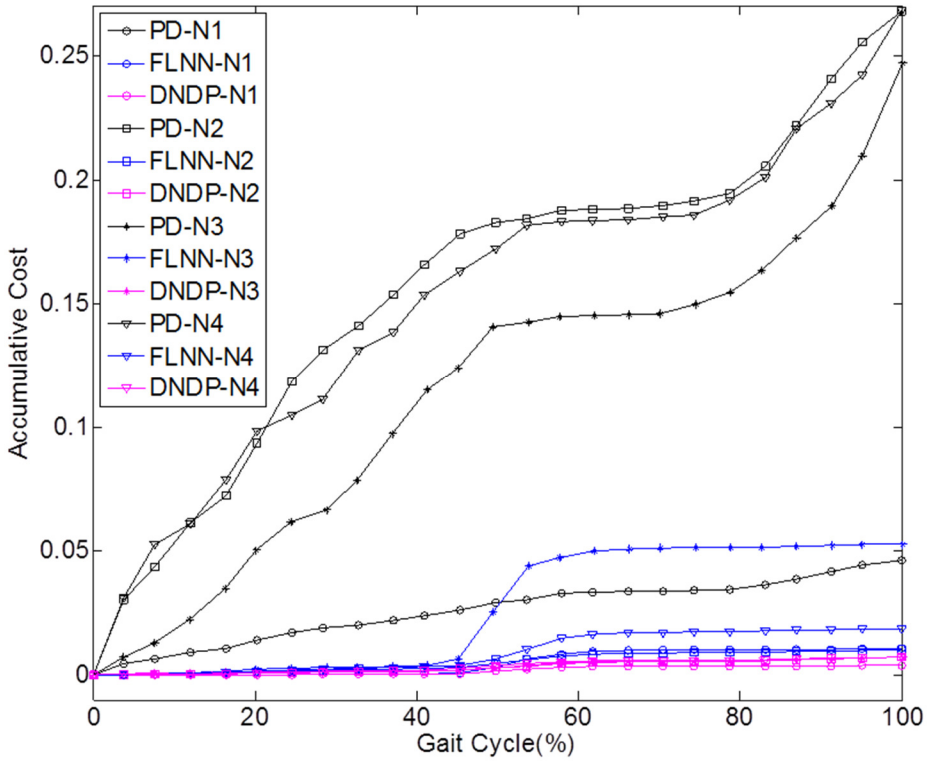

Figure 9.3. Accumulative cost with the measurement and actuator noises.

Accumulative costs from one gait cycle of the simulation scenarios N1 – N4 with the presence of the measurement and actuator noises are showed in Figure 9.3 for all control algorithms. Table 9.3 reports the accumulative cost (per sample) over the entire simulation period which includes 20 steps of the gait with normal walking speed and different levels of noises. It can be seen that as the measurement/actuator noises increase, the DNDP-based control outperforms other control methods by producing robust tracking performance with lower accumulative cost.

Table 9.3. Accumulative cost after 20 steps of normal walking speed with increasing measurement/actuator noises

Noise levels	PD	FLNN	DNDP
2% measurement noise (N1)	0.715	0.239	0.075
5% measurement noise (N2)	3.96	2.003	0.118
5% measurement noise and 2% actuator noise (N3)	3.961	2.079	0.120
5% measurement noise and 5% actuator noise (N4)	3.966	2.336	0.130

Similar setups are repeated here to evaluate the performance of the DNDP-based control in the presence of variations in walking speed. The system is simulated with 5% measurement noise, 5% actuator noise, and 4 different walking setups (Table 9.2).

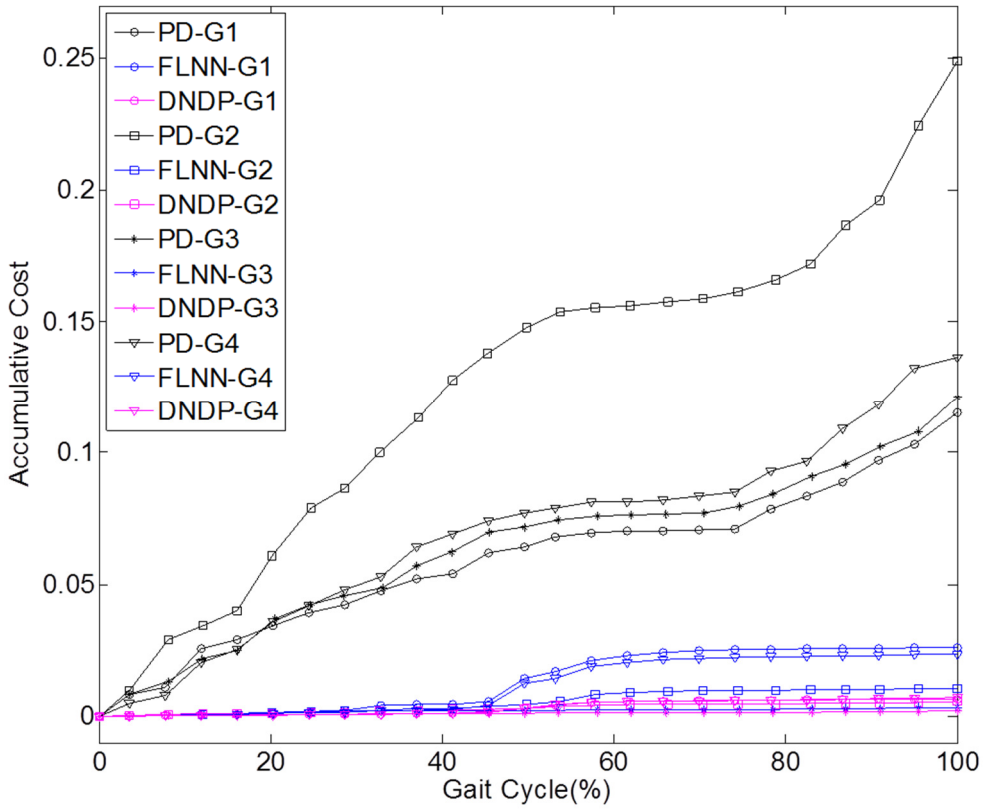

Figure 9.4. Accumulative cost with the changing gaits.

Figure 9.4 shows the accumulative cost of the 11th step of the scenarios G1 and G2 (when the walking speed was changed from *Normal* to *Fast* and from *Normal* to *Slow*,

respectively) and of the 16th step of the scenarios G3 (*Fast* to *Slow*), and G4 (*Slow* to *Fast*). Accumulative costs calculated from the entire simulation duration of the scenarios G1 – G4 are shown in Table 9.4.

It can be seen from Figure 9.4 and Table 9.4 that when the walking speed changes, the DNDP-based control is still able to provide lower accumulative performance cost compared to other control strategies.

Table 9.4. Accumulative cost with 5% measurement noise, 5% actuator noise, and combinations of different walking speeds.

Gait	PD	FLNN	DNDP
10 normal + 10 fast (G1)	2.140	0.567	0.100
10 normal + 10 slow (G2)	3.910	1.915	0.106
10 normal + 5 fast + 5 slow (G3)	2.233	0.461	0.082
10 normal + 5 slow + 5 fast (G4)	2.206	0.490	0.084

9.5 Conclusions

In this chapter, the performance and potential of a model-free adaptive dynamic programming-based controller for a prosthetic ankle joint were evaluated. By optimizing the performance metric which was defined in term of the deviation of the ankle kinematics from its desired profiles, the control approach in this chapter could guarantee the stability and increase the efficiency of the gait by reducing the unnecessary works for the biological knee and hip joints. Simulation scenarios indicated that with the DNDP-based control, the prosthetic ankle joint was able to provide stable, robust, and reduced performance cost during gait. Future works should evaluate the effectiveness of the proposed control structure with different performance indices such as dynamic effort (i.e., integration of squares of all joint torques over time), or metabolic energy consumption.

Chapter 10: Conclusions and Future Research

The design of an intelligent prosthetic ankle that is able to perceive user gait and adapt its performance in real time was addressed in this dissertation. Inability to support body weight during gait as well as inadequate function of the prosthetic foot can lead to gait anomalies that adversely affect the health of individuals with amputation below the knee. While transtibial osteomyoplastic amputation procedure has been advocated to improve end-bearing as well as retention of muscle activity in the affected limb, the clinical outcomes of the procedure were not validated in the literature. Further, gait assessment for individuals with transtibial amputation was performed in a gait laboratory primarily to detect asymmetry in gait and study energy expenditure during locomotion. Such studies were not conducted to study gait under normal work-related activities or to study the environment in the prosthetic socket during gait. Further, the prosthetic ankle was a passive device with minimal energy storage and return capability. Even the active devices were not designed to detect user intent or adapt to changing gait and environmental conditions. For the first time in the literature, a systematic procedure has been demonstrated to study the gait of individuals with TOA and design control strategies that not only guarantee tracking of the ankle displacement profiles that can replicate normal human gait, but can also adapt to changing gait conditions and optimize the performance in real time. The stability and robustness of the proposed design has been rigorously proven and the performance has been validated using actual gait data collected during the course of this dissertation.

The following are some of the results of the research presented in this dissertation.

a) A gait monitoring device and gait analysis software were developed in this dissertation to provide a method to assess the gait asymmetry and quantitatively evaluate the outcomes of the transtibial osteomyoplastic amputation procedure (Chapter 3, Chapter 4, Chapter 5, and [111, 122]). Simultaneous presence of the load at the distal area of the residual limb and activities of the residual muscles were successfully confirmed for the first time. Using the procedure developed in this dissertation, additional evidence was obtained to validate the effectiveness of the TOA procedure.

b) For the first time, the residuum socket interface force and the residual muscle activities of individuals with TOA were captured in real time during work-related gait activities. Contraction/elongation of the residual muscles inside the socket and their relationships to the variations of the RSI forces in individuals with TOA during gait were also studied. The dependence of the interfacial socket force and residual muscle activities on the type of prosthetic feet and type of gait was clearly demonstrated and filled an important gap in the literature (Chapter 4, Chapter 5, and [111, 122]).

c) Socket forces and residual muscle activities captured from the participants in this dissertation provided a new method to recognize the gait types and detect gait events. This method allowed the synthesis of ankle displacement profile similar to that of a normal ankle to be used in the control of a prosthetic foot (Chapter 6 and [142]).

d) Finally, learning-based control strategies with hierarchical structures were implemented to adaptively compensate for the unknown, changing ankle

dynamics and drive the prosthetic ankle joint along the desired trajectories. With the learning capabilities of these control strategies and the incorporation of the actual gait data, the prosthetic ankle joint could not only replicate the healthy ankle movement, but also improve the gait stability and optimize the gait performance (Chapter 7, Chapter 8, Chapter 9, and [158, 159]).

It is anticipated that the results from this dissertation will lead to better understanding on the effect of the amputation procedure and prosthetic components on the long-term health of the individual.

Limitations and future directions

This dissertation focused on a specific group of individuals with unilateral TOA, using the socket design for their residual limb but with different foot components, thus allowing for general interpretation of the results. In order to obtain more specific conclusions on the effect of gait and prostheses on socket force and residual muscle contraction, systematic gait studies should be designed with a larger group size and consistency in the type of prosthetic feet. Kinematic and kinetic measurements (e.g., joint movement, joint force) as well as quantitative metric of metabolic energy consumption should also be incorporated.

In this dissertation, control of the prosthetic ankle joint was carried out in a framework which was based on modeling and simulation. Such frameworks enabled a quick evaluation of the performance of prosthetic devices under different operating conditions without introducing the risk of injury due to prosthetic malfunctions when testing on human subjects. Although the control performance was promising, designing a controlled prosthetic foot is a long-term task and several milestones need to be

addressed before the proposed approach can be applied. First and foremost, a mechanical design and prototype foot which satisfy the requirement on rigidity, mobility, and power has to be built. Dynamical model of the ankle joint during gait should be obtained using mathematical modeling and refined with actual gait measurement. The control approach will then be tested and adjusted on the refined model. Additional, issues such as accuracy of gait recognition, parameterization of the gait patterns, real-time approximation of the ground reaction torque should be addressed. Finally, performance of the controlled prosthetic foot should be tested through both mechanical property testing and quantitative gait analysis. Extension of the study to individuals with bilateral TOA as well as transfemoral (above-knee) amputation is also the scope for future research.

References

[1] K. Ziegler-Graham, E. J. MacKenzie, P. L. Ephraim, T. G. Travison, and R. Brookmeyer, "Estimating the prevalence of limb loss in the United States: 2005 to 2050," *Arch Phys Med Rehabil,* vol. 89, pp. 422-429, 2008.

[2] Y.-L. Chou, S.-S. Shi, G.-F. Huang, and T.-S. Lin, "Interface pressure and gait analysis in different walking speeds and on the below-knee amputees with multiple axis prosthetic foot prosthesis," *Biomedical Engineering - Applications Basis Communications,* vol. 15, pp. 207-211, 2003.

[3] S. A. Gard, "Use of quantitative gait analysis for the evaluation of prosthetic walking performance," *Journal of Prosthetics and Orthotics,* vol. 18, pp. 93-103, 2006.

[4] A. H. Hansen, "Scientific methods to determine functional performance of prosthetic ankle-foot systems," *Journal of Prosthetics and Orthotics,* vol. 17, pp. 23-29, 2005.

[5] M. J. Hsu, D. H. Nielsen, S. J. Lin-Chan, and D. Shurr, "The effects of prosthetic foot design on physiologic measurements, self-selected walking velocity, and physical activity in people with transtibial amputation," *Arch Phys Med Rehabil,* vol. 87, pp. 123-129, Jan 2006.

[6] H. v. d. Linde, C. J. Hofstad, A. C. H. Geurts, K. Postema, J. H. B. Geertzen, and J. v. Limbeek, "A systematic literature review of the effect of different prosthetic components on human functioning with a lower-limb prosthesis," *Journal of Rehabilitation Research and Development,* vol. 41, pp. 555-570, 2004.

[7] J. S. Rietman, K. Postema, and J. H. B. Geertzen, "Gait analysis in prosthetics: opinions, ideas and conclusions," *Prosthetics and Orthotics International,* vol. 26, pp. 50-57, 2002.

[8] T. Pohjolainen, H. Alaranta, and M. Karkkainen, "Prosthetic use and functional and social outcome following major lower limb amputation," *Prosthetics and Orthotics International,* vol. 14, pp. 75-79, 1990.

[9] C. R. Walker, R. Ingram, M. Hullin, and S. W. McCreath, "Lower limb amputation following injury: a survey of long-term functional outcome," *Injury,* vol. 25, pp. 387-392, 1994.

[10] W. K. Brodzka, H. Thornhill, S. Zarapkar, J. Malloy, and L. Weiss, "Long-term function of persons with atherosclerotic bilateral below-knee amputation living in the inner city," *Arch Phys Med Rehabil,* vol. 71, pp. 895-900, 1990.

[11] T. R. Dillingham, L. Pezzin, E. MacKenzie, and A. R. Burgess, "Use and satisfaction with prosthetic devices among persons with trauma-related amputations: a long-term outcome study," *Am J Phys Med Rehabil,* vol. 80, pp. 563-571, 2001.

[12] R. A. Sherman, "Utilization of prostheses among US veterans with traumatic amputation: a pilot survey," *Journal of Rehabilitation Research and Development,* vol. 36, pp. 100-108, 1999.

[13] H. Bateni and S. J. Olney, "Kinematic and kinetic variations of below-knee amputee gait," *Journal of Prosthetics and Orthotics,* vol. 14, pp. 2-13, 2002.

[14] I. Kovac, V. Medved, and L. Ostojic, "Spatial, temporal and kinematic characteristics of traumatic transtibial amputees' gait," *Collegium Antropologicum,* vol. 34, pp. 205-213, 2010.

[15] N. P. Fey, A. K. Silverman, and R. R. Neptune, "The influence of increasing steady-state walking speed on muscle activity in below-knee amputees," *Journals of Electromyography and Kinesiology,* vol. 20, pp. 155-161, 2010.

[16] L. Torburn, C. M. Powers, R. Guiterrez, and J. Perry, "Energy expenditure during ambulation in dysvascular and traumatic below-knee amputees: a comparison of five prosthetic feet," *Journal of Rehabilitation Research and Development,* vol. 32, pp. 111-119, 1995.

[17] R. Gailey, K. Allen, J. Castles, J. Kucharik, and M. Roeder, "Review of secondary physical conditions associated with lower-limb amputation and long-term prosthesis use," *Journal of Rehabilitation Research and Development,* vol. 45, pp. 15-29, 2008.

[18] Össur. (2015). *Proprio Foot*. Available: http://www.ossur.com/?PageID=12704

[19] BIOM. (2015). *BIOM - Personal Bionics*. Available: http://www.biom.com/

[20] S. I. Wolf, M. Alimusaj, L. Fradet, J. Stegel, and F. Braatz, "Pressure characteristic at the stump/socket interface in transtibial amputees using an adaptive prosthetic foot," *Clinical Biomechanics,* vol. 24, pp. 860-865, 2009.

[21] A. E. Ferris, J. M. Aldridge, C. A. Rábago, and J. M. Wilken, "Evaluation of a Powered Ankle-Foot Prosthetic System During Walking," *Archives of Physical Medicine and Rehabilitation,* vol. 93, pp. 1911-1918, 2012.

[22] A. M. Grabowski and S. D'Andrea, "Effects of a powered ankle-foot prosthesis on kinetic loading of the unaffected leg during level-ground walking," *Journal of NeuroEngineering and Rehabilitation,* vol. 10, pp. 1-12, 2013.

[23] S. H. K. R. Gadigota, "Development of a prosthetic activity monitor for gait detection and classification in transtibial amputees," Master of Science, School of Electrical and Computer Engineering, University of Oklahoma, Norman, OK, 2011.

[24] H. Uustal and E. Baerga, "Chapter 6: prosthetics and orthotics," in *Physical Medicine and Rehabilitation Board Review*, S. Cuccurullo, Ed., ed New York: Demos Medical Publishing, 2004.

[25] J. Perry, *Gait Analysis: Normal and Pathological Function*, 1 ed. Thorofare, NJ: SLACK Incorporated, 1992.

[26] E. Ayyappa, "Normal human locomotion, part 1: basic concepts and terminology," *Journal of Prosthetics and Orthotics,* vol. 9, pp. 10-17, 1997.

[27] Orthogate. (2015). *Ankle anatomy*. Available: http://www.orthogate.org/patient-education/ankle/ankle-anatomy.html

[28] D. A. Winter, *Biomechanics and motor control of human movement*, 4 ed. Hoboken, N.J.: Wiley, 2009.

[29] F. C. Anderson and M. G. Pandy, "Dynamic optimization of human walking," *Journal of Biomechanical Engineering,* vol. 123, pp. 381-390, 2001.

[30] M. Ackermann and A. J. van den Bogert, "Optimality principles for model-based prediction of human gait," *Journal of Biomechanics,* vol. 43, pp. 1055-1060, 2010.

[31] D. A. Winter, *The biomechanics and motor control of human gait: normal, elderly and pathological*, 2 ed. Waterloo, Ontario, Canada: University of Waterloo Press, 1991.

[32] H. J. Hermens, B. Freriks, C. Disselhorst-Klug, and G. Rau, "Development of recommendations for SEMG sensors and sensor placement procedures," *Journal of Electromyography and Kinesiology,* vol. 10, pp. 361-374, 2000.

[33] C. Kirtley, "Muscles," in *Clinical gait analysis - theory and practice*, ed: Churchill Livingstone, 2006, pp. 149-150.

[34] A. H. Hansen, D. S. Childress, S. C. Miff, S. A. Gard, and K. P. Mesplay, "The human ankle during walking: Implications for design of biomimetic ankle prostheses," *Journal of Biomechanics,* vol. 37, pp. 1467-1474, 2004.

[35] E. Singer, G. Ishai, and E. Kimmel, "Parameter estimation for a prosthetic ankle," *Annals of Biomedical Engineering,* vol. 23, pp. 691-696, 1995.

[36] B. M. Kelly, P. H. Pangilinan, G. M. Rodriguez, V. S. Bodeau, and R. C. Mipro. (2015). *Lower limb prosthetics*. Available: http://emedicine.medscape.com/article/317358-overview

[37] J. Ertl, "Prosthetic primer: Pain and the inactive residual extremity syndrome," *inMotion,* vol. 10, Sept, Oct, 2000 2000.

[38] J. W. Ertl, J. P. Ertl, W. J. Ertl, and J. Stokosa. (2015). *The Ertl osteomyoplastic transtibial amputation reconstruction - description of techniques and long-term results*. Available: http://ertlreconstruction.com/documents/transtibial-technique.pdf

[39] B. C. Taylor and A. Poka, "Osteomyoplastic transtibial amputation: technique and tips," *Journal of Orthopaedic Surgery and Research,* vol. 6, pp. 1-4, 2011.

[40] C. P. Dionne, "Work Task Performance in Amputees with Trans-Tibial Amputation Due to a Traumatic Event (TTAT)," *IRB Number: 15948,* 2011.

[41] C. P. Dionne, "Residual Limb Measures During Biomechanical Work-Related Activities in Adult Oklahomans with Unilateral-Trans-Tibial Amputation due to a Traumatic Event," *IRB Number: 15713,* 2011.

[42] S. Commuri, J. Day, C. Dionne, and W. Ertl, "Assessment of pressures within the prosthetic socket of a person with osteomyoplastic amputation during varied walking tasks," *Journal of Prosthetics and Orthotics,* vol. 22, pp. 127-137, 2010.

[43] M. C. Faustini, R. R. Neptune, R. H. Crawford, W. E. Rogers, and G. Bosker, "An experimental and theoretical framework for manufacturing prosthetic sockets for transtibial amputees," *IEEE Transactions on Neural Systems and Rehabilitation Engineering,* vol. 14, pp. 304-310, 2006.

[44] J. R. Engsberg, S. W. Sprouse, M. L. Uhrich, B. R. Ziegler, and F. D. Luitjohan, "Preliminary investigation comparing rectified and unrectified sockets for transtibial amputees," *Journal of Prosthetics and Orthotics,* vol. 15, pp. 119-124, 2003.

[45] T. Dumbleton, A. W. P. Buis, A. McFadyen, B. F. McHugh, G. McKay, K. D. Murray, and S. Sexton, "Dynamic interface pressure distributions of two transtibial prosthetic socket concepts," *Journal of Rehabilitation Research and Development,* vol. 46, pp. 405-416, 2009.

[46] M. Zhang, A. R. Turner-Smith, A. Tanner, and V. C. Roberts, "Clinical investigation of the pressure and shear stress on the transtibial stump with a prosthesis," *Medical Engineering & Physics,* vol. 20, pp. 188-198, 1998.

[47] M. B. Silver-Thorn, J. W. Steege, and D. S. Childress, "A review of prosthetic interface stress investigations," *Journal of Rehabilitation Research and Development,* vol. 33, pp. 253-266, 1996.

[48] A. F. T. Mak, M. Zhang, and D. A. Boone, "State-of-the-art research in lowe-limb prosthetic biomechanics socket interface: a review," *Journal of Rehabilitation Research and Development,* vol. 38, pp. 161-174, 2001.

[49] P. Sewell, S. Noroozi, J. Vinney, and S. Andrews, "Developments in the trans-tibial prosthetic socket fitting process: a review of past and present research," *Prosthetics and Orthotics International,* vol. 24, pp. 97-107, 2000.

[50] X. Jia, M. Zhang, and W. C. C. Lee, "Load transfer mechanics between trans-tibial prosthetic socket and residual limb - dynamic effects," *Journal of Biomechanics,* vol. 37, pp. 1371-1377, 2004.

[51] J. C. H. Goh, P. V. S. Lee, and S. Y. Chong, "Comparative study between patellar-tendon-bearing and pressure cast prosthetic sockets," *Journal of Rehabilitation Research and Development,* vol. 41, pp. 491-502, 2004.

[52] B. Rogers, G. Bosker, M. Faustini, G. Walden, R. R. Neptune, and R. Crawford, "Case report: variably compliant transtibial prosthetic socket fabricated using solid freeform fabrication," *Journal of Prosthetics and Orthotics,* vol. 20, pp. 1-7, 2008.

[53] T. L. Beil, G. M. Street, and S. J. Covey, "Interface pressures during ambulation using suction and vacuum-assisted prosthetic sockets," *Journal of Rehabilitation Research and Development,* vol. 39, pp. 693-700, 2002.

[54] H. Seelen, S. Anemaat, H. Janssen, and J. Deckers, "Effects of prosthesis alignment on pressure distribution at the stump/socket interface in transtibial amputees during unsupported stance and gait," *Clinical Rehabilitation,* vol. 17, pp. 787-796, 2003.

[55] A. Eshraghi, N. A. Abu Osman, H. Gholizadeh, S. Ali, S. K. Saevarsson, and W. A. Wan Abas, "An experimental study of the interface pressure profile during level walking of a new suspension system for lower limb amputees," *Clin Biomech (Bristol, Avon),* vol. 28, pp. 55-60, 2013.

[56] P. Dou, X. Jia, S. Suo, R. Wang, and M. Zhang, "Pressure distribution at the stump/socket interface in transtibital amputees during walking on stairs, slope, and non-flat road," *Clinical Biomechanics,* vol. 21, pp. 1067-1073, 2006.

[57] W. C. C. Lee, M. Zhang, X. Jia, and J. T. M. Cheung, "Finite element modeling of the contact interface between transtibial residual limb and the prosthetic socket," *Medical Engineering & Physics,* vol. 26, pp. 655-662, 2004.

[58] S. Portnoy, Z. Yizhar, N. Shabshin, Y. Itzchak, A. Kristal, Y. Dotan-Marom, I. Siev-Ner, and A. Gefen, "Internal mechanical conditions in the soft tissues of a residual limb of a trans-tibial amputee," *Journal of Biomechanics,* vol. 41, pp. 1897-909, 2008.

[59] R. Amali, S. Noroozi, J. Vinney, P. Sewell, and S. Andrews, "Predicting interfacial loads between the prosthetic socket and the residual limb for below-knee amputees - a case study," *Strain,* vol. 42, pp. 3-10, 2006.

[60] X. Jia, M. Zhang, X. Li, and W. C. C. Lee, "A quasi-dynamic nonlinear finite element model to investigate prosthetic interface stresses during walking for transtibial amputees," *Clinical Biomechanics,* vol. 20, pp. 630-635, 2005.

[61] N. A. Abu Osman, W. D. Spence, S. E. Solomonidis, J. P. Paul, and A. M. Weir, "Transducers for the determination of the pressure and shear stress distribution at the stump—socket interface of trans-tibial amputees," *Proceedings of the Institution of Mechanical Engineers, Part B: Journal of Engineering Manufacture,* vol. 224, pp. 1239-1250, 2010.

[62] S. Portnoy, J. v. Haare, R. P. J. Geers, A. Kristal, I. Siev-Ner, H. A. M. Seelen, C. W. J. Oomens, and A. Gefen, "Real-time subject-specific analyses of dynamic internal tissue loads in the residual limb of transtibial amputees," *Medical Engineering & Physics,* vol. 32, pp. 312-323, 2010.

[63] M. B. I. Reaz, M. S. Hussain, and F. Mohd-Yasin, "Techniques of EMG signal analysis: detection, processing, classification and applications," *Biological Procedures Online,* vol. 8, pp. 11-35, 2006.

[64] R. R. Neptune, K. Sasaki, and S. A. Kautz, "The effect of walking speed on muscle function and mechanical energetics," *Gait & Posture,* vol. 28, pp. 135-143, 2008.

[65] E. C. Prinsen, N. Mj, and J. S. Rietman, "Adaptation strategies of the lower extremities of patients with a transtibial or transfemoral amputation during level walking: a systematic review," *Arch Phys Med Rehabil,* vol. 92, pp. 1311-1325, 2011.

[66] H. Sadeghi, P. Allard, and M. Duhaime, "Muscle power compensatory mechanism in below-knee amputee gait," *American Journal of Physical Medicine and Rehabilitation,* vol. 80, pp. 25-32, 2001.

[67] B. Silver-Thorn, C. T, and B. Kuhse, "Preliminary investigation of residual limb plantarflexion and dorsiflexion muscle activity during treadmill walking for trans-tibial amputees," *Prosthetics and Orthotics International,* vol. 36, pp. 435-442, 2012.

[68] S. Huang and D. P. Ferris, "Muscle activation patterns during walking from transtibial amputees recorded within the residual limb-prosthetic interface," *Journal of NeuroEngineering and Rehabilitation,* vol. 9, pp. 1-16, 2012.

[69] M. Seyedali, J. M. Czerniecki, D. C. Morgenroth, and M. E. Hahn, "Co-contraction patterns of trans-tibial amputee ankle and knee musculature during gait," *Journal of NeuroEngineering and Rehabilitation,* vol. 9, pp. 1-9, 2012.

[70] J. D. Miller, M. S. Beazer, and M. E. Hahn, "Myoelectric walking mode classification for transtibial amputees," *IEEE Transaction on biomedical engineering,* vol. 60, pp. 2745-2750, 2013.

[71] C. Kirtley, *Clinical Gait Analysis - Theory and Practice*: Churchill Livingstone, 2006.

[72] E. Ayyappa, "Normal human locomotion, part 2: motions, ground reaction force and muscle activity," *Journal of Prosthetics and Orthotics,* vol. 9, pp. 49-62, 1997.

[73] D. T. H. Lai, R. K. Begg, and M. Palaniswami, "Computational intelligence in gait research: a perspective on current applications and future challenges," *IEEE Transactions on Information Technology in Biomedicine,* vol. 13, pp. 687-702, 2009.

[74] K. Kaufman, "Future directions in gait analysis," in *Gait analysis in the science of rehabilitation*, ed, 1998.

[75] T. Chau, "A review of analytical techniques for gait data. Part 2: neural network and wavelet methods," *Gait & Posture,* vol. 13, pp. 102-120, 2001.

[76] M. Kohle, D. Merkl, and J. Mastner, "Clinical gait analysis by neural networks: issues and experiences," in *10th IEEE Symposium on Computer-Based Medical Systems*, Marribor, Slovenia, 1997, pp. 138-143.

[77] R. Versluys, P. Beyl, M. V. Damme, A. Desomer, R. V. Ham, and D. Lefeber, "Prosthetic feet: state-of-the-art review and the important of mimicking human ankle-foot biomechanics," *Disability and Rehabilitation: Assistive Technology,* vol. 4, pp. 65-75, 2009.

[78] D. H. Gates, J. Lelas, U. D. Croce, H. Herr, and P. Bonato, "Characterization on ankle function during stair ambulation," in *26th Annual International Conference of the IEEE EMBS*, San Francisco, CA, USA, 2004, pp. 4248-4252.

[79] W. Tao, T. Liu, R. Zheng, and H. Feng, "Gait Analysis Using Wearable Sensors," *Sensors (Basel),* vol. 12, pp. 2255-2283, 2012.

[80] VICON. (2015). *Vicon life science*. Available: http://www.vicon.com/motion-capture/life-sciences

[81] OrganicMotion. (2015). *Markerless mocap for the life sciences*. Available: http://www.organicmotion.com/life-sciences/

[82] MiniSun. (2015). *Intelligent device for energy expenditure and activity (IDEEA)*. Available: http://www.minisun.com/IDEEA_Overview.asp

[83] K. R. Archer, R. C. Castillo, E. J. Mackenzie, and M. J. Bosse, "Gait symmetry and walking speed analysis following lower-extremity trauma," *Phys Ther,* vol. 86, pp. 1630-1640, 2006.

[84] A. S. Soares, E. Y. Yamaguti, L. Mochizuki, A. C. Amadio, and J. C. Serrao, "Biomechanical parameters of gait among transtibial amputees: a review," *Sao Paulo Med J,* vol. 127, pp. 302-309, 2009.

[85] R. Baker, "Gait analysis methods in rehabilitation," *J Neuroengineering Rehabil,* vol. 3, pp. 1-10, 2006.

[86] D. Rusaw and N. Ramstrand, "Motion-analysis studies of transtibial prosthesis users: a systematic review," *Prosthetics and Orthotics International,* vol. 35, pp. 8-19, 2011.

[87] J.-M. Casillas, V. Dulieu, M. Cohen, I. Marcer, and J.-P. Didier, "Bioenergetic comparison of a new energy-storing foot and SACH foot in traumatic below-knee vascular amputations," *Archives of Physical Medicine and Rehabilitation,* vol. 76, pp. 39-44, 1995.

[88] D. H. Nielsen, D. G. Shurr, J. C. Golden, and K. Meier, "Comparison of energy cost and gait efficiency during ambulation in below-knee amputees using

different prosthetic feet - A preliminary report," *Journal of Prosthetics and Orthotics,* vol. 1, pp. 24-29, 1989.

[89] L. Torburn, J. Perry, E. Ayyappa, and S. L. Shanfield, "Below-knee amputee gait with dynamic elastic response prosthetic feet: A pilot study," *Journal of Rehabilitation Research and Development,* vol. 27, pp. 369-384, 1990.

[90] K. Postema, H. J. Hermens, J. de Vries, H. F. Koopman, and W. H. Eisma, "Energy storage and release of prosthetic feet. Part 1: Biomechanical analysis related to user benefits," *Prosthetics and Orthotics International,* vol. 21, pp. 17-27, 1997.

[91] A. Gitter, J. M. Czerniecki, and D. M. DeGroot, "Biomechanical analysis of the influence of prosthetic feet on below-knee amputee walking," *Am J Phys Med Rehabil,* vol. 70, pp. 142-148, 1991.

[92] P. M. Stevens, "Current concepts regarding externally powered lower limb prostheses," *Technology & Innovation,* vol. 15, pp. 301-309, 2014.

[93] S. K. Au, J. Weber, and H. Herr, "Powered ankle-foot prosthesis improves walking metabolic economy," *IEEE Transactions on Robotics,* vol. 25, pp. 51-66, 2009.

[94] R. Jiménez-Fabián and O. Verlinden, "Review of control algorithms for robotic ankle systems in lower-limb orthoses, prostheses, and exoskeletons," *Medical Engineering & Physics,* vol. 34, pp. 397-408, 2012.

[95] J. Hitt, T. Sugar, M. Holgate, R. Bellman, and K. Hollander, "Robotic transtibial prosthesis with biomechanical energy regeneration," *International Journal of Industrial Robot,* vol. 36, pp. 441-447, 2009.

[96] R. Versluys, A. Desomer, G. Lenaerts, M. V. Damme, P. Beyl, G. V. d. Perre, L. Peeraer, and D. Lefeber, "A pneumatically powered below-knee prosthesis: design specifications and first experiments with an amputee," in *2nd Biennial IEEE/RAS-EMBS International Conference on Biomedical Robotics and Biomechanics*, Scottsdale, AZ, USA, 2008, pp. 372-377.

[97] M. Alimusaj, L. Fradet, F. Braatz, H. J. Gerner, and S. I. Wolf, "Kinematics and kinetics with an adaptive ankle foot system during stair ambulation of transtibial amputees," *Gait & Posture,* vol. 30, pp. 356-363, 2009.

[98] H. A. Varol, F. Sup, and M. Goldfarb, "Real-time gait model intent recognition of a powered knee and ankle prosthesis for standing and walking," in *2nd Biennial IEEE/RAS-EMBS International Conference on Biomedical Robotics and Biomechatronics*, Scottsdale, AZ, USA, 2008, pp. 66-72.

[99] H. Huang, T. A. Kuiken, and R. D. Lipschutz, "A strategy for identifying locomotion modes using surface electromyography," *IEEE Transactions on Biomedical Engineering,* vol. 56, pp. 65-73, 2009.

[100] L. J. Hargrove, A. M. Simon, A. J. Young, R. D. Lipschutz, S. B. Finucane, D. G. Smith, and T. A. Kuiken, "Robotic leg control with EMG decoding in an amputee with nerve transfers," *New England Journal of Medicine,* vol. 369, pp. 1237-1242, 2013.

[101] S. Srinivasan, E. R. Westervelt, and A. H. Hansen, "A low-dimensional sagittal-plane forward-dynamic model for asymmetric gait and its application to study the gait of transtibial prosthesis users," *Journal of Biomechanical Engineering,* vol. 131, pp. 1-9, 2009.

[102] Tekscan. (2015). *FlexiForce sensors - User manual*. Available: http://www.tekscan.com/pdf/A201-force-sensor.pdf

[103] TheElectrodeStore. (2015). *Disposable surface electrodes*. Available: http://www.electrodestore.com/emg/emg-surface-electrodes/disposable-surface-electrodes

[104] Atmel. (2015). *Microcontrollers*. Available: http://www.atmel.com

[105] L. F. Teixeira-Salmela, N. S, M. Mh, G. D, and L. F. Requiao, "Effects of cadence on energy generation and absorption at lower extremity joints during gait," *Clin Biomech (Bristol, Avon),* vol. 23, pp. 769-778, 2008.

[106] E. Isakov, O. Keren, and N. Benjuya, "Trans-tibial amputee gait: time-distance parameters and EMG activity," *Prosthetics and Orthotics International,* vol. 24, pp. 216-220, 2000.

[107] J. Perry, L. A. Boyd, S. S. Rao, and S. J. Mulroy, "Prosthetic weight acceptance mechanics in transtibial amputees wearing the single axis, Seattle Lite, and Flex Foot," *IEEE Transactions on Rehabilitation Engineering,* vol. 5, pp. 283-289, 1997.

[108] J. D. Ventura, G. K. Klute, and R. R. Neptune, "The effect of prosthetic ankle energy storage and return properties on muscle activity in below-knee amputee walking," *Gait & Posture,* vol. 33, pp. 220-226, 2011.

[109] S. J. Mattes, P. E. Martin, and T. D. Royer, "Walking symmetry and energy cost in persons with unilateral transtibial amputations: matching prosthetic and intact limb inertial properties," *Arch Phys Med Rehabil,* vol. 81, pp. 561-568, 2000.

[110] E. Isakov, H. Burger, J. Krajnik, M. Gregoric, and C. Marincek, "Influence of speed on gait parameters and on symmetry in trans-tibial amputees," *Prosthetics and Orthotics International,* vol. 20, pp. 153-158, 1996.

[111] A. Mai, S. Commuri, C. P. Dionne, J. Day, W. J. J. Ertl, and J. L. Regens, "Residual muscle contraction and residuum socket interface force in men with transtibial osteomyoplastic amputation," *Journal of Prosthetics and Orthotics,* vol. 25, pp. 151-158, 2013.

[112] X. Jia, S. Suo, F. Meng, and R. Wang, "Effects of alignment on interface pressure for transtibial amputee during walking," *Disability and Rehabilitation: Assistive Technology,* vol. 3, pp. 339-343, 2008.

[113] M. Zhang and W. C. C. Lee, "Quantifying the regional load-bearing ability of trans-tibial stumps," *Prosthetics and Orthotics International,* vol. 30, pp. 25-34, 2006.

[114] P. Convery and A. W. P. Buis, "Socket/stump interface dynamic pressure distributions recored during the prosthetic stance phase of gait of a transtibial amputee wearing a hydrocast socket," *Prosthetics and Orthotics International,* vol. 23, pp. 107-112, 1999.

[115] K. Yigiter, G. Sener, and K. Bayar, "Comparison of the effects of patellar tendon bearing and total surface bearing sockets on prosthetic fitting and rehabilitation," *Prosthetics and Orthotics International,* vol. 26, pp. 206-212, 2002.

[116] Freedom-Innovations. (2015). *Renegade Foot*. Available: http://www.freedom-innovations.com/renegade/index.html

[117] College-Park. (2015). *Venture Foot*. Available: http://www.college-park.com/spec_sheets/CPI_Venture%20SpecSheet.pdf

[118] H. G. Ragnarsdottir, A. V. Clausen, H. Thorhallsdottir, and H. Jonsson, "System and method for motion-controlled foot unit," US Patent 7,431,737, 2008.

[119] J. H. Hong and M. S. Mun, "Relationship between socket pressure and EMG of two muscles in trans-femoral stumps during gait," *Prosthetics and Orthotics International,* vol. 29, pp. 59-72, 2005.

[120] R. D. Schrock, J. H. Zettl, E. M. Burgess, and R. L. Romano, "A preliminary report of basic studies from prosthetics research study," *Bulletin of Prosthetics Research,* pp. 90-105, 1968.

[121] E. M. Burgess and A. J. Moore, "A study of interface pressures in the below-knee prosthesis (physiological suspension: an interim report)," *Bulletin of Prosthetics Research,* pp. 58-70, 1977.

[122] A. Mai, S. Commuri, C. P. Dionne, J. Day, W. J. J. Ertl, and J. L. Regens, "Effect of prosthetic foot on residuum-socket interface pressure and gait characteristics in an otherwise healthy man with transtibial osteomyoplastic amputation," *Journal of Prosthetics and Orthotics,* vol. 24, pp. 211-220, 2012.

[123] E. G. Culham, M. Peat, and E. Newell, "Below-knee amputation: a comparison of the effect of the SACH foot and single axis foot on electromyography patterns during locomotion," *Prosthetics and Orthotics International,* vol. 10, pp. 15-22, 1986.

[124] C. P. Dionne, W. J. J. Ertl, and J. Day, "Physical therapy management of patients following an Ertl osteomyoplastic transtibial amputation procedure," *Journal of Prosthetics and Orthotics,* vol. 21, pp. 64-70, 2009.

[125] A. L. Hof, H. Elzinga, W. Grimmius, and J. P. K. Hallbertsma, "Speed dependence of avaraged EMG profiles in walking," *Gait & Posture,* vol. 16, pp. 78-86, 2002.

[126] J. Markowitz, K. P, E. Mf, E. K, B. C, and H. Herr, "Speed adaptation in a powered transtibial prosthesis controlled with a neuromuscular model," *Philosophical Transactions of the Royal Society B-Biological Sciences,* vol. 366, pp. 1621-1631, 2011.

[127] L. J. Hargrove, E. Scheme, K. Englehart, and B. S. Hudgins, "Multiple binary classifications via linear discriminant analysis for improved controllability of a

powered prosthesis," *IEEE Trans Neural Syst Rehabil Eng,* vol. 18, pp. 49-57, 2010.

[128] L. Hargrove, A. M. Simon, R. D. Lipschutz, S. B. Finucane, and T. A. Kuiken, "Real-time myoelectric control of knee and ankle motions for transfemoral amputees," *Journal of the American Medical Association,* vol. 305, pp. 1542-1544, 2011.

[129] MathWorks. (2015). *MathWorks - MATLAB and Simulink for Technical Computing*. Available: http://www.mathworks.com/index.html

[130] M. Millard, J. McPhee, and E. Kubica, "Multi-step forward dynamic gait simulation," *Computational Methods in Applied Sciences,* vol. 12, pp. 25-43, 2008.

[131] M. Peasgood, E. Kubica, and J. McPhee, "Stabilization of a dynamic walking gait simulation," *ASME Journal of Computational and Nonlinear Dynamics,* vol. 2, pp. 65-72, 2007.

[132] D. G. Thelen and F. C. Anderson, "Using computed muscle control to generate forward dynamic simulations of human walking from experiment data," *Journal of Biomechanics,* vol. 39, pp. 1107-1115, 2006.

[133] M. G. Pandy, "Computer modeling and simulation of human movement," *Annual Review of Biomedical Engineering,* vol. 3, pp. 245-273, 2001.

[134] Y. Xiang, J. S. Arora, and K. Abdel-Malek, "Physics-based modeling and simulation of human walking: a review of optimization-based and other approaches," *Medical and Bioengineering Application,* vol. 42, pp. 1-23, 2010.

[135] S. Pejhan, F. Farahmand, and M. Parnianpour, "Design optimization of an above-knee prosthesis based on the kinematics of gait," in *30th Annual International IEEE EMBS Conference*, Vancouver, Bristish Columbia, Canada, 2008, pp. 4274-4277.

[136] P. Brugger and H.-B. Schemiedmayer, "Simulating prosthetic gait - lessons to learn," *Proceedings in Applied Mathematics and Mechanics,* vol. 3, pp. 64-67, 2003.

[137] B. Dariush, V. Ng-Thow-Hing, and D. G. Thelen, "Simulation system, method and computer-readable medium for human augmentation devices," US Patent 7,251,593, 2007.

[138] D. Orin, "Application of robotics to prosthetic control," *Annals of Biomedical Engineering,* vol. 8, pp. 305-316, 1981.

[139] A. K. Silverman and R. R. Neptune, "Muscle and prosthesis contributions to amputee walking mechanics: A modeling study," *Journal of Biomechanics,* vol. 45, pp. 2271-2278, 2012.

[140] V. D. Kalanovic, D. Popovic, and N. Skang, "Feedback error learning neural network for trans-femoral prosthesis," *IEEE Transactions on Rehabilitation Engineering,* vol. 8, pp. 71-80, 2000.

[141] F. M. L. Amirouche, *Computational Methods in Multibody Dynamics*. Englewood Cliffs, NJ: Prentice Hall, 1992.

[142] A. Mai and S. Commuri, "Gait identification for an intelligent prosthetic foot," in *IEEE International Symposium on Intelligent Control (ISIC)*, Denver, CO, USA, 2011, pp. 1341-1346.

[143] G. K. Klute, J. S. Berge, and A. D. Segal, "Heel-region properties of prosthetic feet and shoes," *Journal of Rehabilitation Research and Development,* vol. 41, pp. 535-546, 2004.

[144] H. Pontzer, J. H. Holloway, D. A. Raichlen, and D. E. Lieberman, "Control and function of arm swing in human walking and running," *Journal of Experimental Biology,* vol. 212, pp. 523-534, 2009.

[145] S. H. Collins, P. G. Adamczyk, and A. D. Kuo, "Dynamic arm swinging in human walking," *Proceedings of the Royal Society B: Biological Sciences,* vol. 276, pp. 3679-3688, 2009.

[146] F. L. Lewis, S. Jagannathan, and A. Yesilderek, *Neural network control of robot manipulators and nonlinear systems*. London, UK: Taylor & Francis, 1999.

[147] J. J. E. Slotine and W. Li, *Applied nonlinear control*: Prentice-Hall, Incorporated, Englewood Cliffs, N.J., 1991.

[148] D. M. Dawson, J. Hu, and T. C. Burg, *Nonlinear control of electric machinery*: Taylor & Francis, 1998.

[149] J. C. Ambrósio and A. Kecskeméthy, "Multibody dynamics of biomechanical models for human motion via optimization," in *Multibody Dynamics*. vol. 4, J. García Orden, J. Goicolea, and J. Cuadrado, Eds., ed: Springer Netherlands, 2007, pp. 245-272.

[150] R. Beckett and K. Chang, "An evaluation of the kinematics of gait by minimum energy," *Journal of Biomechanics,* vol. 1, pp. 147-159, 1968.

[151] M. Wojtyra, "Multibody simulation model of human walking," *Mechanics Based Design of Stuctures and Machines,* vol. 31, pp. 357-379, 2003.

[152] S. Srinivasan, I. A. Raptis, and E. R. Westervelt, "Low-dimensional sagittal plane model of normal human walking," *Journal of Biomechanical Engineering,* vol. 130, pp. 1-9, 2008.

[153] V. E. Berbyuk, G. V. Grasyuk, and N. I. Nishchenko, "Mathematical modeling of the dynamics of the human gait in the sagittal plane," *Journal of Mathematical Scienes,* vol. 96, pp. 3047-3056, 1999.

[154] M. A. Shandiz, F. Farahmand, and H. Zohour, "Dynamic simulation of the biped normal and amputee human gait," in *12th International Conference on Climbing and Walking Robots and the Support Technologies for Mobile Machines*, Istanbul, Turkey, 2009, pp. 1113-1120.

[155] J. Si and Y.-T. Wang, "On-line learning control by association and reinforcement," *IEEE Transactions on Neural Networks,* vol. 12, pp. 264-276, 2001.

[156] C. Lu, J. Si, and X. Xie, "Direct heuristic dynamic programming for damping oscillations in a large power system," *IEEE Transactions on Systems, Man, and Cybernetics - Part B: Cybernetics,* vol. 38, pp. 1008-1013, 2008.

[157] R. Enns and J. Si, "Helicopter trimming and tracking control using direct neural dynamic programming," *IEEE Transactions on Neural Networks,* vol. 14, pp. 929-939, 2003.

[158] A. Mai and S. Commuri, "Adaptive dynamic programming-based control of an ankle prosthetic joint," in *Lecture Note in Electrical Engineering*. vol. 325, ed: Springer, 2015, pp. 91-105.

[159] A. Mai and S. Commuri, "Intelligent control of a prosthetic ankle using gait recognition," *IFAC Journal of Control Engineering Practice,* Submitted (2015).

Appendices

Appendix A1 – Link segment and ankle joint dynamics

$$M = \begin{bmatrix} M_{aa} & M_{ak} & M_{ah} \\ M_{ka} & M_{kk} & M_{kh} \\ M_{ha} & M_{hk} & M_{hh} \end{bmatrix}$$

$$= \begin{bmatrix} m_f r_f^2 + I_f & m_f r_f L_s \cos(\theta_a - \theta_k) & m_f r_f L_t \cos(\theta_a - \theta_h) \\ m_f r_f L_s \cos(\theta_a - \theta_k) & m_f L_s^2 + m_s r_s^2 + I_s & (m_f L_s L_t + m_s r_s L_t)\cos(\theta_k - \theta_h) \\ m_f r_f L_t \cos(\theta_a - \theta_h) & (m_f L_s L_t + m_s r_s L_t)\cos(\theta_k - \theta_h) & m_f L_t^2 + m_s L_t^2 + m_t r_t^2 + I_t \end{bmatrix}$$

$$V = \begin{bmatrix} V_{aa} & V_{ak} & V_{ah} \\ V_{ka} & V_{kk} & V_{kh} \\ V_{ha} & V_{hk} & V_{hh} \end{bmatrix}$$

$$= \begin{bmatrix} 0 & m_f r_f L_s \dot{\theta}_k \sin(\theta_a - \theta_k) & m_f r_f L_t \dot{\theta}_h \sin(\theta_a - \theta_h) \\ -m_f r_f L_s \dot{\theta}_a \sin(\theta_a - \theta_k) & 0 & (m_f L_s L_t + m_s r_s L_t)\dot{\theta}_h \sin(\theta_k - \theta_h) \\ -m_f r_f L_t \dot{\theta}_a \sin(\theta_a - \theta_h) & -(m_f L_s L_t + m_s r_s L_t)\dot{\theta}_k \sin(\theta_k - \theta_h) & 0 \end{bmatrix}$$

$$G = \begin{bmatrix} G_a \\ G_k \\ G_h \end{bmatrix} = \begin{bmatrix} m_f r_f g \sin\theta_a \\ (m_f L_s + m_s r_s) g \sin\theta_k \\ (m_f L_t + m_s L_t + m_t r_t) g \sin\theta_h \end{bmatrix}$$

$I_f = m_f (\alpha_f L_f)^2$; $I_s = m_s (\alpha_s L_s)^2$; $I_t = m_t (\alpha_t L_t)^2$;

m_f, L_f, I_f – mass, length, and inertia around the center of mass of the foot

m_s, L_s, I_s – mass, length, and inertia around the center of mass of the shank

m_t, L_t, I_t – mass, length, and inertia around the center of mass of the thigh

$\alpha_{f,s,t} = \dfrac{\text{radius of gyration}}{\text{segment length}}$; $\alpha_f = 0.475(\text{foot})$; $\alpha_s = 0.302(\text{shank})$; $\alpha_t = 0.323(\text{thigh})$

$r_f = \dfrac{L_f}{2}$ – distance from the ankle joint to the center of the mass of the foot

$r_s = \dfrac{L_s}{2}$ – distance from the ankle/knee joint to the center of the mass of the shank

$r_t = \dfrac{L_t}{2}$ – distance from the knee/hip joint to the center of the mass of the thigh

Appendix A2 – Proof of Lemma 8.3.1

The physical/design constraints of the prosthetic ankle joint guarantee that the actual ankle angular position θ_a and velocity $\dot{\theta}_a$ are always bounded. In addition, the gait-

based kinematic references $\left(\theta_r^g, \dot{\theta}_r^g, \ddot{\theta}_r^g\right)$ are also bounded since they are approximated by finite Fourier series (Discussions). The tracking error $\left(\theta_{ar}^g - \theta_a\right)$ is therefore finite and since $r = \dot{e}_a + \lambda e_a$, the filtered tracking error r is also finite, i.e., $r \in L_\infty$.

By replacing $\dot{e}_a$ in (8.2)by $r - \lambda e_a$, one can show that

$$\|x\| \le C_2 + C_3 \|r\|$$

where $C_2 > 0$ and $C_3 > 0$ depend on the initial tracking error $e_a(0)$, the bound $B_{\theta_r^g}$ and design parameter λ. With the input vector x in a compact set $x \in S_x \subset \mathbb{R}^{N_x \times 1}$, the approximation (8.1) holds.

Appendix A3 – Proof of Lemma 8.3.2

From Taylor series expansion of $\sigma\left(V_f^T x\right)$, $\left(H.O.T\right) = \sigma - \hat{\sigma} - \hat{\sigma}' \tilde{V}_f^T x$, then

$$\begin{aligned} \|H.O.T\| &= \left\|\sigma - \hat{\sigma} - \hat{\sigma}' \tilde{V}_f^T x\right\| \\ &\le \|\sigma - \hat{\sigma}\| + \|\hat{\sigma}'\| \left\|\tilde{V}_f^T\right\|_F \|x\| \\ &\le \|\sigma - \hat{\sigma}\| + \|\hat{\sigma}'\| \left\|\tilde{V}_f^T\right\|_F \left(C_2 + C_3 \|r\|\right) \end{aligned}$$

Since the sigmoid activation functions and their derivatives are bounded, i.e., $\|\sigma\| < 1$, $\|\hat{\sigma}\| < 1$ and $\|\hat{\sigma}'\| \le B_\sigma$, we have

$$\|H.O.T\| \le 1 + C_2 B_\sigma \left\|\tilde{V}_f^T\right\|_F + C_3 B_\sigma \left\|\tilde{V}_f^T\right\|_F \|r\|$$

with $\tilde{Z}_f = \begin{bmatrix} \tilde{W}_f & \Theta \\ \Theta & \tilde{V}_f \end{bmatrix}$, we have $\left\|\tilde{W}_f\right\|_F, \left\|\tilde{V}_f\right\|_F \le \left\|\tilde{Z}_f\right\|_F$, then

$$\|H.O.T\| \le 1 + C_2 B_\sigma \left\|\tilde{Z}_f^T\right\|_F + C_3 B_\sigma \left\|\tilde{Z}_f^T\right\|_F \|r\|$$

Appendix A4 – Proof of Lemma 8.3.3

Since $\|\varepsilon\| \le \varepsilon_B$, $\|\tau_{ad}\| \le B_d$, and $\|\tilde{\tau}_{aG}\| \le B_G$,

$$\begin{aligned}
\|\delta\| &= \left\|\tilde{W}_f^T \hat{\sigma}' V_f^T x + W_f^T (H.O.T) + \varepsilon + \tau_{ad} - \tilde{\tau}_{aG}\right\| \\
&\le \left\|\tilde{W}_f^T\right\|_F \|\hat{\sigma}'\| \left\|V_f^T\right\|_F \|x\| + \left\|W_f^T\right\|_F \|H.O.T\| + \varepsilon_B + B_d + B_G \\
&\le B_\sigma B_Z \left\|\tilde{Z}_f^T\right\|_F (C_2 + C_3 \|r\|) + B_Z \left(1 + C_2 B_\sigma \left\|\tilde{Z}_f^T\right\|_F + C_3 B_\sigma \left\|\tilde{Z}_f^T\right\|_F \|r\|\right) + \\
&\quad + \varepsilon_B + B_d + B_G \\
&\le \varepsilon_B + B_d + B_G + B_Z + 2C_2 B_\sigma B_Z \left\|\tilde{Z}_f^T\right\|_F + 2C_3 B_\sigma B_Z \left\|\tilde{Z}_f^T\right\|_F \|r\| \\
&\le C_4 + C_5 B_Z \left\|\tilde{Z}_f^T\right\|_F + C_6 B_Z \left\|\tilde{Z}_f^T\right\|_F \|r\|
\end{aligned}$$

where

$$\begin{aligned}
C_4 &= \varepsilon_B + B_d + B_G + B_Z \\
C_5 &= 2C_2 B_\sigma \\
C_6 &= 2C_3 B_\sigma
\end{aligned}$$